Development of methods and technology for human blood hemostasis assessment

Praveen Kaliappan Sekar

A dissertation

submitted in partial fulfillment of the

requirements for the degree of

Doctor of Philosophy

University of Washington

2022

Reading Committee:

Dayong Gao, Co-Chair

Jae-Hyun Chung, Co-Chair

Yanyun Wu

Program Authorized to Offer Degree:

Mechanical Engineering

University of Washington

Abstract

Development of methods and technology for human blood hemostasis assessment

Praveen Kaliappan Sekar

Chairs of the Supervisory Committee:
Professor Dayong Gao
Professor Jae-Hyun Chung
Department of Mechanical Engineering

The primary response of the human body to an injury or trauma is the formation of a thrombus (clot) to stop bleeding, which is referred to as hemostasis. It is a complex biological process involving multiple blood components including platelets, plasma coagulation factors and erythrocytes (red blood cells). Rapid, accurate, and comprehensive assessment of hemostasis is essential in many clinical settings for managing patients who undergo invasive procedures, experience hemorrhages, or receive antithrombotic therapies to treat clotting disorders. Currently available hemostasis assays can be broadly classified into platelet function assays, tests for coagulation function, and recently developed 'global' hemostasis assays which include thromboelastography (TEG) and thromboelastometry (ROTEM). Major challenges or drawbacks of these assays include incomplete or partial evaluation of individual faceted clotting elements,

being expensive, time-consuming, and requiring highly trained personnel to conduct, analyze and interpret the results. In this dissertation, two new techniques for blood hemostasis assessments are introduced and tested for various hemostatic conditions. The first approach is a comprehensive platelet functional assay using a nano thin-film sensor. The second approach is a multiparameter whole blood hemostasis assay using a carbon nanotube paper-composite sensor. Finally, the development of an automated hemostasis analyzer for potential clinical applications is also presented in this dissertation.

Platelets are highly specialized discoid-shaped blood cells that play a vital role in the hemostatic response. In the event of a vascular injury, platelets undergo a series of highly complex, regulated, and multi-stage functional changes, including adhesion to the intimal matrix, intracellular calcium influx leading to platelet conformational change of morphology and integrins, activation, granule secretion, aggregation, and cytoskeletal contraction to form and stabilize a hemostatic plug that occludes the site of damage to stop bleeding. One of the major limitations of existing platelet assays is that they focus on a single functional response and thereby provide only a partial analysis of platelet function. The first approach presented in this dissertation is to address this long-standing technological limitation in platelet function assays. The newly developed approach evaluated platelets based on multiple functional stages of hemostasis using a sensitive nano thin-film capacitance sensor. Human platelet-rich plasma-based platelet function evaluations were conducted to demonstrate the feasibility of this approach for various platelet physiological conditions including drug-induced functional disorders. Sensor responses to platelet adhesion and after activation showed excellent sensitivities towards platelet counts, platelet activation levels, and platelet activation pathways. Close similarities between the

obtained signal and platelet cytoskeletal reorganization after activation were observed through a fluorescence microscopy study. In comparison to the conventional optical-based evaluation system, the developed low-cost electrical-based sensing platform offers superior performance characteristics in assaying platelet function, such as high sensitivity, continuous multiparameter evaluation, label-free and easy-to-use.

The second approach presented in this thesis is focused on providing a more comprehensive analysis of the overall blood hemostatic potential. Even though the newly developed platelet assay can offer a good snapshot of the *in vivo* blood hemostatic status by providing a comprehensive analysis of platelet function, it did not evaluate the contributions from other cellular components and plasma coagulation factors. Additionally, the sensor system is expensive to fabricate, and the assay is technically challenging and time-consuming. Therefore, an all-encompassing hemostasis assay with a more convenient workflow using a novel carbon nanotube-paper composite (CPC) capacitance sensor was developed. The CPC capacitance response to blood clotting at 1.3 MHz provided three sensing parameters with distinctive sensitivities towards coagulation function (factors), platelets, and erythrocytes. Whole blood-based hemostasis assessments were conducted to demonstrate the potential functionality of the device for various hemostatic conditions, including pathological conditions such as hemophilia and thrombocytopenia. Results showed good agreements when compared to a conventional thromboelastography assay. Overall, the presented sensor system is a promising new biomedical device for convenient whole blood-based global assessment of hemostasis. Plans for further scientific explorations, including studying the effects of other physiological clotting parameters are also presented in this dissertation.

Most clinical hemostasis assays are still restricted to specialized laboratories because they need highly trained personnel to conduct, analyze and interpret the results. To address this issue, an automated bench-top prototype using the CPC sensor was developed. The automated hemostasis analyzer was devised with an intent to meet the growing needs in the healthcare landscape for an inexpensive routine hemostasis assessment and triage of patients with bleeding or risks for bleeding. The presented first version of the device is fully automatic, starting from blood aspiration to discard after measurements. The system was designed using conventional solid modeling software and fabricated using evolving low-cost rapid prototyping techniques. Further improvements in the system and a roadmap for extensive clinical studies to establish the functional equivalence of the analyzer to an existing U.S. FDA-approved device are also presented in this dissertation.

TABLE OF CONTENTS

LIST OF FIGURES

LIST OF TABLES

ACKNOWLEDGEMENTS

I am deeply indebted to my supervisors Prof. Dr. Dayong Gao, Prof. Dr. Jae-Hyun Chung and Prof. Dr. Yanyun Wu, whose support, inspiration, suggestions, and encouragement helped me all the time not only in my research but also through my personal life. I would also like to thank my committee members Prof. Dr. Jonathan Himmelfarb and Prof. Dr. Shaoyi Jiang for their input on my research.

My colleagues and collaborators greatly supported me in my research work. These kind people include but are not limited to Xin M. Liang, Zhiquan Shu, Sijie Sun, Ren Shen, Cifeng Fang, Ye Chen and so on in Dr. Gao's Lab, and Seong-Joong Kahng, Vigneshwar Sakthivelpathi in Dr. Chung's Lab and Prof. Dr. Anthony B. Dichiara from the School of Environmental and Forest Sciences, University of Washington.

I want to thank all the staff in the Department of Mechanical Engineering for their long-term support. I want to thank all the friends and staff in the Washington Nanofabrication Facility (WNF) for their help and patience with my micro-fabrication learnings. My conversations with them have helped me a lot throughout, all these years, and I am grateful for the opportunity to work in the WNF.

I would like to acknowledge the financial support from UW-CoMotion through their Innovation Gap Fund for my research.

Especially, I give my special thanks to my family and friends. This dissertation would never have been completed without their encouragement and affection.

DEDICATION

To my wife and mom for their boundless love in my life

Chapter 1. INTRODUCTION

1.1 HEMOSTASIS AND THROMBOSIS

The maintenance of blood fluidity within the vascular system is imperative for the overall well-being of the human body. Normal hemostasis (or hemostasis) generally refers to biological processes that lead to the formation of blood clots at the site of injury (Becker et al., 2013; Gale, 2011). It's a highly complex physiological process that involves multiple interlinked steps that culminate with the formation of a stable thrombus to staunch bleeding and promote vascular healing (Golebiewska and Poole, 2015). On the other hand, thrombosis refers to pathological clot formation from undesired activation of hemostasis ('hemostasis in the mistaken place and time'). Under healthy hemostatic conditions (also called as 'eucoagulable state'), there is a delicate equilibrium between the pathological states of hypercoagulability and hypocoagulability in the circulating blood (Fig. 1.1). Numerous clinical drugs have been developed over the years to help maintain this delicate equilibrium in patients with hemostatic (or clotting) disorders (McFadyen et al., 2018).

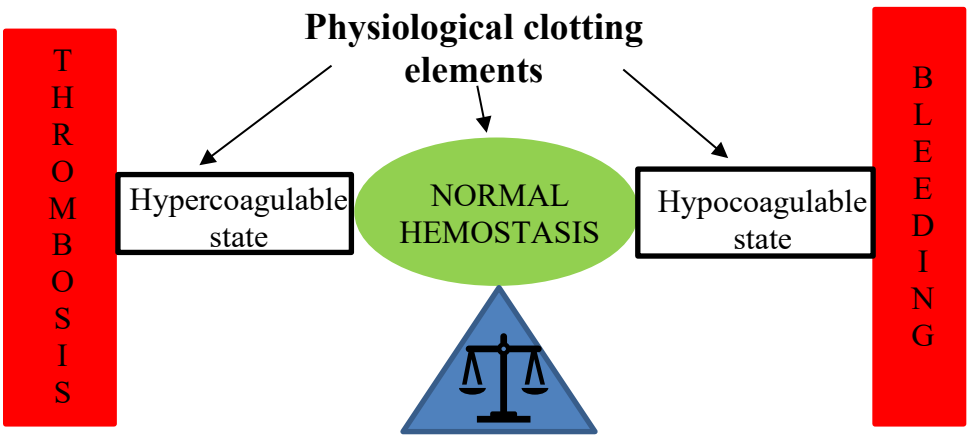

Fig. 1.1. The balance of normal hemostasis.

The mechanism of hemostasis (Fig. 1.2) *in vivo* involves the following steps: 1. Blood vessel constriction, 2. Primary hemostasis involves the formation of a platelet plug at the site of injury, 3. Secondary hemostasis involves the formation of fibrin mesh to encapsulate the platelet aggregates and other blood cells to form a thrombus, 4. Clot retraction from the contractile forces applied by the activated platelets, which over time increases the clot density and decreases clot size, promoting clot stability and maintaining blood vessel patency, 5. The last step is the dissolution of the clot through the activation of plasmin that breaks up the fibrin. This dissertation will focus on novel techniques to evaluate steps 2, 3, and 4 in an isolated and combined fashion.

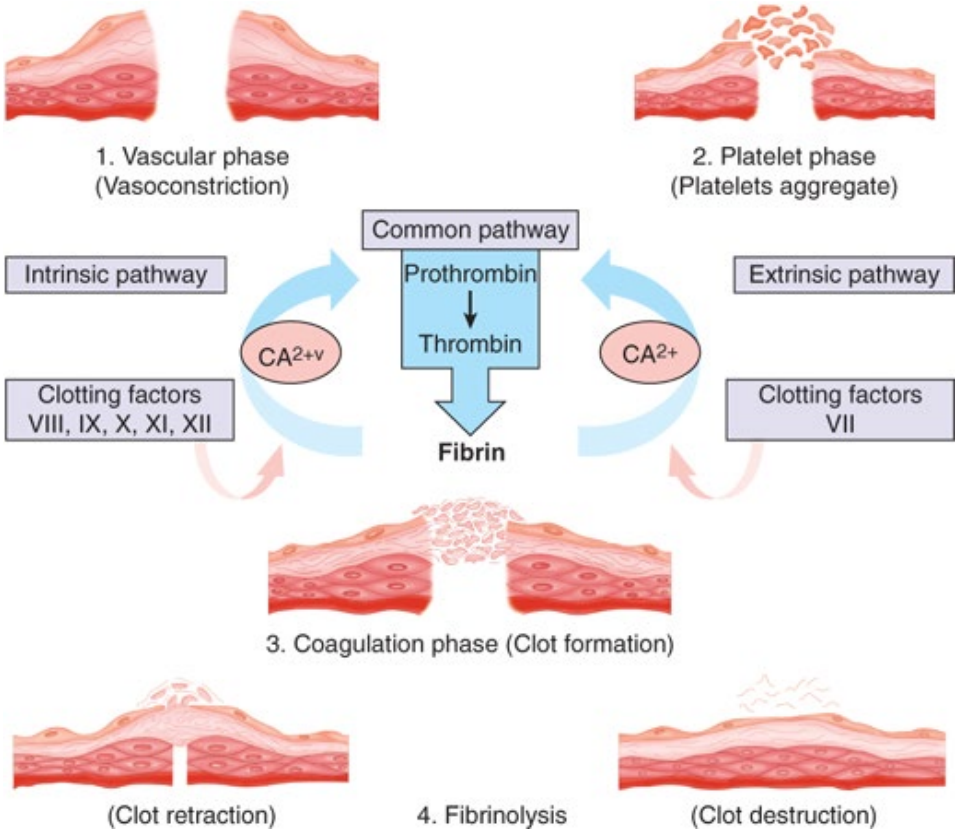

Fig. 1.2. Mechanisms in hemostasis.

In this section, first, a brief technical summary about the mechanisms in hemostasis is presented, followed by a review of the currently existing assays with an emphasis on their principle, pros and cons, and what aspects of hemostasis they measure. Then the significance and clinical applications for these assays are discussed.

1.1 PLATELETS IN HEMOSTASIS

Platelets were once considered to be passive participants in hemostasis, but are now well-recognized as an active synthesizer of humoral factors that potentiate clot formation and inflammation (Deepak L. Bhatt and Topol, 2003; Drelich and Bray, 2015). Fig. 1.3 is a summary of the role played by platelets in a thrombus formation. In an 'eucoagulable' state (normal hemostasis), platelets role along the side of the endothelium and are kept in an inactive state by prostacyclin and nitric oxide released by the endothelial cells that line the walls of blood vessels (Fig. 1.3a). The endothelial cells also express CD39 on their surface, which inhibits platelet activation by converting adenosine diphosphate (ADP), a potent platelet agonist, into adenosine monophosphate (AMP). When the integrity of the endothelial layer is damaged, the platelets adhere to the exposed sub-endothelium through interactions between the exposed matrix ligands such as collagen, von Willebrand factor, and fibronectin, and the platelet receptors including integrin $\alpha_{IIb}\beta_3$, glycoprotein Ib-IX (GP Ib-IX), and integrin $\alpha_5\beta_1$ (Fig. 1.3b). Both thrombin from the coagulation cascade (secondary hemostasis) and ADP can stimulate platelets to undergo shape change into an active conformation (Fig. 1.3c). Activated platelets secrete ADP, platelet-derived growth factor, and fibrinogen from their storage granules, and thromboxane A2 (TXA_2) is produced from biosynthesis. ADP and TXA_2 cause other circulating platelets to undergo shape change and further activation (Fig. 1.3d). $\alpha_{IIb}\beta_3$ receptors on the surface of activated platelets bind to fibrinogen in the plasma, leading to the formation of fibrinogen bridges between the

activated platelets, resulting in platelet aggregation to form a loose plug (Fig. 1.3e). The simultaneous formation of a fibrin mesh (secondary hemostasis) reinforces the platelet thrombus. Finally, the thrombus contracts from the contractile force exerted by activated platelets to provide further stabilization to the clot. (Fig. 1.3f).

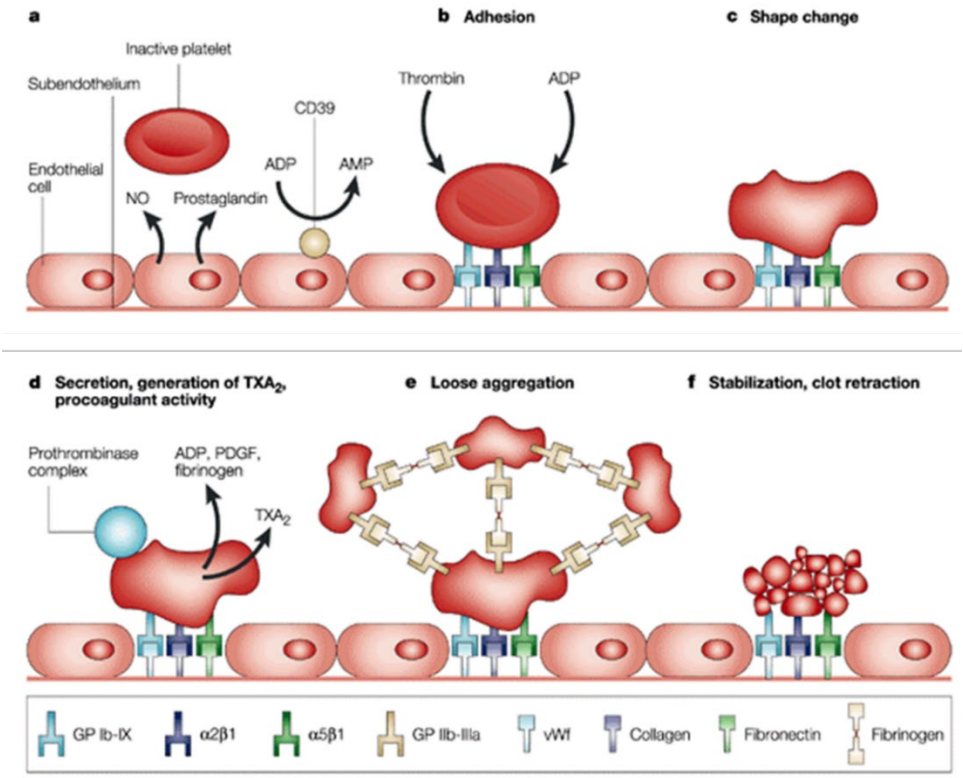

(D L Bhatt and Topol, 2003) -*"Scientific and therapeutic advances in antiplatelet therapy." Nat Rev Drug Discovery 2(1): 15-28.).*

1.2 SECONDARY HEMOSTASIS

Secondary hemostasis also referred to as coagulation cascade, involves the conversion of soluble fibrinogen to insoluble fibrin (Dahlbäck, 2000; Pallister and Watson, n.d.). Secondary hemostasis can be broken down into two pathways (Fig. 1.4): extrinsic and intrinsic, which eventually culminate with the fibrin mesh formation. The extrinsic pathway is initiated when the

blood vessel injury occurs, exposing tissue factor (TF) to the blood cells. TF combines with Factor VIIa creating the TF-VIIa complex, which then activates Factor X to Factor Xa and Factor IX to Factor IXa in the presence of Ca^{2+}. Concurrently, the intrinsic pathway is initiated when Factor XII is actuated to Factor XIIa by negatively charged surface contact. Factor XIIa then stimulates Factor XI to Factor XIa, which in turn converts Factor IX to Factor IXa in the presence of Ca^{2+}. Factor XIa combined with Factor VIIIa in the presence of Ca^{2+} forms a tenase complex activating Factor X to Factor Xa. The activation of Factor X to Factor Xa is where both the extrinsic and intrinsic pathways merge into the common pathway. After the activation of Factor X to Factor Xa to begin the common pathway, Factor Xa combines with Factor Va, phospholipid and Ca^{2+} to form prothrombinase. Prothrombinase converts prothrombin to thrombin. In the last step, thrombin cleaves the plasma fibrinogen to fibrin and activates Factor XIII to Factor XIIIa, which is responsible for the cross-linking of fibrin polymers to form a stable mesh.

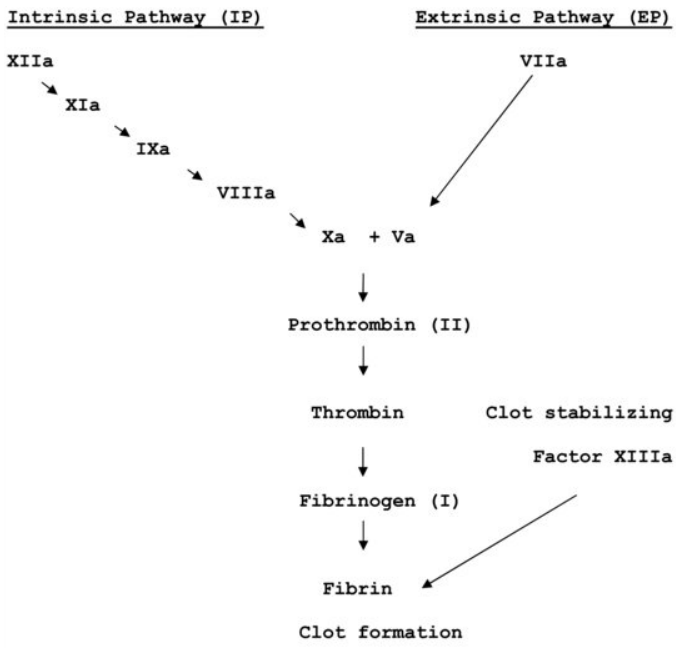

Fig. 1.4. The classical coagulation cascade.

(Pallister and Watson, n.d.). *"Haematology. Bloxham. UK: Scion Publishing, 334-336)*

1.3 ANTITHROMBOTIC DRUGS

An antithrombotic agent is a drug that reduces the undesired formation of blood clots. They are used therapeutically for the prevention and treatment of life-threatening thromboembolic conditions. They are also used in clinical therapies involving extracorporeal assist devices such hemodialysis, membrane oxygenation, mechanical circulatory support and so on, to prevent clotting in the blood transport lines and pumps of these devices *ex vivo* (Huth-Kühne et al., 2009; Sniecinski and Levy, 2015). There are two classes of antithrombotic drugs: anticoagulants and antiplatelet drugs. Anticoagulants slow down the coagulation cascade limiting the formation of fibrin mesh and thereby stunting the growth of a clot. Some of the commonly used anticoagulants include heparin, warfarin, and direct thrombin inhibitors. On the other hand, antiplatelet agents inhibit the platelet function for aggregation. They are generally more effective in arterial circulation compared to anticoagulant drugs (Durila et al., 2010).

1.4 EXISTING ASSAYS FOR BLOOD HEMOSTASIS – WHAT DO THEY MEASURE?

Over the years, several biological assays have been developed and applied for clinical evaluation of hemostatic status. These assays help clinicians in anticipating, avoiding and directing the management of life-threatening disorders due to bleeding or thrombosis (Jackson, 2011; Nair et al., 2010). Broadly, they can be classified into two types, platelet functional assays and tests for coagulation function.

Platelet functional assays evaluate the status of *in vivo* primary hemostasis. This includes the formation of a weak platelet plug from the interaction between platelets and vessel walls. In recent years, the assessment of platelet function has become increasingly essential in a variety of

clinical settings: 1) Identification of patients with bleeding disorders, 2) Monitoring the antiplatelet therapy, 3) Evaluation of perioperative hemostasis, 4) Transfusion medicine. Because of the diverse applications of these tests and the complex functionality of platelets, different methodologies have been developed and tested for clinical applicability. The majority of these assays typically measure the platelet adhesion or aggregation responses to agonists, including thrombin, collagen, ADP and arachidonic acid (Orme et al., 2017). Recently developed thromboelastography and thromboelastometry assays measure the viscoelastic properties of the thrombus to provide an indirect assessment of the platelet function (Carll and Wool, 2020; Whiting and DiNardo, 2014). A summary of the commonly used techniques, their principles and applications are provided in Table 1.1.

Table 1.1. Different methodologies for assessment of platelet function.

METHOD	SAMPLE	APPLICATIONS	PRINCIPLE
Bleeding time	Native WB	Screening test(obsolete)	In vivo measurement of time to stop bleeding
Tests based on platelet aggregation			
1. Light Transmission Aggregation (LTA)	1. Citrated PRP	1. Screening test for bleeding tendency; Diagnostic for platelet defects and monitoring antiplatelet treatment effect	1. Photo-optical measurement of light transmission increase to agonist-induced platelet aggregation
2. Impedance platelet aggregation	2. Citrated WB	2. Screening test for bleeding tendency Diagnostic for platelet defects Monitoring antiplatelet treatment effect	2. Measurement of electrical impedance increase to agonist-induced platelet aggregation
3. Lumiaggregometry	3. Citrated WB	3. Detection of storage/release disorders	3. LTA or wB aggregometry combined with luminescence
4. Platelet works	4. Citrated WB	4. Monitoring of platelet responses to antiplatelet agents	4. Platelet counting pre- and post-activation in whole blood
Tests based on platelet adhesion			
1. PFA-100; innovance PFA-200	1. Citrated WB	1. Assessment of bleeding risk and drug effects Searching severe platelet dysfunctions, revealing of VwD	Time evaluation of high shear WB flow blocked by platelet plug into a hole in the activated surface
2. Impact Cone and Plate(let) Analyzer	2. Citrated WB	2. Screening of primary hemostasis	2. Shear-induced platelet adhesion–aggregation upon the specific surface
3. Global thrombosis test (GTT)	3. Native WB	3. Evaluation of platelet function and thrombolysis	3. Measurement of time cessation of wB flow by high shear-dependent platelet plug formation
Viscoelastic tests			
1. TEG	1. Citrated WB	1. Assessment of global hemostasis plus monitoring antiplatelet treatments effect	1 & 2. Evaluation of the rate of clot formation based on low shear-induced and agonist addition
2. ROTEM Platelet	2. Citrated WB	2. Assessment of global hemostasis plus diagnostic of platelet defects plus monitoring antiplatelet treatments effect	
Flow cytometry	Citrated wB, PRP.	Cell counting, detection platelet activation by the extent of expression of surface and/or cytoplasmic biomarkers	Engineering laser-based detection of suspending fluorescent label platelets in a flowing solution

Abbreviations: PRP, platelet-rich plasma; WB, Whole blood; TEG, thromboelastometry; ROTEM, Rotational thromboelastometry

Coagulation assays (Table 1.2 evaluate the status of secondary hemostasis, which involves the enzymic reactions between the coagulation factors in plasma for insoluble fibrin formation. Conventional coagulation tests include prothrombin time (PT), activated partial thromboplastin time (aPTT), thrombin time (TT) and factor assays. They are all clot-based plasma assays and are either used for screening coagulation disorders or the diagnosis of specific factor disorders such as hemophilia or von Willebrand disease (Ganter and Hofer, 2008). Citrated plasma prepared by two-step centrifugation of whole blood is used as the working sample for these tests.

Table 1.2. Assays for coagulation function assessment.

METHOD	PRINCIPLE
Screening test for coagulation	
1. Prothrombin time (PT)	Measures the time it takes for plasma to clot after initiation by the extrinsic pathway The sample is activated by the addition of complete thromboplastin, a mixture of tissue factor (TF), phospholipids and $CaCl_2$, to the plasma samples.
2. Activated partial thromboplastin time (aPTT)	Measures the time it takes plasma to clot when exposed to substances that activate the contact factors, which assesses the intrinsic and common pathways of coagulation T The sample is activated by the addition of a surface activator such as silica, kaolin or ellagic acid and a diluted phospholipid-enriched extract of thromboplastin lacking TF, historically referred to as partial thromboplastin.
3. INR	INR is a dimensionless number calculated as the ratio of Patient PT to a control PT, using the formula $A = \{\frac{Patient\ PT}{Control\ PT}\}^{ISI}$ *ISI* – International Sensitivity Index
Follow-up (Diagnostic) tests	
1. Thrombin Time (TT)	Measures the last step of coagulation, the conversion of fibrinogen to fibrin, is performed by incubating citrated plasma in the presence of dilute thrombin and measuring the time to clot formation.
2. Reptilase time (RT) and dRVVT	Similar to TT, reptilaste (venom from Bothrops snake) or Russell's viper venom (dRVVT) are used to activate clotting, respectively.
3. Factor assays	Chromogenic or antigen-based tests to diagnose specific coagulation factor deficiencies

As mentioned earlier, hemostasis has contributions from multiple blood components including platelets, coagulation factors and erythrocytes. Thus, an "ideal" hemostasis assay should preferably evaluate all the contributing parameters at relevant physiological conditions. Existing global hemostasis assays have advanced our understanding of this complex dynamical process beyond end point assays and are at the forefront of implementation in the clinic. However, none of them could measure all these processes and they all have their pros and cons. Table 1.3 lists a few of the commonly used techniques from a technical point of view, highlighting what they can and cannot measure

Table 1.3. Aspects of current hemostasis assays.

ASSAY	SAMPLE			PLATELETS		COAGULATION	CLOTTING	
	PPP	PRP	WB	Adhesion	Aggregation	Clotting Factors	Clt. Els.	Lysis
Mutiplate	X	✓	✓	X	✓	X	X	X
Verify Now	X	X	✓	X	✓	X	X	X
Platelet works	X	X	✓	X	✓	X	X	X
Impact – R	X	X	✓	✓	✓	X	X	X
PFA-100	X	X	✓	✓	✓	X	X	X
TT	✓	X	X	X	X	✓	X	X
aPPT	✓	X	X	X	X	✓	X	X
PT	✓	X	X	X	X	✓	X	X
Factor assays	✓	X	X	X	X	✓	X	X
ACT	X	X	✓	X	X	✓	X	X
TEG	(~)	(~)	✓	X	✓	✓	✓	✓
ROTEM	(~)	(~)	✓	X	✓	✓	✓	✓
SonoClot	(~)	(~)	✓	X	✓	✓	✓	✓

Notations: ✓, X and (~), denote yes, no, and may be, respectively. 'may be' denotes that it is possible in theory but not commonly used or advised by the inventors. Clt. Els abbreviates as Clot Elasticity

Among the available techniques, viscoelastic thromboelastography (TEG) and thromboelastometry (ROTEM) are the most commonly used assays because they allow for the analysis of several aspects of hemostasis if not all (Whiting and DiNardo, 2014). In recent years, they are increasingly being utilized for the diagnosis and treatment of patients at high risk of bleeding, including those undergoing surgeries or trauma (Gonzalez et al., 2016; Ramiz et al., 2019; Whiting and DiNardo, 2014). However, their results are heavily operator-dependent and prone to processing/sampling errors. More importantly, the mechanical force introduced by these assays can interfere with the natural clotting process.

Several new systems have been developed over the years working on different technologies such as magnetoelastic transducers (Puckett et al., 2005), piezoelectric quartz crystal (Müller et al., 2010), electrical impedimetric monitors (Lei et al., 2013), microfluidic disk analyzers (Lin et al., 2014), micro post arrays (Judith et al., 2015), microfluidics (Jain et al., 2016), microcantilevers (Li et al., 2016; Padovani et al., 2017), optical coherence elastography (Xu et al., 2019) and acoustic resonators (Chen et al., 2017; X. Chen et al., 2020). There are also some commercially available devices incorporating the conventional coagulation assays, such as electrochemical impedance-based devices i-STAT (Abbott) and CoaguChek XS (Roche Diagnostics) as well as optical-based CoaguChek S (Roche Diagnostics) and ProTime (ITC). They all have their pros and cons, and none of the currently available techniques assess all the functional components in the hemostasis process. For example, the endothelium component which plays a significant role *in vivo* hemostasis is missing in all existing assays. One should note that it is technically very challenging to incorporate all these physiological components in an analysis suitable for routine use, so a prudent trade-off is warranted. This dissertation presents

two new methodologies for blood hemostasis assessment driven by the motivation to address this complex problem.

1.5 SIGNIFICANCE AND APPLICATIONS OF HEMOSTASIS ASSAYS

Rapid, accurate, and clinical assessment of blood hemostasis is imperative in many clinical settings. Broadly, these tests are utilized for screening, diagnosis, and management of hemostatic disorders. This section lists out some of the common clinical applicability for these assays.

1.5.1 Preoperative evaluation of hemostasis

Nearly 48 million surgical procedures are performed each year in the U.S. (Wier et al., 2015). Considering the evolving nature of elective surgery, increased attention has been placed on pre-operative evaluation. Perhaps one of the most important tasks that fall to the consultative hematologist is the preoperative assessment of hemostasis to ensure the absence of any hemorrhagic risk factors in patients scheduled to undergo surgery. Aggressive anti-coagulant dosage for patients already on antithrombotic therapies often leads to unnecessary hemorrhage rather than preventing thrombosis (Koscielny et al., 2004). A risk assessment of bleeding versus thrombosis from hemostasis tests is necessary to ensure the best outcome.

1.5.2 Monitoring anticoagulation and antiplatelet therapy

Over 15 million people worldwide receive antithrombotic therapy to prevent and treat life-threatening thromboembolic events, such as deep venous thrombosis, pulmonary embolism, myocardial infarction and stroke (Ageno et al., 2012; Ahrens et al., 2010; Baron et al., 2013; A. Chen et al., 2020; Kirley et al., 2012; Matchar et al., 2000; Pengo et al., 2006; Seiffge et al., 2020; Wang et al., 2020). Because of the rapidly changing guidelines and individual patient

conditions such as drug resistance or response, the management of antithrombotic therapies is extremely challenging. Frequent laboratory testing of clotting status helps clinicians in making individualized treatment decisions

1.5.3 Blood transfusion management

Blood transfusion is one of the most commonly performed medical procedures (Gonzalez et al., 2016; Rugeri et al., 2007). Severe side-effects defects that occur during massive transfusion are related to preexisting hemostatic abnormalities and concomitant pathologic changes. Routine hemostatic analysis, including blood cellularity, platelet function and coagulation function is essential for the successful determination of appropriate transfusion products as well as management of post-transfusion bleeding.

1.5.4 Screening for pre-existing coagulopathies

Routine blood screening tests are performed when a hemostatic disorder is suspected due to prevailing symptoms or if the patient has a family history of bleeding disorders such as hemophilia (A, B) or von Willebrand (vWF disease) which are generally inherited (Lusher, 1996). Hemophilia A is the most common serious hemorrhagic disorder affecting around 1 in 5000 infants at birth, caused by Factor VIII deficiency. Hemophilia B is caused by a deficiency in factor IX and von Willebrand disease is a quantitative or qualitative deficiency of multimeric vWF protein (Nathwani and Tuddenham, 1992).

1.5.5 Management of extracorporeal blood circulation

An increasing number of patients worldwide are treated with the help of extracorporeal assist devices such as hemodialyzers, membrane oxygenation, mechanical circulatory support for various conditions (Sniecinski and Levy, 2015). They require precise and personalized

anticoagulation dose monitoring on a real-time basis to maintain hemostasis *in vivo*, and to prevent clotting in the blood transport lines and pumps *ex vivo*. Most concerning is the inability to manage anticoagulant dosage precisely which is a common cause of catastrophic hemorrhage and mortality in patients (Annich, 2015).

1.5.6 Management of cardiovascular diseases and other pathological conditions

Cardiovascular diseases (CVDs) are a group of heart and blood vessels disorders. They include Coronary heart disease – a disease of the blood vessels supplying the heart muscle; Cerebrovascular disease – a disease of the blood vessels supplying the brain; Peripheral arterial disease – a disease of blood vessels supplying the arms and legs; Rheumatic heart disease – damage to the heart muscle and heart valves from rheumatic fever, caused by streptococcal bacteria; Congenital heart disease – birth defects that affect the normal development and functioning of the heart caused by malformations of the heart structure from birth; and Deep vein thrombosis and pulmonary embolism – blood clots in the leg veins, which can dislodge and move to the heart and lungs. For the past 50 years and up-till now (2022), CVDs have been the leading cause of death worldwide, accounting for nearly 17.9 million deaths in 2019 (WHO Fact sheet). Hemostasis assays are being increasingly utilized for screening, diagnosis, and monitoring care for these conditions.

In addition, hemostatic abnormalities can also arise from numerous other pathological conditions such as cancer, which can cause a quantitative or a qualitative platelet defect (Kvolik et al., 2010), cirrhosis of the liver, HIV, leukemia, end-stage renal disease and many more (Levi and Opal, 2006). Even through the global pandemic caused by the Corona virus disease (COVID-19), the development of unusual thrombotic complications in more than one-third of

the patients is a serious concern (Lemke and Silverman, 2020). Additionally, some people have been shown to develop a rare hypercoagulable condition after vaccination for COVID-19.

To summarize, these underscore the dire need, importance, and extensive applicability of blood hemostasis assays. The global market for the hemostasis analyzer is currently around 3.8 billion (in 2020) and is projected to reach USD 5.0 billion by 2025 (Fig. 1.5), at a compound annual growth rate (CAGR) of 5.7% between 2020 and 2025 (*MarketsandMarkets* analysis report, June 2020). Furthermore, the increasing prevalence of cardiovascular diseases, blood disorders, and the rising geriatric population, in addition to the rising technological advancements, are predicted to boost the growth of this market in the coming years.

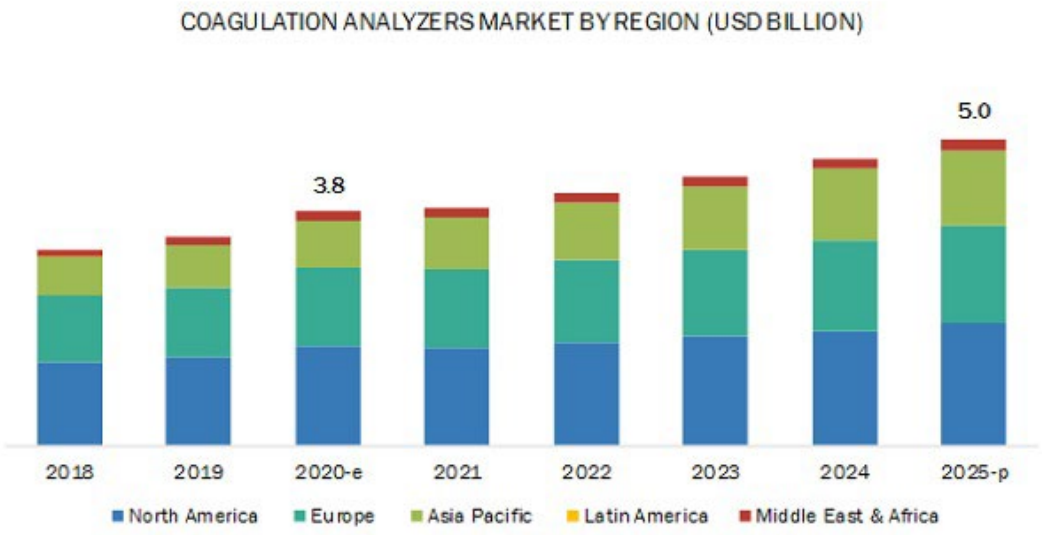

Fig. 1.5. Hemostasis analyzers market trend.

Markets and Markets analysis report June 2020

1.6 DISSERTATION OUTLINE

In summary, this dissertation describes the development of two new techniques for the evaluation of blood hemostasis. The design and fabrication of the sensor systems used for these assays and human blood sample testing results are presented in detail for each technique. Contributions and further ideas for scientific explorations are also presented. A brief synopsis of the chapters in this dissertation is described below.

Chapter 2 presents the development of a muti-stage platelet function assay using a nano thin-film capacitance sensor. The device was fabricated using standard top-down micro-fabrication techniques. A dual-chip design was introduced to reduce the system disposables. An extensive series of experiments using clinically relevant human plasma samples were conducted to demonstrate the sensitivity towards platelet count, platelet activation levels, and multiple activation pathways. A comparison study with a confocal microscope was conducted to gain further insights into the platelet F-actin dynamics after activation.

In Chapter 3, a whole blood-based hemostasis assay using a carbon nanotube capacitance sensor is presented. CPC sensors were fabricated using a bottom-up technique using a composite made of carbon nanotubes and cellulose fibers. The CPC sensor provided a simultaneous evaluation of coagulation function, platelets, and hematocrit. Whole blood-based hemostasis assessments were conducted to demonstrate the potential utility of the developed sensor for various hemostatic conditions including pathological conditions. Results showed good agreement when compared to a conventional thromboelastography.

Chapter 4 presents the development of an automated hematology analyzer using the CPC capacitance sensor. Rapid prototyping and custom-made control circuitry were used to manufacture the device. Open-source PYTHON-based algorithms were utilized for system control.

In the last chapter, a summary of the work and the key scientific contributions are provided. Future work is also discussed

Chapter 2. A COMPREHENSIVE EVALUATION OF PLATELET FUNCTION USING A NANO THIN-FILM CAPACITANCE SENSOR

2.1 ABSTRACT

Accurate and comprehensive assessment of platelet function is essential for managing patients who receive antiplatelet therapies or platelet transfusion either as a treatment for active bleeding or prophylactically. Platelets contribute to hemostasis by undergoing a sequence of highly regulated functional responses, including adhesion, spreading, granular secretion, aggregation, and cytoskeletal contraction. In contrast to the well elucidated molecular mechanisms leading to various delineated functional phases of platelet response, tests of platelet function have lagged. The majority of existing clinical assays only assess a certain stage of platelet function in clot formation, such as platelet adhesion or aggregation function in the presence of agonists such as thrombin, ADP, collagen, and arachidonic acid.

In this chapter, an innovative approach to evaluate platelets in multiple functional stages using a nano thin-film capacitance sensor is introduced. Platelet-Rich plasma-based platelet function evaluations were conducted to demonstrate the potential utility of the technique. Sensor responses to platelet adhesion and after activation showed excellent sensitivities towards platelet counts, platelet activation levels and platelet activation pathways. The sensor signal after platelet activation showed close similarities with the platelet F-actin reorganization observed using a fluorescence microscope. In comparison to the conventional optical-based evaluation system, the developed low-cost electrical-based sensing platform offers superior performance characteristics in assaying platelet function, such as high sensitivity, continuous multiparameter evaluation, label-free and easy-to-use. In summary, the nano-thin film capacitance sensor with the associated

testing protocol is a promising new technique for a comprehensive assessment of platelet function.

2.2 INTRODUCTION

Platelets are highly specialized discoid-shaped blood cells that play a central role in the hemostatic response (Frenette et al., 1995; Gale, 2011; George, 2000). Platelets are also the pivotal mediators of arterial thrombosis which is the leading cause of cardiovascular deaths worldwide (Jackson, 2011; Raskob et al., 2014; Wendelboe and Raskob, 2016). The prevention of acute arterial thrombosis has primarily focused on antiplatelet therapy rather than anticoagulation (Deepak L. Bhatt and Topol, 2003; McFadyen et al., 2018; Michelson, 2004; Orme et al., 2017; Yeung and Holinstat, 2012). Currently available antiplatelet drugs and various therapeutic strategies (such as Dual Antiplatelet Therapy - DAPT) have shown to offer substantial benefits in lowering the morbidity and mortality associated with acute thrombosis, however, there are significant incidences of hemorrhagic or other adverse clinical outcomes, and effective antiplatelet management in these patients remains challenging due to the increased risk of iatrogenic bleeding inherited with therapeutic antagonists, the inability to achieve antithrombotic potency while preserving hemostasis, and the large interpatient variability in responsiveness to treatments including drug resistances (Angiolillo, 2009; Fuentes and Palomo, 2014; Mackenzie et al., 2010; Mega and Simon, 2015; Miyazaki et al., 2017; White, 2011; Wiviott and Steg, 2015). On the other hand, platelet transfusions are widely used for managing patients with active bleeding, or for prophylactic transfusion in patients with thrombocytopenia or platelet dysfunction (Blumberg et al., 2010; Kaufman et al., 2015; Kumar et al., 2015). Together, these highlight the need for a comprehensive platelet function assay in several clinical settings.

As briefed in Section 1.1, in primary hemostasis the initial thrombus formation is largely mediated by platelets. They undergo a sequence of highly complex, regulated, and multi-stage functional changes including adhesion to the intimal matrix, intracellular calcium influx leading to platelet shape change, activation, granular secretion, aggregation, and cytoskeletal contraction (Michelson, 2019; van der Meijden and Heemskerk, 2019). The majority of existing clinical assays only assess certain stages of platelet function in clot formation, such as measuring platelet aggregation either in citrated platelet-rich plasma (c-PRP) by light transmission aggregometry or in citrated whole blood by impedance aggregometry; measuring platelet adherence and aggregation under various shear conditions by either Platelet Function Analyzer or Impact Cone and Plate(let) Analyzer; measuring the viscoelastic property of the clot during formation and fibrinolysis; measuring the secretion of granule contents and thromboxane metabolite production, and measuring the changes in membrane glycoproteins and surface expression of P-selectin and phosphatidylserine ex vivo and in vitro using flow cytometry to assess the state of platelet activation following the addition of various agonists (Collet and Montalescot, 2009; Orme et al., 2017). However, these single-stage-based approaches do not fully capture the complexity of platelets (Harrison, 2005; Pakala and Waksman, 2011). Therefore, each assay or technology has provided an incomplete assessment of platelet function in hemostasis and thrombosis (Harrison, 2009; Paniccia et al., 2015).

With the continuous development of nanotechnology, impedimetric or capacitive sensors with advantages like ultra-sensitivity, high selectivity, low cost, quick readout, improved system robustness, and simplicity, have been developed for various electro biochemical analyses (Chowdhury et al., 2019; Cui et al., 2020; Ertürk and Mattiasson, 2017; Luka et al., 2019;

Mahadhy et al., 2014; Prusty and Bhand, 2020; Zuo et al., 2019). A wide variety of bioassays including DNA hybridization (Mahadhy et al., 2014), antigen-antibody binding (Prusty and Bhand, 2020), detection and quantification of pathogens (Luka et al., 2019; Mattiasson and Hedström, 2016), and cell culture monitoring (Nabovati et al., 2019) have been realized using capacitance sensors. In this study, we present the development of a comprehensive multiparameter platelet function assessment using a nano thin-film capacitance sensor. A major improvement of the proposed approach is that it can evaluate the full spectrum of platelet function in clot formation using the reported microdevice. The capacitance sensor was designed as two microchips, a disposable top silicon chip containing a sample well for a citrated platelet-rich-plasma sample and a sensing electrode coated with Human Fibronectin to support platelet adhesion, and a reusable bottom silicon chip containing the reference electrode. The pattern and/or parameters in dynamic capacitance changes during clot formation, including platelet adhesion, activation and post-activation were continuously measured and were found to be sensitively associated with changes in platelet counts, levels of platelet activation, and platelet activation pathways. The feasibility and the possible clinical utility of this approach were demonstrated using clinically relevant human plasma samples. Finally, to gain further insights into the dynamics of signals changes during platelet activation, a comparative analysis was also conducted through live confocal fluorescence imaging.

2.3 Material and Methods

2.3.1 Nano thin-film sensor fabrication

The nano-thin film capacitance sensor was designed as two silicon chips (SiC) namely the Top (T-) and the Bottom (B-). Fig. 2.1a and b highlight the steps involved in fabricating the T-SiC and the B-SiC. Briefly, the SiCs were fabricated on 4-inch p-type silicon (Si) substrates

using standard photolithography, pattern etching and deposition processes. Si substrates with LPCVD silicon nitride (Si_3N_4, 500 nm) were purchased from Rogue Valley Microdevices, Medford, OR. For fabricating the T-SiC, a 15 μm layer of AZ 9260 photoresist (AZ electronic materials, NC, U.S.A.) was spin-coated (SUSS MicroTec LabSpin8) on the substrate, baked at 110 ^{0}C for 180 secs, then exposed to UV-light using a precision mask aligner (AB-M Semi-Auto aligner) and finally developed using AZ-400 K developer (AZ electronic materials, NC, U.S.A.). The Si_3N_4 layer was then patterned using Reactive Ion Etching (RIE Vision 320) to access the underlying substrate. Next, a Deep Reactive Ion Etch (DRIE SPTS Rapier Si) was used to etch the Si to get the desired cylindrical sample well with the circular Si_3N_4 membrane at the bottom.

To prevent etching the Si_3N_4 layer, dry etching was stopped a few cycles before the membrane and the remaining Si was removed using a highly selective Si wet-etch (KOH, 80 ^{0}C). The DRIE Si etch also partially separated the individual T-SiC. Next, 20 nm Cr and 150 nm Au layers were consecutively deposited with an e-beam evaporator (CHA SEC-600) using a shadow mask to fabricate the sensing electrode. At this stage, the T-SiCs in the wafer were held together by tiny silicon holders which were carefully punctured to release the individual chips. The fabrication steps for B-SiC (Fig. 2.1b) involved depositing Cr/Au (20/150 nm) on Si substrate using a shadow mask. Individual B-SiCs were separated using a DRIE Si etch similar to the T-SiCs. The SiCs had Au pads (2.5 x 1.5 cm) for electrical contacts.

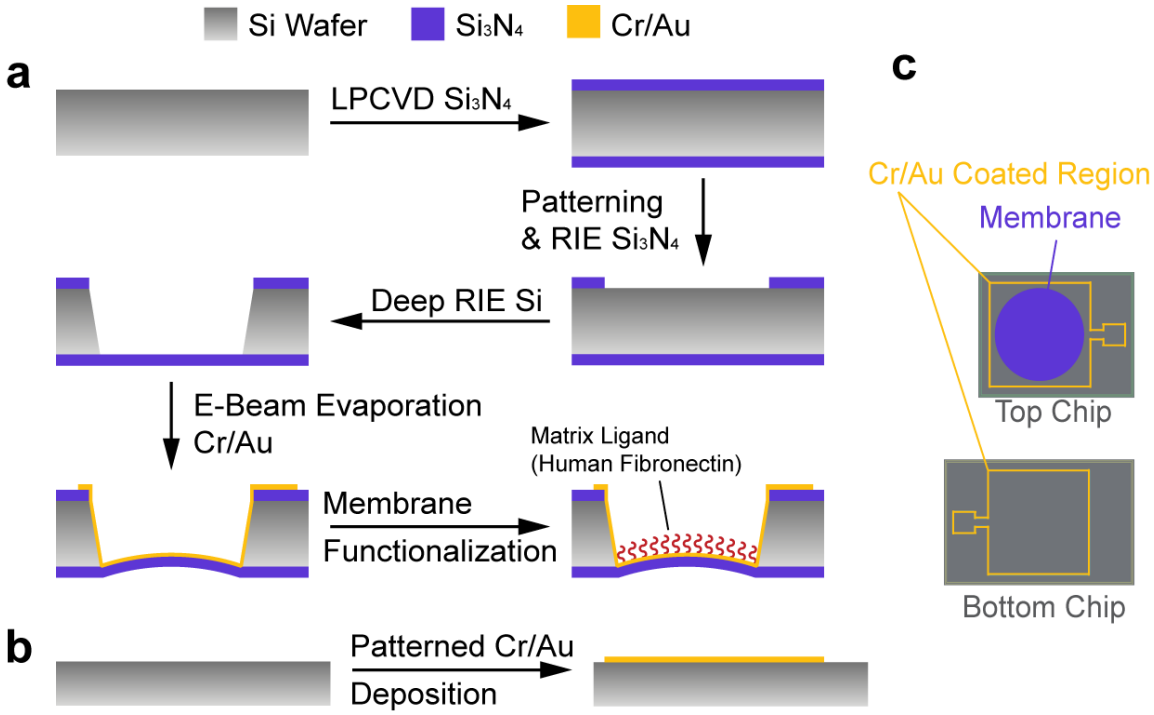

Fig. 2.1. Nano-thin film capacitance sensor fabrication.

Fabrication flow chart for Top silicon chip (a) and Bottom silicon chip (b), and assembly (c) to form a nano thin-film capacitance sensor.

2.3.2 Sensor biofunctionalization

Briefly, the sensing electrode in the T-SiC was coated with human fibronectin (FN; BD Biosciences, NJ, U.S.A.) to facilitate platelet adhesion. Before biomolecular coatings, the sensing electrode was first treated with oxygen plasma for 45 s at 100 W to clean the gold surface. Next, 1-Dodecanethiol (1 mM; Sigma-Aldrich, MO, U.S.A) in 200 proof ethanol (Sigma-Aldrich, MO, U.S.A) was added to the sample well and placed in a parafilm sealed container for 24 - 48 hours. The gold surface was then rinsed with DI water followed by 200-proof ethanol (3X) and allowed to dry at room temperature. FN solution (50 µg ml^{-1}) in phosphate buffered saline (PBS, pH 7.4; Sigma-Aldrich, MO, U.S.A) was prepared and added to the sample well and incubated at 37 ^{0}C for 2-8 hours. Finally, the device was carefully rinsed with PBS, dried, and transferred to fresh sterile containers before measurement. All experiments

were conducted within a day of FN coating. Thiol-coated sensors were stored at 2 - 8 ^{0}C to retain the composition and high quality of the molecular layer.

2.3.3 Capacitance measurement system

The experimental setup for capacitance measurements consists of the presented nano thin-film capacitance sensor, an LCR meter (Keithley EL 4980AL, OH, U.S.A), two micro-positioners (Signatone S-725 P (L/R) M, CA, U.S.A) with holders (Signatone SCA-50-4) and needle probes (SCAT5T-4 12.5 µm radius) for electrical contacts, 3D printed plastic fixtures and a laptop with data acquisition program (PYTHON), as shown in Fig. 2.2.

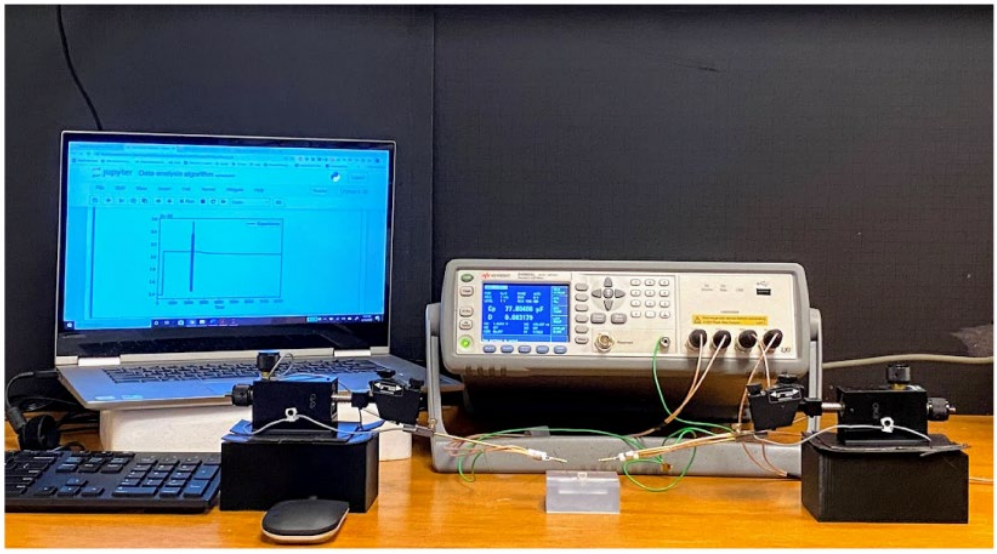

Fig. 2.2. Overall experimental setup for platelet function assay.

Keithley EL 4980AL meter was used for continuous capacitance measurements.

Table 2.4 lists the device setup, which was chosen to complement the best resolution range for the LCR meter and to obtain the most precise sensor capacitance readings.

Table 2.4. LCR Meter settings.

Parameters	Values
Cable Length	1 m
Signal Frequency	100 kHz
Voltage (V_{AC})	1 V
Temperature	25 ^{0}C
Correction	Open
Integration Time	0.129 sec

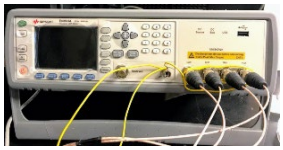

The nano thin-film sensor was connected to the LCR meter using needle probes in holders positioned using micro positioners. Plastic fixtures (Fig. 2.3) were used to provide an isolated testing environment, preventing any sample contamination during data acquisition. The plastic fixtures also minimized the variability in SiCs alignment between measurements. The bottom fixture had stoppers in *x-y* to precisely align the T-SiC over the B-SiC. The top fixture had a cylindrical opening for access to the sample well. A plastic lid was used to close this opening during measurements. A standalone laptop was used to remotely initialize and log the capacitance data. During measurements, the B-SiC was isolated from the bio-sample, therefore only the T-SiC was discarded after single data acquisition.

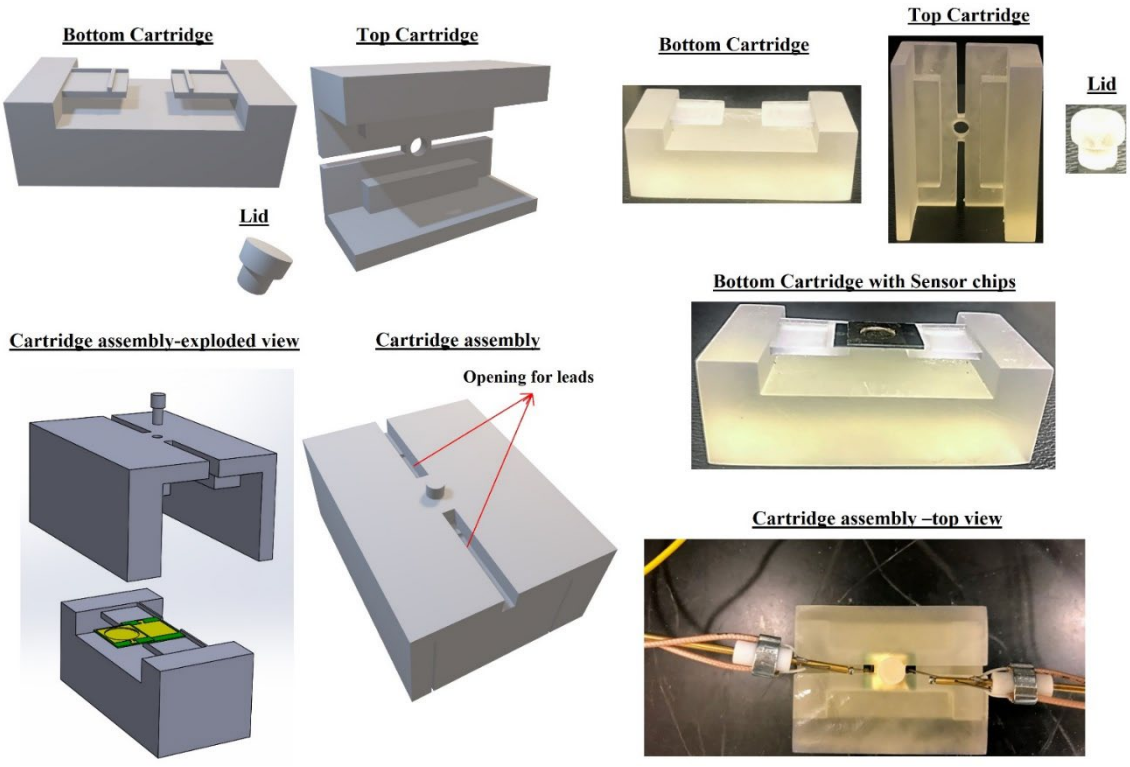

Fig. 2.3. Plastic cartridges for a dual-chip platelet sensor.

2.3.4 Platelet functional assay protocol

The schematic of the overall experimental protocol is shown in Fig. 2.4. For a multiparameter platelet functional assay using the presented sensor system, initially, the silicon chips are placed in the cartridge. A baseline capacitance was measured for 5 min. Then, 45 µL of citrated Platelet-Rich Plasma (c-PRP) was added to the sample well ([1]Add c-PRP), followed by a 30 min equilibration time for the platelets to attach to the FN coated sensing electrode ([2]Adhesion). Before stimulation, a washout procedure was conducted to remove any free-floating platelets in the medium ([3]Cell wash). For the washout procedure, 30 µL of the c-PRP was carefully removed and immediately replenished with Tyrode's buffer (Boston Bioproducts, U.S.A; Composition: 0 mM HEPES, 127 mM NaCl, 5.5 mM dextrose, 12 mM $NaHCO_3$, 0.5 mM NaH_2PO_4, 5 mM KCl and 1 mM $MgCl_2$ at pH 7.5). This step was repeated 5 times with a 20-sec

interval to ensure that after activation no additional platelets or microaggregates in the suspension land on the microthrombus or the sensing electrode. Platelets attached to the sensing electrode were activated by adding 10 µl of thrombin (Enzyme Research Laboratories, U.S.A) or adenosine 5'-diphosphate (ADP; Sigma Aldrich, U.S.A) solution at a specified concentration ([4]After activation). For the platelet count study, thrombin (3.5 U ml^{-1}) was used for activation and ADP (50 µM) was used to stimulate the platelets in the inhibitor studies. Measurement was conducted for an additional 80 min after stimulation. All measurements were conducted at room temperature (23 ^{0}C).

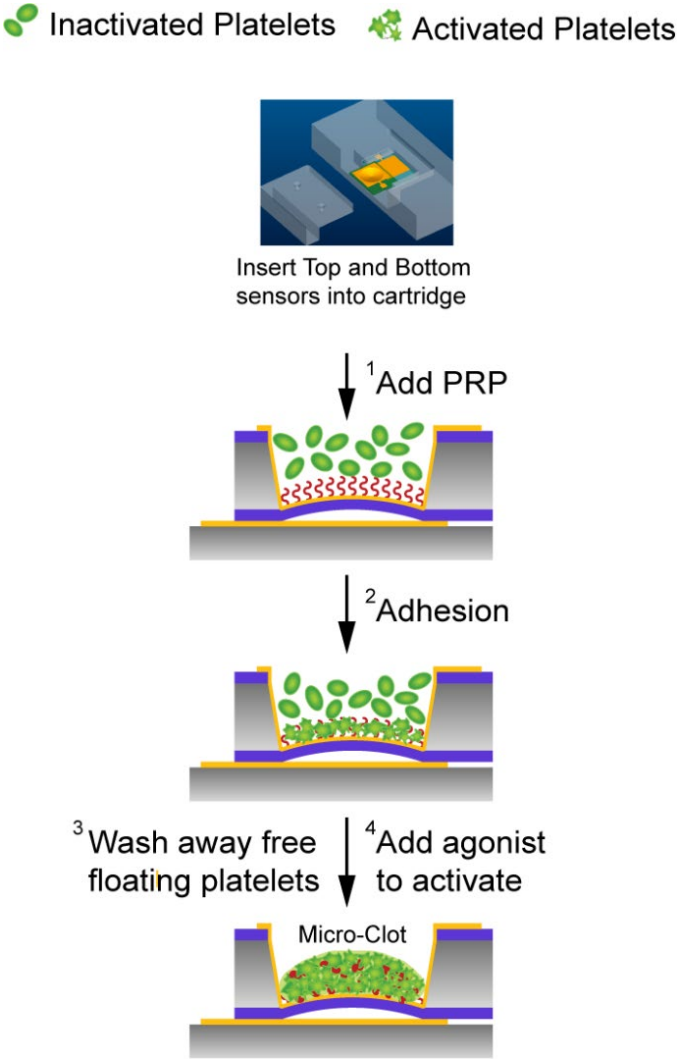

Fig. 2.4. Schematic of the platelet function assay using the sensor.

2.3.5 Analysis of capacitance signal markers for platelet function assessment

Sensor capacitance was measured at a sampling rate of 7 Hz. A representative overall capacitance signal for a platelet assay is shown in Fig. 2.5.

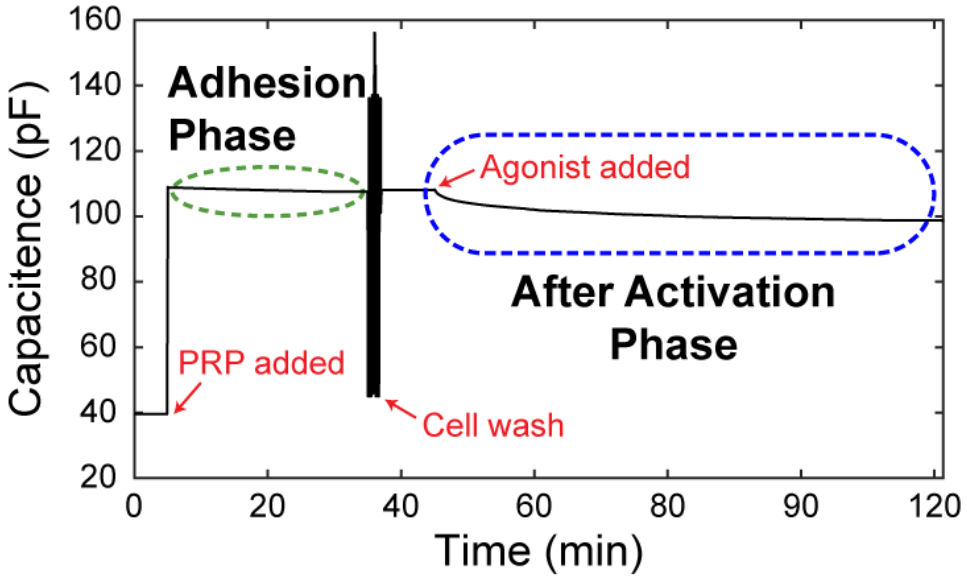

Fig. 2.5. A representative overall capacitance signal for a human plasma sample activated using human α-thrombin (3.5 U ml^{-1}).

From the measured overall capacitance two regions, namely the adhesion and activation phase (marked in Fig. 2.5) were chosen as they represent the specific functional stages of platelets. From the two regions of interest, three signal parameters, namely ΔC_{adh}, ΔC_{act} and S_{act}, were chosen for analysis as shown in Fig. 2.6.

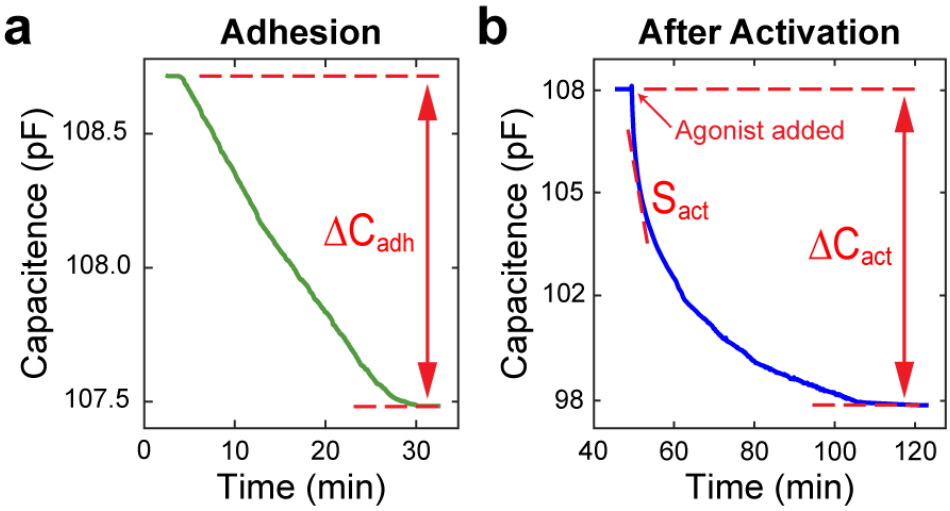

Fig. 2.6. Zoom-in view of the regions of interest in the sensor responses with the signal markers, ΔC_{adh},ΔC_{act} and S_{act} chosen for analysis.

ΔC_{adh} and ΔC_{act} was the maximum decrement in capacitance during the adhesion and after activation phases, respectively. S_{act} was the rate of change in capacitance after activation and was evaluated as an averaged slope between 200-250 sec after the addition of the agonist. An automated data analysis for convenient, accurate and objective determination of the signal markers was performed in PYTHON. This code is provided in Appendix Section A. In sensor capacitance graphs, the initial time ($t = 0$) was defined as the time point 20 sec after the addition of c-PRP for the adhesion phase and 20 sec after the addition of agonist for after the activation phase.

2.3.6 PRP samples

Under the protocol approved by the Human Subjects Division (HSD) at the University of Washington-Internal Review Board (UW-IRB), written informed consent was obtained from all volunteer subjects who participated in the study. All volunteers with no previously known platelet abnormality or clotting disorder and had not received any platelet medication including Non-Steroidal Anti-inflammatory Drugs (NSAIDs) in the two weeks before sample collection

participated in this study. Human whole blood was collected by a licensed phlebotomist at the University of Washington Medical Center Blood Draw Lab. The blood draw was performed using a 21G needle to standard 3.2% citrate tubes (Tiger Medical, NJ, U.S.A.) and the first ml was discarded to prevent tissue factor contamination. Blood tubes were transported in a styrofoam box at room temperature and used within 6 hours from the blood draw. PRP was obtained by centrifuging the whole blood at 200 *g* for 10 min and was carefully transferred to sterile tubes using a transfer pipette. Platelet count was performed using a hemocytometer and adjusted using Tyrode's buffer to 250 x 10^3 μl^{-1} for all experiments except for the platelet count study. For inhibitor studies, the c-PRP samples from healthy volunteers were incubated with the drug for 20 mins. Inhibition of cyclooxygenase (COX-1) was done by adding a predefined concentration (0, 0.1, 0.51 mM) of aspirin (Sigma-Aldrich, MO, U.S.A). $P2Y_{12}$ platelet receptor inhibition was achieved by adding ticagrelor (Sigma-Aldrich, MO, U.S.A) of desired concentrations (219, 785, 2800 ng/ml). Aspirin and ticagrelor solutions were prepared by dissolving the drug in dimethyl sulfoxide (DMSO; Sigma-Aldrich, MO, U.S.A) and diluting with Tyrode's buffer to the desired concentration before adding to the c-PRP samples. In the inhibitor studies, an appropriate amount of Tyrode's buffer was added to the control samples to maintain approximal cell counts and hemodilution as the drug-treated samples.

2.3.7 Fluorescence microscopy and image analysis

c-PRP samples were incubated with SiR-actin cytoskeleton probe (6 mM, Cytoskeleton, Inc., CO, U.S.A.) for 30 min at 37 ^{0}C to fluorescently label the platelet F-actin. SiR-actin is fluorogenic, cell-permeable and highly specific for F-actin (Lukinavičius et al., 2014). It stains the endogenous platelet F-actin without the need for genetic manipulation or overexpression. Glass coverslips used for imaging were coated with FN following a protocol similar to coating

the sensing electrode for capacitance measurements. For inhibitor studies, the samples were co-incubated with aspirin (0.51 mM) or ticagrelor (785 ng ml^{-1}) along with the fluorophore. The dynamic reorganization of platelet F-actin was visualized using an inverted confocal microscope (Leica SP5 confocal microscope) with a high magnification objective (63x oil). Z-section images at 0.29 µm increments were obtained every 10 min for 80 min. ADP (50 µM) was added 20 secs before the second stack (0 min time mark in the graphs). Image analysis was performed in Fiji using the maximum intensity projections of the Z-section images at each time point. Only isolated and fully spread platelets were chosen for analysis. At each timepoint, the spread area of the F-actin labeled platelets were measured using a canny edge detection algorithm. A representative stack with the trace is shown in Fig. 2.7. To quantify the F-actin reorganization, the fluorescence intensities of SiR-actin were analyzed within the individually traced area. A corrected total cell fluorescence (CTFC) was used for analysis to get an intensity value independent of the background signal. CTCF was calculated using the equation, *Integrated Density – (Area of the selected cell X background grey mean value).*

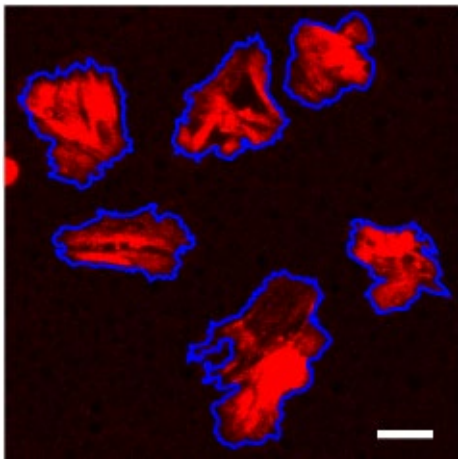

Fig. 2.7. A representative platelet spread area tracing using the canny edge detection algorithm.

Platelet f-actin was stained with a SiR probe. Blue trace output from the edge detection program accurately captures the shape of the platelets. Scale bar, 5µm.

2.3.8 Statistical analysis of data

To ensure excellent data repeatability and reliability, the sample size for measurements was predetermined to be five healthy donors to account for biological variability. For inhibitory studies, blood samples from healthy volunteers were divided into two portions and either incubated with inhibitors (aspirin or ticagrelor) or left untreated as a control. All of the data distributions were found to be normal (Shapiro–Wilk Goodness of Fit for normal distribution, $p > 0.05$) and were analyzed using parametric methods for statistical analysis. Analysis of variance (ANOVA) with Tukey's post-hoc was used to compare the results with three or more groups. * denotes a *p*-value less than 0.05 and was considered statistically significant. ** denotes a *p*-value less than 0.01 and NS denotes not significant. Data analyses were performed using GraphPad Prism 9 to guarantee high reliability.

2.4 RESULTS

2.4.1 Calibration and characterization of the capacitance-based platelet sensor

The nano thin-film sensor consists of two SiCs which were precisely aligned to form an electrical capacitor. A c-PRP sample was added to a sample well in the T-SiC. This dual-chip design minimized the disposables by eliminating the bio sample contact with the B-SiC making them reusable for measurements. The active sensing region was a Cr/Au coated Si_3N_4 membrane in the T-SiC, which was biofunctionalized with 50 µg ml^{-1} of FN to support cell attachment. The sensing electrode had a dome shape as a result of the residual stresses in the thin film from metallization (Fig. 2.8).

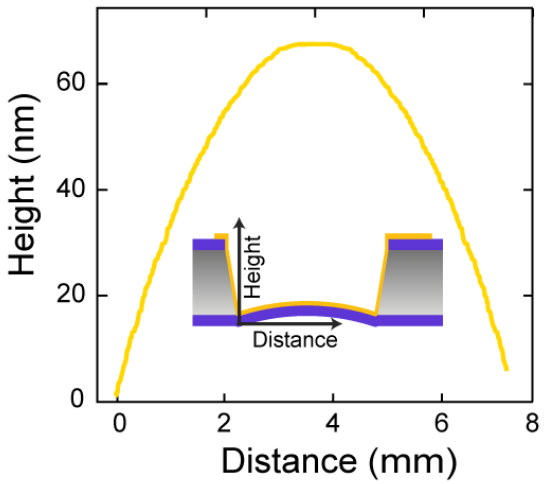

Fig. 2.8. The structural profile of sensing electrode.

Optical profilometry measurements show the upward bend shape from the residual stresses induced from sensor fabrication

Micro positioners with needle probes were used for electrical contacts to minimize system instability by avoiding repetitive solder junctions between the measurement system and individual microsensors. This design provided a capacitance signal with low noise in the order of 204 aF (*peak-to-peak*; Fig. 2.9).

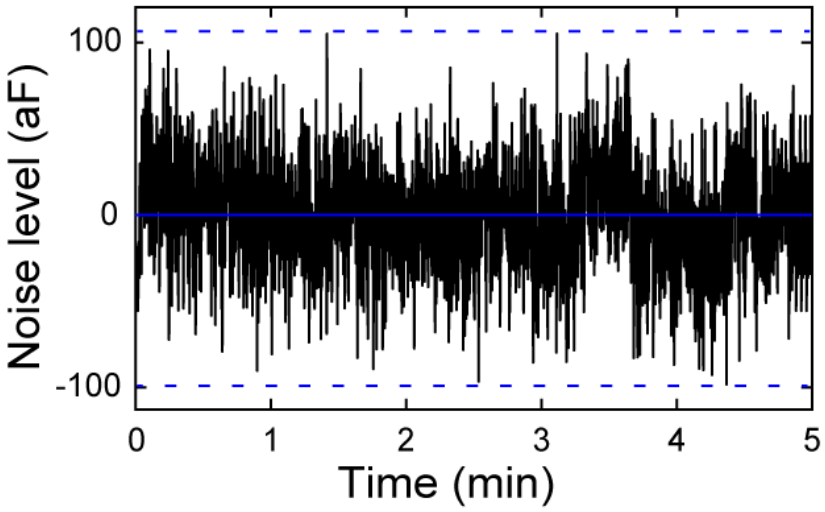

Fig. 2.9. A representative nano thin-film sensor noise level.

DI water in the sample well; peak-to-peak noise, 203 aF; and RMS noise, 32 aF.

Temperature perturbation in a DI water sample during capacitance measurement was observed to be less than 0.15^0 C (Fig. 2.10), therefore it was reasonable to believe that the electrical current through the sample did not significantly alter its thermal environment.

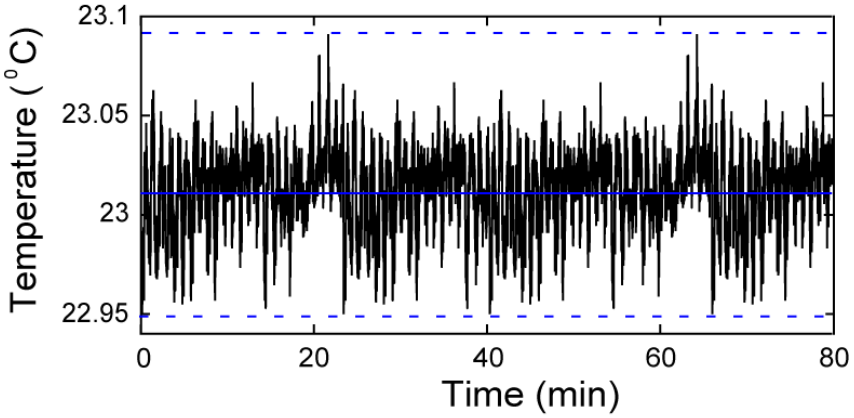

Fig. 2.10. A representative sample liquid temperature through the course of measurement.

Liquid temperature measurement shows that the electrical current did not induce thermal stress during measurement; peak-to-peak, 0.15 ^{0}C; and RMS 0.021 ^{0}C.

To evaluate the variability among different microfabricated devices, three randomly selected T-SiCs were tested for capacitance change (δC) from the addition of *NaCl* solutions (0 - DI water, 0.01, 0.1, 0.5, 1 M) to the sample well. As illustrated in Fig. 2.11a, the sensors exhibited excellent performance similarity in capacitance measurement with a maximum percentage difference of 3.6 %. Two-way ANOVA tests revealed that δC exhibited no statistically significant difference between the individual T-SiCs ($F(2,30) = 0.0365$, $p = 0.964$; two-way ANOVA), and a strong significant dependence with the molar concentration of *NaCl* ($F(4,30) = 298.7$, $p < 0.0001$; two-way ANOVA; Fig. 2.11b). Results also showed no significant differences among multiple trails for all the sensors ($F(2,12) \geq 0.0264$, $p \geq 0.963$; $n = 3$; one-way ANOVA). Overall, these results indicated that all the T-SiCs share a high resemblance in electrical performance characteristics.

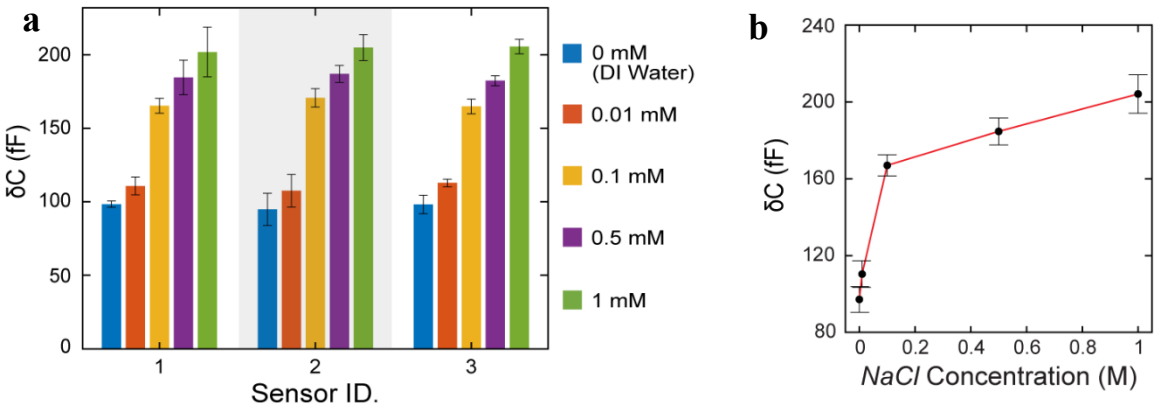

Fig. 2.11. Capacitance change (δC) from sample addition for different concentrations of *NaCl* for three randomly tested sensors.

(a) Sensors exhibit excellent repeatability (within trails) and similarities in capacitance change measurements. Data represented as Mean ± S.D. with three replicate measurements using each sensor. (b) Capacitance increases with increasing molar concentration of NaCl ((0, 0.01, 0.1, 0.5, 1 M). Electrical double-layer capacitance increases with increasing molar concentration of NaCl, and δC sensitively followed this increment. Data represented as Mean ± S.D. with 9 replicate measurements.

2.4.2 Sensor signal validation for platelet adhesion and activation

Sensor capacitance was measured continuously during the assay as shown in Fig. 2.5 and two regions of interest signifying the platelet attachment (Adhesion phase, green) and after activation (After activation phase, blue) were chosen for analyses. The analyses for the capacitance signal markers are described in detail in Section 2.3.5. For a c-PRP suspension with a predefined platelet count (250 x10^3 platelets μl^{-1}), it was found that the capacitance during the adhesion phase linearly decreased with increasing equilibration time and reached a steady-state value (Fig. 2.6a). To ensure that the signal was from cell adhesion to the underlying matrix ligand, experiments were conducted with an equivalent amount of Tyrode's buffer devoid of platelets following the same experimental procedure. Capacitance was stable for the suspension without

platelets with a *peak-to-peak* change of 0.318 fF (Fig. 2.12), which confirmed that the signals in Fig. 2.6a were caused by platelet adhesion to the FN-coated sensing electrode.

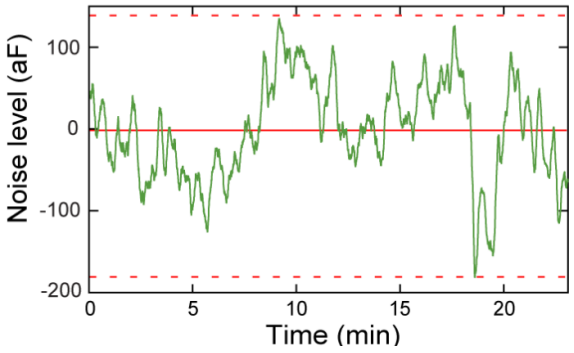

Fig. 2.12. Stability of the adhesion capacitance signal for a control sample devoid of platelets.

An equivalent volume of Tyrode's buffer devoid of platelets; peak-to-peak noise, 0.318 fF

When the attached platelets were activated using thrombin (final concentration: 3.5 U ml^{-1}), it was found that the sensor capacitance exponentially decreased to a steady-state value (Fig. 2.6b). For a sample without platelet activation (Thrombin addition), the capacitance signal was stable with a *peak-to-peak* change of 1.827 fF (Fig. 2.13) confirming the validity of the signals observed in Fig. 2.6b.

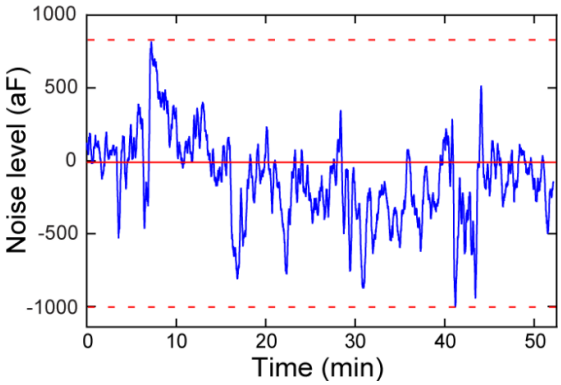

Fig. 2.13. Stability of the capacitance signal for a control sample without platelet stimulation.

Platelets attached to the sensing electrode without any agonist addition; peak-to-peak noise, 1.827 fF

From the two regions of interest, three signal markers namely ΔC_{adh} (Adhesion), ΔC_{act} and S_{act} (After activation) were chosen for analysis to quantify the hemostatic potential of the platelets for adhesion (ΔC_{adh}) and after activation (ΔC_{act}, S_{act}) respectively. Results from a parametric study to optimize the size of the sensing membrane (3, 5, 7, 10 mm), showed that a 7-mm circular membrane was sufficient to accommodate enough platelets for accurate analysis (Fig. 2.14a-c). Between the 7- and 10-mm membranes, the capacitance signal markers (ΔC_{adh}, ΔC_{act}, S_{act}) increased by increments that were not statistically significant (ΔC_{adh}: $p = 0.38$, ΔC_{act}: $p = 0.99$, S_{act}: $p = 0.99$; ANOVA post-hoc). Therefore, to minimize the sample volume required for the assay, a 7-mm design was chosen for all the studies.

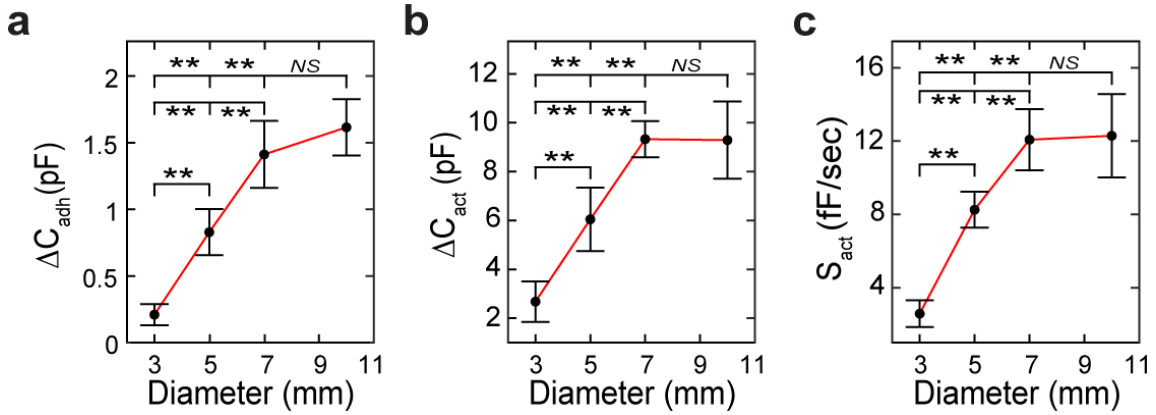

Fig. 2.14. Effects of sensing electrode diameter on the capacitance signal markers

Between 7- and 10-mm diameters, the signal marker increment was statistically insignificant (p-values were calculated from ANOVA)

2.4.3 Impact of platelet count and platelet function variations on the sensor response to platelet adhesion

To examine the ability of the sensor to evaluate platelet adhesion to an intimal matrix ligand, c-PRP samples from healthy volunteers were modulated for a predefined platelet count or platelet function. It was found that with decreasing platelet count (250, 100, 10 and 1 x 10^3 platelets μl^{-1}) the linear capacitance decrement from cell adhesion was strongly attenuated (Fig.

2.15a). The maximum drop in sensor capacitance increased with increasing cell seeding density (Fig. 2.15b), which indicated a correlation of ΔC_{adh} and platelet count ($F(3,16) = 46.23$, $p < 0.00001$; one-way ANOVA).

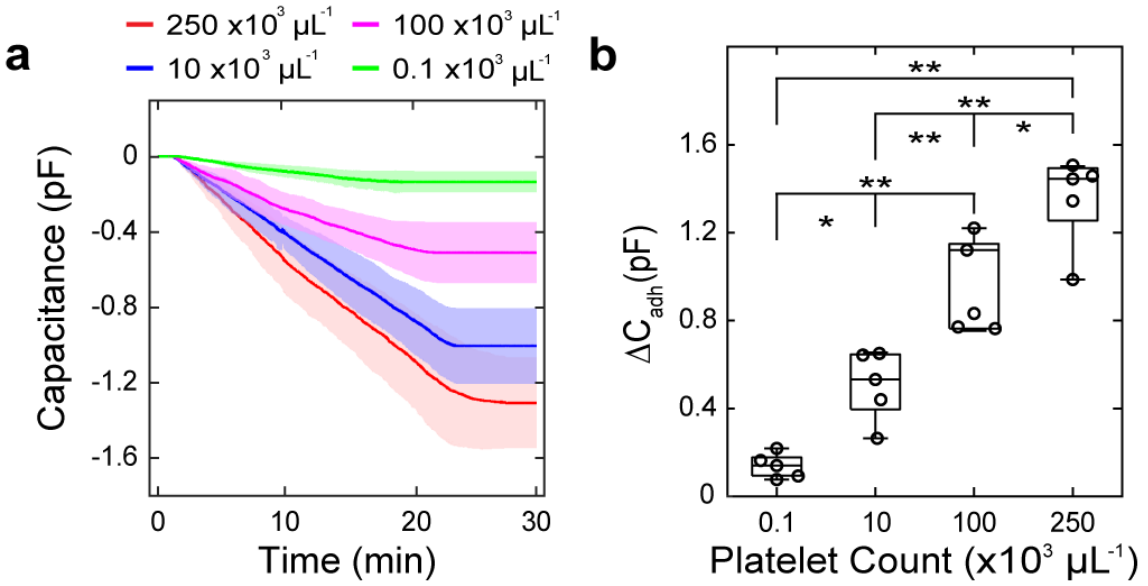

Fig. 2.15. Sensor responses to platelet adhesion are sensitive to platelet count.

(a) Dynamics of capacitance signal for plasma samples with varying platelet count. (b). ΔC_{adh} increases with increasing platelet count in the samples

Measurements using c-PRP samples incubated with aspirin (0, 0.1,0.51,1.3 mM) showed that a high dose (1.3 mM) of aspirin provided a smaller capacitance decrement relative to healthy samples (Fig. 2.16a). ΔC_{adh} for 1.3 mM aspirin was significantly lower compared to untreated samples ($p = 0.0095$, ANOVA post-hoc; Fig. 2d). No significant difference in ΔC_{adh} was observed for other aspirin doses ($p \geq 0.95$, ANOVA post-hoc; Fig. 2.16b). This finding implied that a higher dose of aspirin may have a direct effect on the platelet receptors for fibronectin (GP IIb/IIIa and GP Ic/IIa), in addition to the previously believed cyclooxygenase-1 (COX-1) inhibition for thromboxane (TxA_2) synthesis (Patrono, 1994; Vane and Botting, 2003). Similar observations such as reduced expression of GP IIb/IIIa receptor (McKenzie et al., 2003) and shedding of platelet receptors GPIbα and GPV upon incubation with aspirin (Aktas et al., 2005)

have been reported in earlier studies. Taken together, these observations shed light on the gaps in the current understanding of the mechanism of action of aspirin which is one of the widely used antiplatelet drugs.

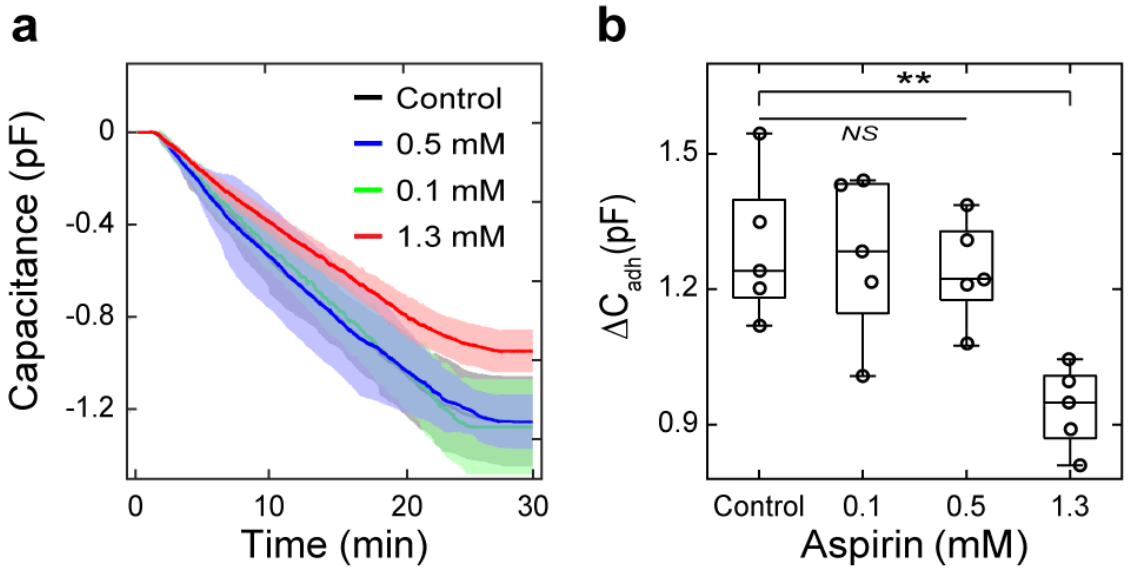

Fig. 2.16. High-dose (1.3mM) aspirin inhibits platelet adhesion (stickiness) to FN.

A high dose aspirin treatment (1.3 mM) showed a reduced capacitance decrement (a) and ΔC_{adh} (b)

Results from testing c-PRP samples incubated with a predefined concentration of ticagrelor (0, 219, 785, 2800 ng ml^{-1}) showed no significant differences in the sensor capacitance trend (Fig. 2.17a) and ΔC_{adh} ($F(3,16) = 0.675$, $p = 0.58$; one-way ANOVA; Fig. 2.17b) all doses.

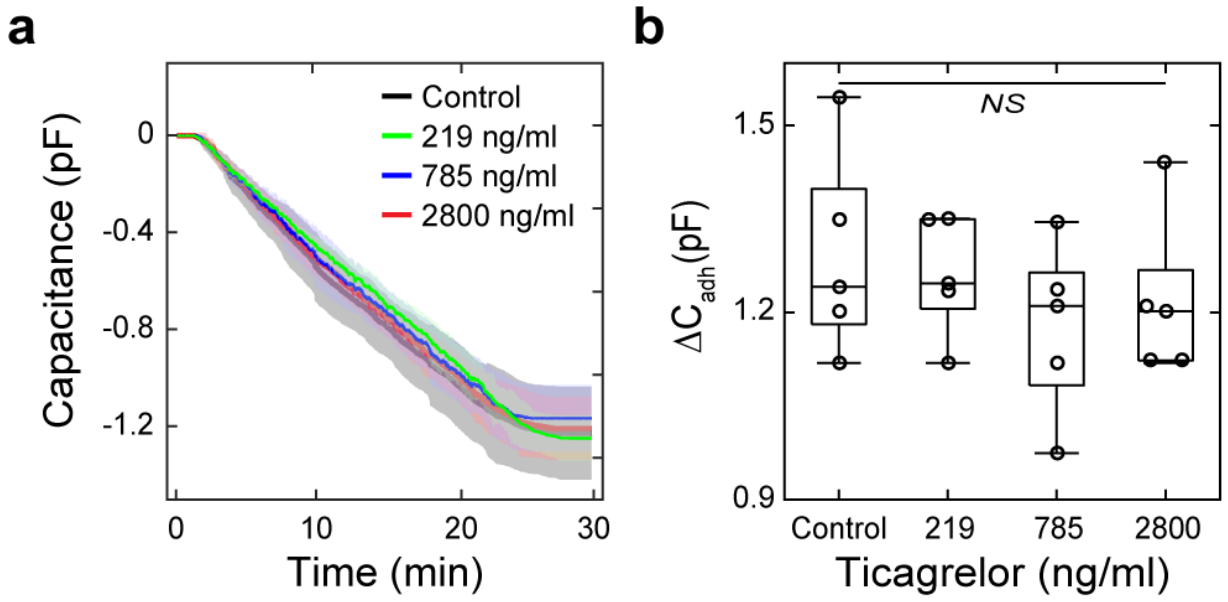

Fig. 2.17. Ticagrelor shows no significant impact on the adhesion ability of platelet for all doses.

No significant differences in capacitance decrement (a) and ΔC_{adh} (b), were observed from Ticagrelor incubation.

Overall, the above results show that the sensor responses to platelet adhesion were sensitive to variations in platelet count and platelet receptor function.

2.4.4 Capacitance signal after platelet stimulation is sensitive to activation levels

To ensure that attached platelets were under conditions of maximal activation for capacitance measurements, first the relationship between agonist (Thrombin and ADP) concentration and platelet activation levels was studied. The c-PRP samples were modulated to a platelet count close to 250 x 10^3 platelets μl^{-1} and stimulated with a predefined concentration of thrombin (0.1, 3.5, 10 U ml^{-1}) or ADP (5, 10, 15, 25, 50, 75 µM). Results showed that the exponential capacitance decrement after platelet activation increased with higher thrombin concentrations (Fig. 2.18a). This finding indicates that the sensor signal is sensitive to platelet activation levels. Statistical analyses revealed significant correlation between thrombin concentration and ΔC_{act}

($F(2,12) = 108.6$, $p < 0.00001$; one-way ANOVA; Fig. 2.18b), and with S_{act} ($F(2,12) = 16.07$, $p < 0.0001$; one-way ANOVA; Fig. 2.18c). For 3.5 and 10 U ml^{-1} thrombin concentrations, the ΔC_{act} and S_{act} increased by statistically insignificant increments ($p \geq 0.29$, ANOVA post-hoc). The similar capacitance response between the two concentrations suggests that thrombin had a saturating effect for concentrations at or higher than 3.5 U ml^{-1}, similar to previous observation (Liang et al., 2010).

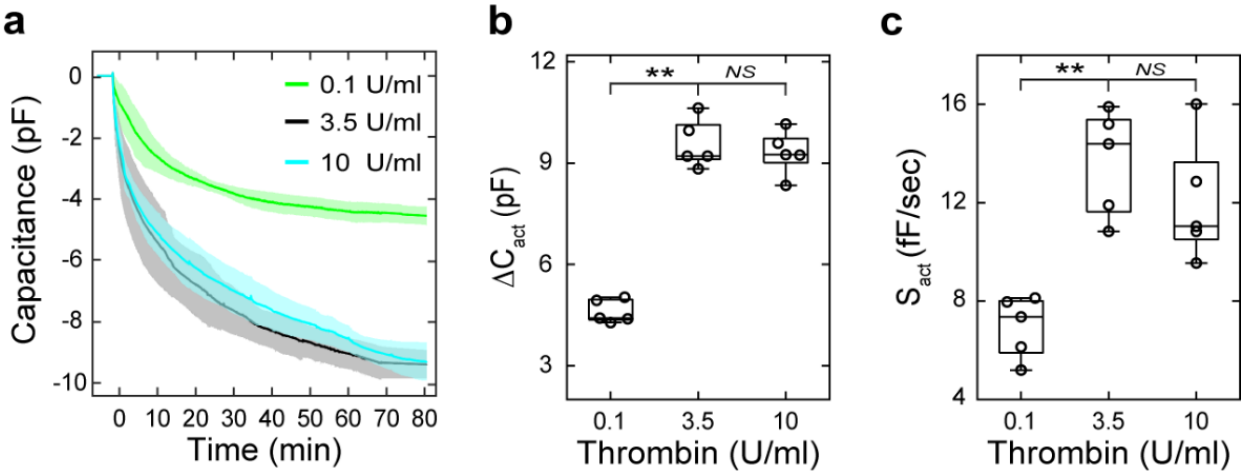

Fig. 2.18. Sensor responses after platelet activation are sensitive to activating thrombin concentration.

(a) Capacitance decrement increased with increasing concentration of thrombin (b) ΔC_{act} and (c) S_{act} showed a positive correlation with thrombin concentration. Between 3.5- and 10 U ml^{-1} of thrombin no significant differences were observed in the capacitance signal markers.

When platelets were activated using a predefined concentration of ADP (5, 10, 15, 25, 50 and 75 µM), two different sensor responses depending on the concentration levels were observed. For a lower ADP concentration (5, 10, 15 µM), a biphasic capacitance signal (Fig. 2.19a) containing primary and secondary curves with a distinctive point of inflection was observed. It is to note that the biphasic capacitance response was similar to the platelet aggregation curves obtained from Light Transmission Aggregometry (LTA) studies (Jin et al., 2002; Li et al., 2003).

The inflection point denoted the release of platelet granules which amplifies the aggregation of platelets in the medium producing a secondary curve (Lages and Weiss, 1980; Miller, 2009). The close similarity between the two signals suggests that the sensor measurement is sensitive to platelet aggregation and granular secretion. This also means that this device can potentially be used to monitor platelet dysfunction for aggregation and granular release (such as Storage Pool Disorder, Glanzmann's Thrombasthenia and Afibrinogenemia).

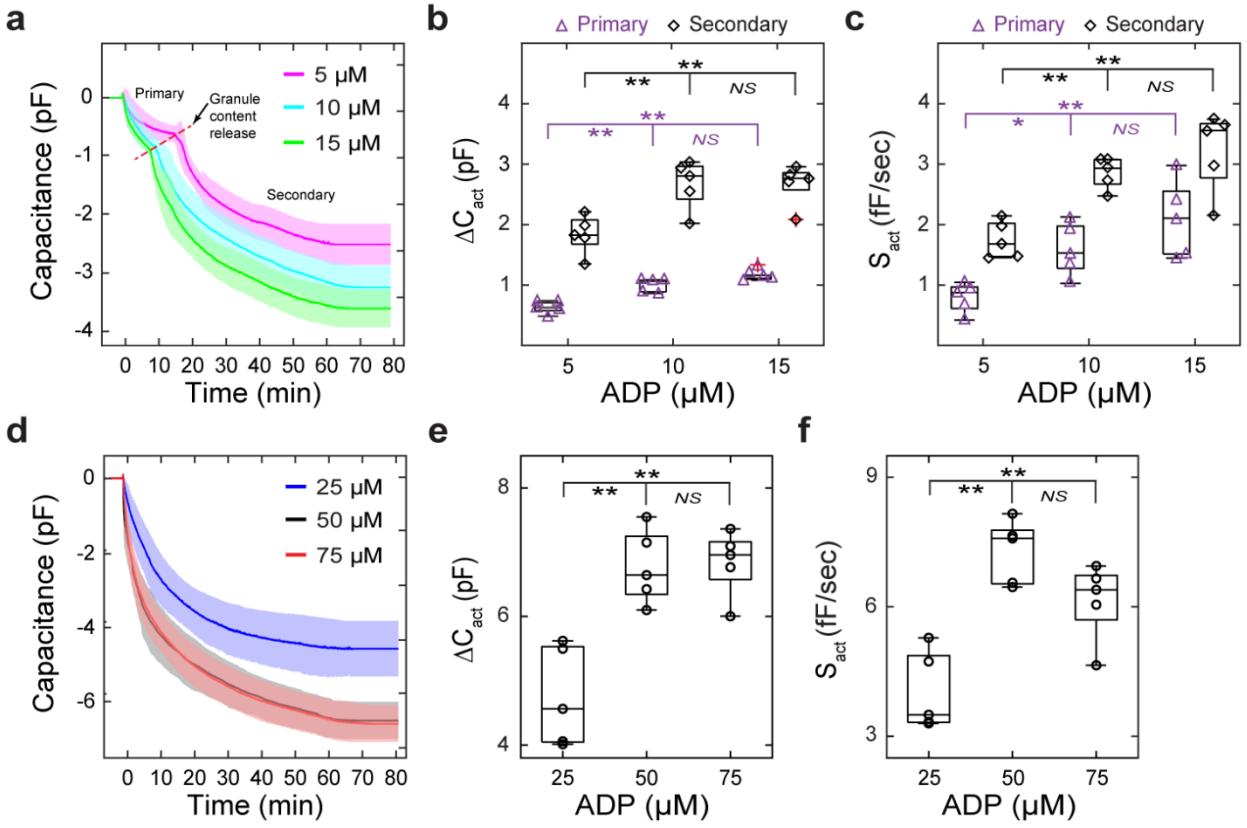

Fig. 2.19. Impact of ADP concentration on sensor signal after platelet activation.

(a) A biphasic capacitance signal trend was observed for lower ADP concentrations (b) ΔC_{act} and (c) S_{act} for both primary and secondary signal curves showed a positive correlation with ADP concentrations. (d,e,f) Medium and high dose ADP produced a monophasic response after platelet activation. A saturation in capacitance decrement and signal markers (ΔC_{act}, S_{act}) was observed at 50 μM ADP concentration.

Analyses on the sensor capacitance obtained from the low-dose ADP study revealed a significant trend between ADP concentration (5, 10, 15 µM) and ΔC_{act} (Primary (Δ): $F(2,12) = 14.52$, $p < 0.001$; Secondary (◊): $F(2,12) = 8.959$, $p = 0.0042$; one-way ANOVA; Fig. 2.19b), and with S_{act} (Primary (Δ): $F(2,12) = 16.20$, $p < 0.001$; Secondary (◊): $F(2,12) = 14.67$, $p < 0.001$, one-way ANOVA; Fig. 2.19c). No significant differences in the signal markers (ΔC_{act}, S_{act}) were observed between 10 and 15 µM ADP ($p \geq 0.15$; ANOVA post-hoc). ADP concentrations at or greater than 25 µM provided a monophasic capacitance decrement with platelet activation (Fig. 2.19d) similar to thrombin activated samples (Fig. 2.18a). Statistical analyses revealed significant trends between the ADP concentration (25, 50, 75 µM) and the signal markers (ΔC_{act}: $F(2,12) = 17.66$, $p < 0.001$; S_{act} : $F(2,12) = 15.58$, $p < 0.001$; one-way ANOVA; Fig. 2.19e-f). No significant difference in ΔC_{act} ($p = 0.98$; ANOVA post-hoc; Fig. 2.19e) and S_{act} ($p = 0.21$; ANOVA post-hoc; Fig. 2.19f) was observed between 50 and 75 µM ADP, which indicated that a 50 µM ADP may be the critical concentration required for maximal platelet activation.

2.4.5 Effects of platelet count and platelet inhibitors on sensor responses after maximal activation of platelets

To examine the effects of platelet count and platelet inhibitors on the sensor responses after platelet activation, the c-PRP samples from healthy volunteers were treated *in vitro* to modulate the platelet count or platelet function. Results showed that the exponential capacitance decrement after platelet stimulation increased with increasing platelet count (1, 10, 100 and 250 x 10^3 platelets μl^{-1}; Fig. 2.20a). The magnitude of capacitance decrement increased with increasing platelet count, which indicated a trend in ΔC_{act} and platelet count ($F(3,16) = 92.37$, $p < 0.00001$;

one-way ANOVA; Fig. 2.20b). Results also showed a similar increasing trend in S_{act} with increasing platelet count (F (3,16) = 43.62, $p < 0.00001$; one-way ANOVA; Fig. 2.20c).

Measurements using c-PRP samples incubated with aspirin (0, 0.1,0.51,1.3 mM), which inhibits TxA_2 formation, showed that the capacitance reduction decreased with increasing aspirin concentration (Fig. 2.20d). ΔC_{act} (F (3,16) = 123.0, $p < 0.00001$; one-way ANOVA; Fig. 2.20e) and S_{act} (F(3,16) = 90.71, $p < 0.00001$; one-way ANOVA; Fig. 2.20f) dose-dependently decreased with increasing concentration of the drug. Results from samples incubated with ticagrelor (0, 219, 785, 2800 ng ml^{-1}), which inhibits the $P2Y_{12}$ receptor for ADP activation also showed a similar dose-dependent attenuation in capacitance decrement (Fig. 2.20g), ΔC_{act} (F (3,16) = 187.6, $p < 0.00001$; one-way ANOVA; Fig. 2.20h) and S_{act} (F (3,16) = 104.1, $p <$ 0.00001; one-way ANOVA; Fig. 2.20i).

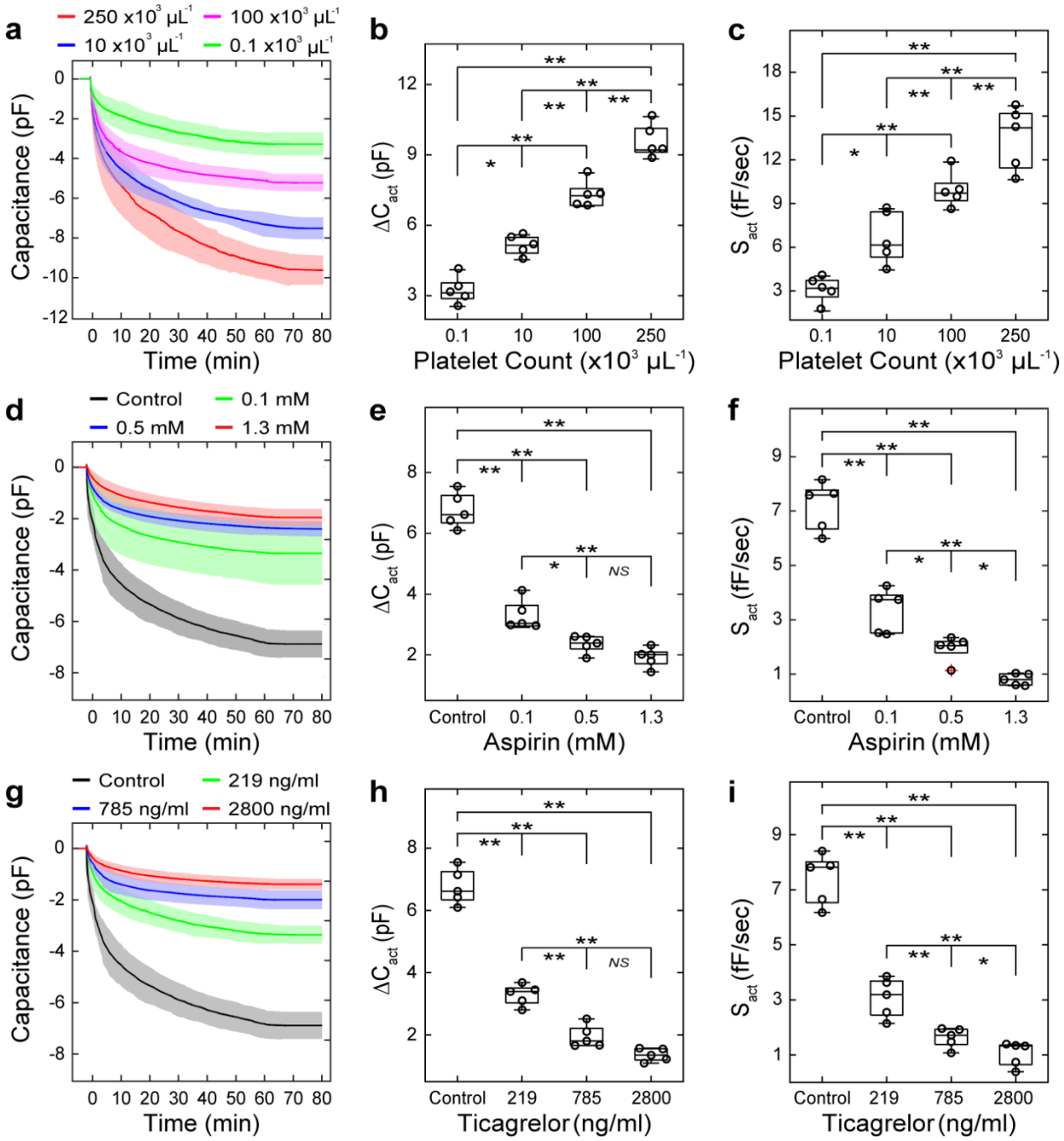

Fig. 2.20. Effects of platelet count and platelet inhibitors in sensor responses after activation.

(a) Capacitance decrement increased with platelet count in the plasma samples (b, c) ΔC_{act} and S_{act} showed a positive correlation with platelet count. (d -i) Sensor responses and the capacitance signal markers are sensitive to thromboxane TxA_2 and $P2Y_{12}$ signaling pathways. (f, i) Between the medium and high dose platelet inhibitors, a significant difference was observed only in S_{act}.

Together, the above results (Fig. 4) show that the sensor is sensitive to both platelet count and platelet activation pathways (TxA_2 and ADP signaling).

Between the medium (0.51 mM) and high (1.3 mM) dose aspirin data, a statistically significant difference was observed in S_{act} ($p = 0.038$; ANOVA post-hoc; Fig. 2.20f) but no significant difference was found in ΔC_{act} ($p = 0.43$; ANOVA post-hoc; Fig. 2.20e). Analyses on the signal markers obtained from the ticagrelor study also revealed a similar trend between the medium (785 ng ml^{-1}) and high (2800 ng ml^{-1}) dose of the drug (ΔC_{act} : $p = 0.13$; S_{act}: $p = 0.040$; ANOVA post-hoc; Fig. 2.20h-i). This finding implied that a higher concentration of inhibitors (Aspirin -1.3 mM; Ticagrelor - 2800 ng ml^{-1}) may have an immediate short-term functional inhibition in platelets, however, their cumulative long-term effect may be similar to a medium dose of the drug.

To examine the ability of the sensor to differentiate between different antiplatelet drugs, the signal markers obtained from aspirin and ticagrelor studies were compared (Fig. 2.21a-d). Analysis revealed a statistically significant difference in ΔC_{act} and S_{act} for low-medium (ΔC_{act} : $p \leq 0.016$; S_{act}: $p \leq 0.0015$; ANOVA post-hoc; Fig. 2.21a-d) and low-high (ΔC_{act} : $p < 0.0001$; S_{act}: $p < 0.0015$; ANOVA post-hoc; Fig. 2.21a-d) dose pairs of data. For a medium-high dose pair, a significant difference was observed only in S_{act} ($p \leq 0.042$; ANOVA post-hoc; Fig. 2.21c-d) but not in ΔC_{act} ($p \geq 0.12$; ANOVA post-hoc; Fig. 2.21a-b), similar to previous results (Fig. 2.20e-i). No significant differences in the signal markers were observed between aspirin and ticagrelor at the identical dosage levels (ΔC_{act} : $p \geq 0.17$; S_{act}: $p \geq 0.19$; ANOVA post-hoc), which suggests that both the drugs may have similar levels of inhibition on platelet function.

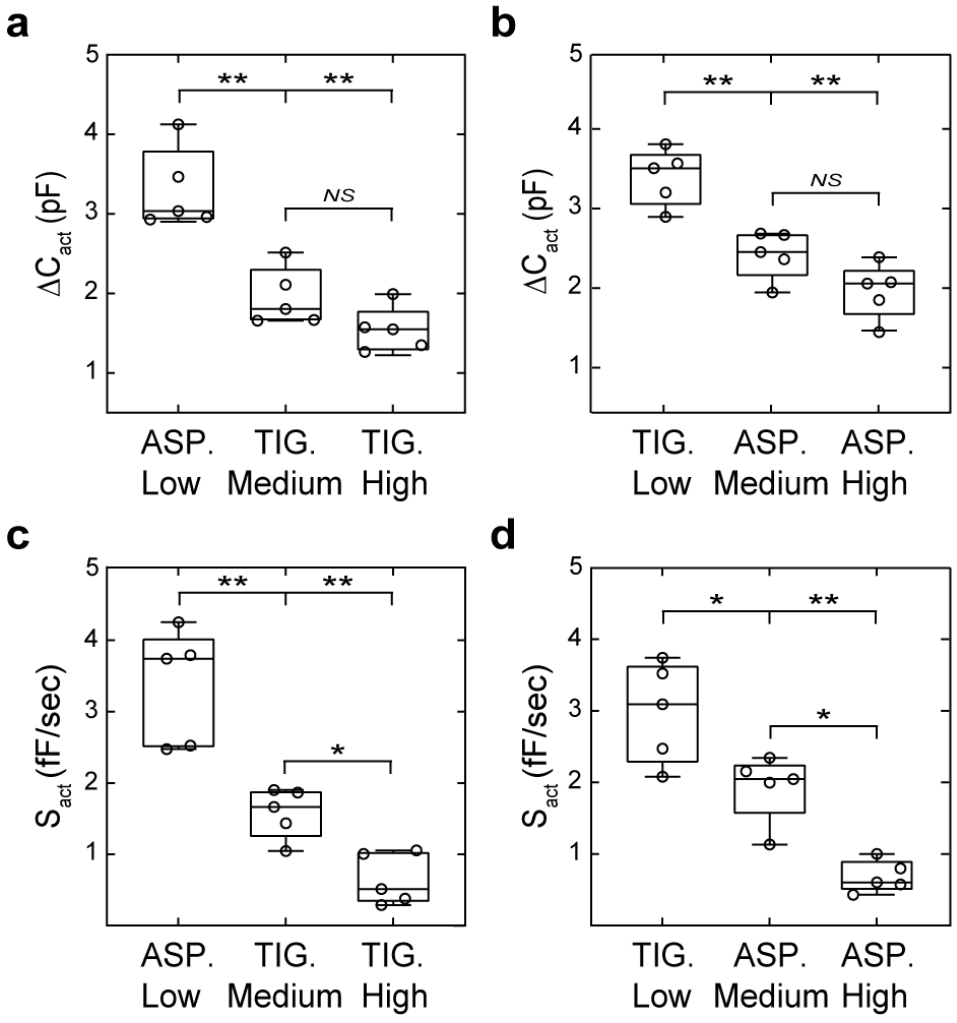

Fig. 2.21. Comparison between intra-drug dosage levels of Aspirin and Ticagrelor.

ASP and TiG refer to Aspirin and ticagrelor, respectively.

2.4.6 Platelet F-actin reorganization measurements using a confocal microscope

To gain further insights into the sensor responses after platelet activation, the development and reorganization of the platelet F-actin was visually observed using an inverted fluorescence microscope. This approach enabled live imaging of the dynamics of the actin cytoskeleton after stimulation for a duration similar to the capacitance measurements. As before, platelets were seeded on FN-coated substrates followed by a washout procedure to remove the free-floating platelets and activated using a 50 µM ADP concentration. Platelets were incubated with either

0.51 mM of aspirin or 785 ng ml^{-1} of ticagrelor or left untreated as a control. Before activation, the morphology of the completely spread platelets was spindle-like, circular, triangular, or polygonal and the stress-fiber-like actin structures formed filament bundles that traverse across the platelets (Fig. 2.22, Pre-Activation).

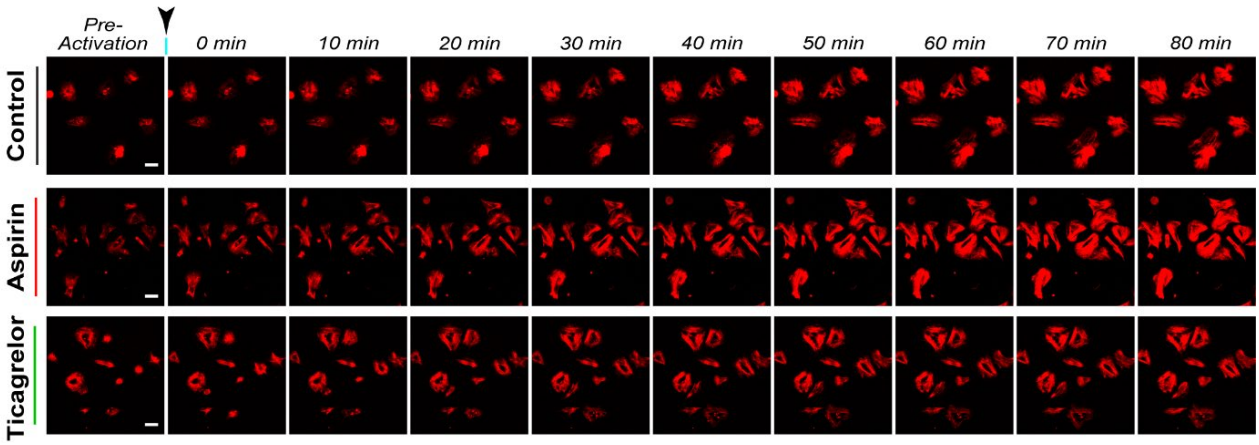

Fig. 2.22. Cytoskeletal reorganization of actin filaments in activated platelets.

From the obtained Z-stack images at each time point (Fig. 2.22), the actin spread areas and the fluorescent intensities within the area were chosen for analyses (described in detail in Section 2.3.7.) The platelet spread areas (Fig. 2.23a) and the fluorescent intensities of the epifluorescence channel (Fig. 2.23b) exponentially increased after ADP addition (cyan dotted lines with marker) and reached a steady-state value. Interestingly, there was a 10 min delay in the signal saturation for fluorescent intensities relative to the actin spread areas for all three conditions. This finding suggested that the actin structures dynamically reorganized even after reaching their final spread area, reaffirming the similar observation observed by another research group (Paknikar et al., 2019)

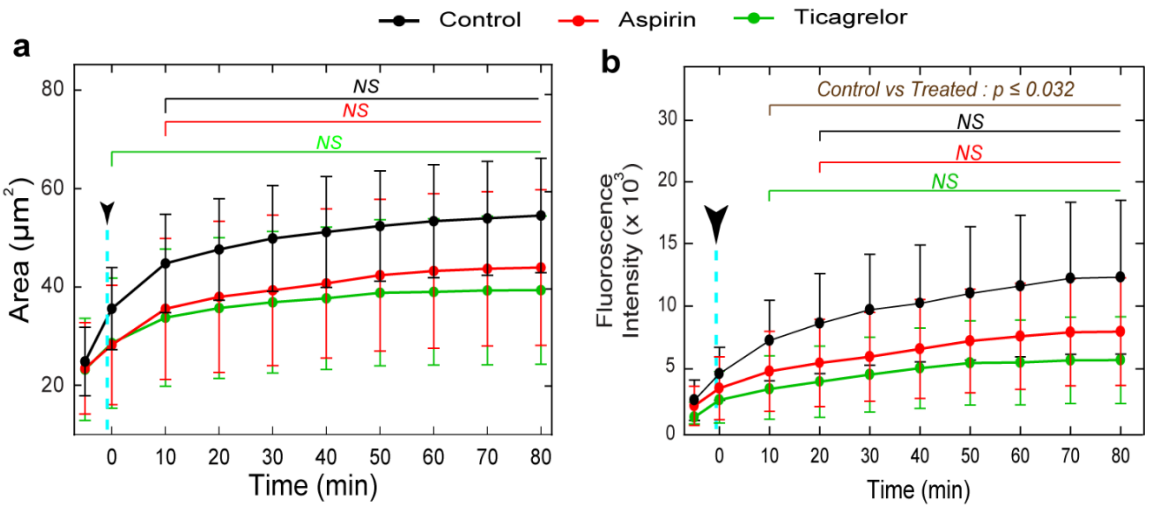

Fig. 2.23. Platelet spread areas and epifluorescence signal intensity increases with platelet stimulation.

Data represented as Mean ± S.D. for 30 individual platelets. Cyan dotted lines indicate the addition of 50 μM of ADP.

This dynamic F-actin reorganization after platelet stimulation should be the major factor affecting the signal responses after platelet activation. To examine this hypothesis, the continuous capacitance data was converted to discrete (5 min) points and compared with the fluorescent intensities obtained from the confocal study (Fig. 2.24). The timepoints for saturation in the capacitance values matched perfectly with the fluorescence intensities for all conditions. No statistically significant differences in fluorescence intensity ($p \geq 0.062$; ANOVA post-hoc; Fig. 2.23b) and discrete capacitance values ($p \geq 0.3444$; ANOVA post-hoc; Fig. 2.24) were observed between aspirin (0.51 mM) and ticagrelor (785 ng ml^{-1}) treated platelets. However, the capacitance signal for ticagrelor treated platelets saturated 10 min earlier than the aspirin-treated samples. A similar trend in signal saturation was also observed in the fluorescent intensities between the two conditions. These findings implied that aspirin and ticagrelor have different effective time courses of drug action on the platelet function response, even though they exert similar levels of inhibitory effects on platelets.

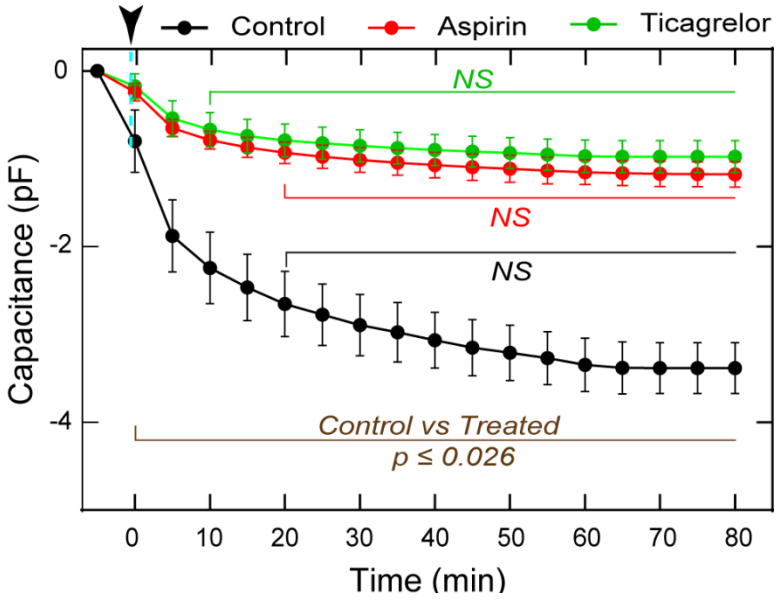

Fig. 2.24. Discretized capacitance signal for control, medium dose (0.51mM) aspirin and medium dose ticagrelor (785 ng ml^{-1}) conditions.

Data represented as Mean ± S.D. for 5 trails. Cyan dotted lines indicate the addition of 50 µM of ADP.

Furthermore, it is to note that the capacitance signal differentiated control and drug-treated conditions 10 min earlier than fluorescence intensity values (Control vs Drug-treated: Fluorescence intensity – $p \leq 0.032$ for $t \geq 10$ min, Capacitance – $p \leq 0.026$ for $t \geq 0$; ANOVA post-hoc). This result demonstrated the superior characteristics of the presented technique. It may be a quicker alternative to study the healthy and abnormal platelets, as it has better granularity (continuous) in system responses with additional advantages such as being devoid of eliminating phototoxic inhibition of the cells.

2.5 DISCUSSION

In physiological hemostasis, timely recruitment of platelets at the site of vascular injury is crucial to prevent bleeding. In this chapter, a new capacitance-based approach to evaluate platelet function in terms of adhesion and after activation in a single device was reported. The presented experimental protocol provides a relatively simple approach to eliminate the effects of fibrin formation and plasma clotting factors through a wash-out procedure, resulting in a measurement that was highly sensitive to several attributes on platelet function. The presented multiparameter approach may provide a more integrated assessment of platelet function by combining the aspects of adhesion, granular secretion, and aggregation, with a unique ability to detect platelet dysfunctions arising from many causes, in contrast to existing single parameter-based assays. Because the nano thin-film sensors share a remarkable resemblance in terms of electrical characteristics, the calibration and characterization process is greatly simplified by allowing the values obtained using a single sensor to be applied for an entire batch of mass-produced devices. Additionally, the dual-silicon chip design shielded the B-SiC from bio sample contamination making them reusable for multiple measurements.

From this study, a critical thrombin (3.5 U mL^{-1}) and ADP (50 μM) concentration for maximal platelet activation was obtained. This finding implied that physiologically elevated levels of these agonists do not necessarily lead to procoagulant platelet activity. Results also showed that thrombin caused an elevated activation response in platelets relative to ADP, reaffirming the higher potency of thrombin observed in previous studies (Davie and Kulman, 2006; D M Monroe et al., 2002).

A unique feature of the presented system is that it can provide a relatively simpler approach to studying the relationships between different physiological parameters and platelet function. For example, the ease in biofunctionalization of the sensor with matrix proteins (on the Cr/Au-Si_3N_4 membrane) makes this approach capable of assaying the effects of different matrix ligands for platelet adhesion and activation. In this study, the nano thin-film sensors were coated with FN (50 μg ml^{-1}) to support platelet adhesion and spreading. Because FN does not activate platelets, it is an appropriate intimal matrix to exclusively assay the thrombotic potential of platelets for pre- and post-activation phases of primary hemostasis (CHO and MOSHER, 2006; Ill et al., 1984; Pierschbacher and Ruoslahti, 1984). By stimulating the platelets attached to the sensor with different soluble agonists (such as collagen, TxA_2), it would be relatively straightforward to study their roles in the hemostatic response. In summary, this technique can serve as a new approach for studying platelet physiology and evaluating the impacts of different matrix ligands and agonists on the platelet hemostatic responses.

Arterial thrombi are typically rich in platelets (‘white’ clots) compared to venous clots (‘red’ clots due to trapped erythrocytes), hence the prevention for acute arterial thrombosis have primarily focused on antiplatelet therapies rather than anticoagulation (Jackson, 2011; Lippi and Favaloro, 2018). It was shown that the sensor system is sensitive to inhibition of TxA_2 generation (aspirin) and $P2Y_{12}$ receptor (ticagrelor), which are the predominantly focused platelet inhibitory pathways (Orme et al., 2017; Yeung and Holinstat, 2012). The results demonstrated that the sensor system could not only differentiate between normal and drug-treated samples but also show significant differences between the drug dosage levels (Fig. 2.20d-f). It was found that a high dose of aspirin (1.3 mM) and ticagrelor (2800 ng ml^{-1}) caused a short-

term inhibitory effect in the platelet functional response (i.e., S_{act}), but their cumulative long-term effect (i.e., ΔC_{act}) was similar to the medium dose of the drugs (Aspirin – 0.51 mM; Ticagrelor - 785 ng ml^{-1}). Another interesting finding in this work was that aspirin and ticagrelor had a distinctly different effective time course of drug action (Fig. 2.24), even though they wielded similar levels of antiplatelet effects. Finally, it was also found that a high dose (1.3 mM) of aspirin treatment inhibits the ability of platelets to attach to FN, which implied that aspirin could have a direct influence on the functionality of platelet receptors GP IIb/IIIa and GP Ic/IIa. Taken together, these results suggest that the presented sensor system can provide new in-depth insights into the antiplatelet effects of different inhibitors, in terms of receptor inhibition, immediate short-term (S_{act}) and cumulative long-term (ΔC_{act}) functional inhibition, and also the effective drug action time, which has not been possible previously. We believe that this comprehensive multiparameter evaluation of different platelet functions may provide better monitoring and compliance that are currently needed to guide antiplatelet therapies and to understand the effects of different antiplatelet drugs at different stages of the hemostatic response.

Additionally, some interesting insights into the dynamics of platelet cytoskeletal reorganization were also gained from this study. It is believed that the complete formation of the stress fiber-like actin structures may require more time compared to the initially platelet spreading phase, and it reaches a steady state when the maximum cytoskeletal contraction has occurred (Henriques et al., 2012; Lam et al., 2011). Results from the live microscopy studies showed that the actin filaments reorganized even after reaching their final spread area. However, a much more comprehensive study in the electro-chemical direction is required to fully understand this phenomenon.

Finally, the presented sensor system along with the standardized experimental and automated data analysis protocol is a promising new diagnostic device for a comprehensive evaluation of platelet function, encompassing multiple aspects of platelet function, in addition to serving as a potential tool for mechanistic studies in the field of experimental hematology and platelet physiology.

2.6 CONCLUSION

In conclusion, the presented nano thin-film capacitance sensor has enabled a comprehensive multiparameter assessment of platelet function in terms of the hemostatic ability for adhesion, aggregation, granular secretion, and cytoskeletal contraction. By conducting measurements using plasma samples modulated for a desired platelet count or function, and activated using varying concentrations of platelet agonists, it was shown that the sensor system is sensitive to platelet counts, platelet activation levels and multiple activation pathways. Capacitance responses after platelet activation showed an excellent correlation with the fluorescent intensity of stress-fiber-like F-actin filaments. Compared to a live imaging technique, this capacitance-based approach was rapid in differentiating between normal and drug-treated platelets.

The presented technique does have some limitations. From a hematological perspective, the assay does not evaluate the contributions from plasma clotting factors and other blood cells in hemostasis. Additionally, the sensor design is highly complex and expensive to fabricate making it not ideal for routine analysis in a clinical setting. An alternative sensor design could be a coplanar electrode setup instead of the parallel-plate configuration. This modification can reduce the microfabrication costs and also pave way for cheaper manufacturing alternatives like screen printing and ink jet printing.

Chapter 3. A SIMULTANEOUS MULTIPARAMETER ASSESSMENT OF WHOLE BLOOD HEMOSTASIS USING A CARBON-NANOTUBE-PAPER COMPOSITE CAPACITANCE SENSOR

3.1 ABSTRACT

In Chapter 2, a nano-thin film capacitance sensor was developed and applied for the evaluation of platelet function in hemostasis. However, *in vivo* hemostasis encompasses an ensemble of interactions between the cellular (platelets, erythrocytes) and non-cellular (coagulation factors) blood components. Therefore, for an accurate and clinically relevant hemostasis evaluation, a simultaneous assessment of multiple clotting elements is required. The majority of the existing assays also have this limitation as shown in Table 1.3.

In this chapter, a new approach to simultaneously evaluate coagulation function, platelet function or count, and hematocrit using a carbon nanotube-paper composite (CPC) capacitance sensor is presented. The CPC capacitance response to blood clotting at 1.3 MHz provided three sensing parameters with distinctive sensitivities towards key physiological clotting elements. Whole blood-based hemostasis assessments were conducted to demonstrate the potential utility of the technique for various hemostatic conditions, including pathological conditions, such as hemophilia and thrombocytopenia. Results showed good agreement when compared to a conventional thromboelastography analyzer. In summary, the CPC capacitance sensor system is a promising new biomedical device for convenient whole-blood-based wide-ranging hemostasis evaluation.

3.2 INTRODUCTION

Rapid and accurate assessment of hemostatic parameters is imperative in various clinical settings to diagnose, treat, and monitor patients with impaired hemostasis (Levy et al., 2010; Mallett and Armstrong, 2015; Tynngård et al., 2015). Traditional laboratory-based clotting assays and devices are not only time-consuming and expensive but also provide insufficient information due to a partial analysis of various individual facetted clotting elements, such as coagulation function (activated partial thromboplastin time - aPTT, prothrombin time - PT, thrombin time - TT), fibrinogen, platelet function (platelet functional analyzer and aggregometry) or blood cellularity (hematology analyzers). Evolving whole blood-based viscoelastic assays such as thromboelastography (TEG) also lack sensitivity and specificity to platelet counts and platelet dysfunction, and can often provide an inaccurate assessment of hemostatic status in the settings of abnormal hematocrit (Bolliger et al., 2012; Ranucci and Baryshnikova, 2020; Spiezia et al., 2008). As a result, each current assay or testing technology has provided an incomplete assessment of bleeding and thrombosis status and risks (Chee and Greaves, 2003; Ganter and Hofer, 2008). This has also stymied the fields of clinical and experimental hematology given the interdependence among the clotting elements.

Over the years, electrical permittivity sensors have been extensively developed to characterize various blood physiological properties that are of relevance for numerous medical applications including hemostasis (Chiba et al., 2015; Hayashi et al., 2010, 2008; Heileman et al., 2013; Pethig, 1984; Ur, 1970). The permittivity change of whole blood in the MHz range was from the accumulation of charge carriers at the interface between erythrocyte membrane and its cytoplasm (Chelidze, 2002), and this was found to change significantly during cellular

aggregation, formation of fibrin mesh networks encapsulating the aggregates and retraction of the clot from the contractile force exerted by activated platelets (Asami and Sekine, 2007; Hayashi et al., 2008). So far, two systems that measure blood permittivity using an impedance technique have demonstrated a good sensitivity to both coagulation and platelet function (Hayashi et al., 2015; D. Maji et al., 2018). One study has reported an independent evaluation of hematocrit level without clotting (Hayashi et al., 2017). These studies confirmed that measuring blood permittivity can provide a sensitive analysis of both cellular and non-cellular blood components that play a key role in hemostasis. However, these impedance-based devices were not able to offer concurrent information on all the key clotting elements from a single assay, and also have limitations in being translated into clinical practice. The physical electrical contact with the blood samples irreversibly contaminates the sensing surface from corrosive elements in the blood (such as proteins and ions). Also, these single-use disposable sensors require precious metal (such as Au or Pt) electrodes to reduce oxidation and electrostatic contamination, coupled with a highly specialized impedance analyzer, making them expensive to use in clinical settings. Moreover, physical electrical contact can also interfere with the natural progression of the clotting process in the blood samples. Addressing the challenges in electrical sensor resolution and sensitivity can lead to insights into key components of hemostasis that arise from studying blood permittivity.

This chapter presents the development of a capacitance-based approach for blood permittivity measurement using a carbon nanotube-paper composite (CPC) capacitance sensor. Sensors were fabricated adapting previously reported techniques (Dichiara et al., 2017; Zhang et al., 2021). A major progression of the proposed approach is that the capacitance signal obtained

from a single measurement could provide three parameters with distinctive sensitivity towards coagulation function, platelet count or function, and hematocrit. The CPC sensor exhibited a high fringing field to detect permittivity changes in a blood sample placed in a glass vial on top of the sensor, eliminating the need for physical electrical contact. The feasibility and sensitivity of this approach were demonstrated using clinically relevant human blood samples. The results were compared against a conventional TEG analyzer to validate the effectiveness of the sensor. To demonstrate potential clinical usefulness, the reduced hemostatic ability, in terms of coagulation function, platelets and hematocrit were evaluated for hemophilia and thrombocytopenia conditions.

3.3 Material and Methods

3.3.1 CPC capacitance sensor fabrication

Carbon nanotube-paper composite (CPC) film made of multiwall carbon nanotubes (MWCNTs) and cellulose fibers was prepared and fabricated as a capacitance sensor using previously reported techniques (Dichiara et al., 2017; Zhang et al., 2021). Briefly, bleached softwood pulp pre-adsorbed with cationic polyacrylamide (CPAM, Percol 3035) (BASF, RP, DE) was mixed with a dispersion of sodium dodecyl sulfate (Sigma Aldrich, MO, U.S.A.) and MWCNTs (Cheap Tubes Inc., VT, U.S.A.). The resulting aqueous suspension was subsequently filtered, pressed, and dried to form electrically conductive sheets of 60 g m^{-2} containing 10% (w/w)-MWCNTs. The sheets were cut into 5 mm wide strips with 20 mm in length. Silver epoxy (MG Chemicals, BC, CA) was patterned at both ends to provide electrical contact. The SEM images of the CPC surface confirmed that the cellulose fibers were uniformly coated with the MWCNTs (Fig. 3.1).

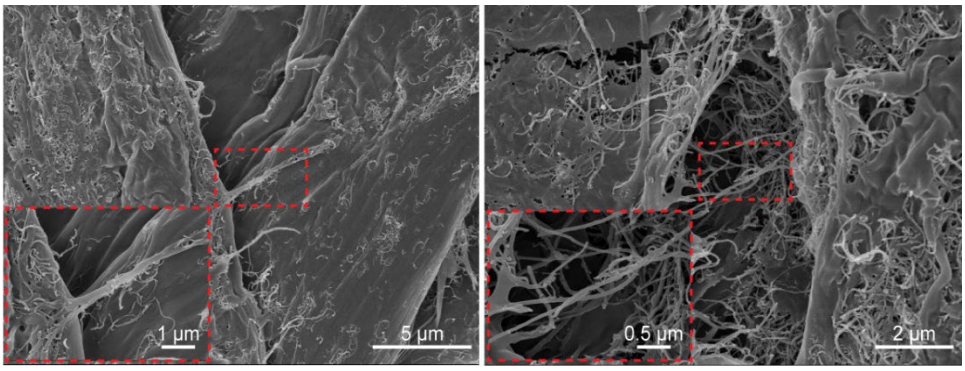

Fig. 3.1. Representative SEM images of the carbon nanotube paper-composite.

Images of the CPC surface showed that the cellulose fibers were uniformly coated with the MWCNTs.

Controlled water printing and stretching techniques were used to fabricate the CPC capacitance sensors with a V-shaped crack. V-shaped crack demonstrated higher sensitivity in comparison to a straight-line crack (Zhang et al., 2021) due to a larger surface area (approximately 1.4 times). Water was printed on the CPC specimens using a noncontact liquid bridge printing method (Kahng et al., 2018). Then stretching was applied using a tensile test stage to fabricate the sensor electrodes with a gap of 1 mm. The average capacitance for six sensors from the same batch was found to be 314 ± 12 fF (3.8 %; CV). A randomly selected pair of sensors were used for all measurements. Standard cold soldering through copper plates was utilized for external wiring. The fractured CPC was coated with polyurethane and vacuum-sealed on cover glass (0.17 mm thickness, Thermo Scientific, MA, U.S.A). A polyester film was used to protect the sensor from oxidation and environmental exposure. Fig. 3.2 shows the schematic and the real-time photograph of the CPC sensor.

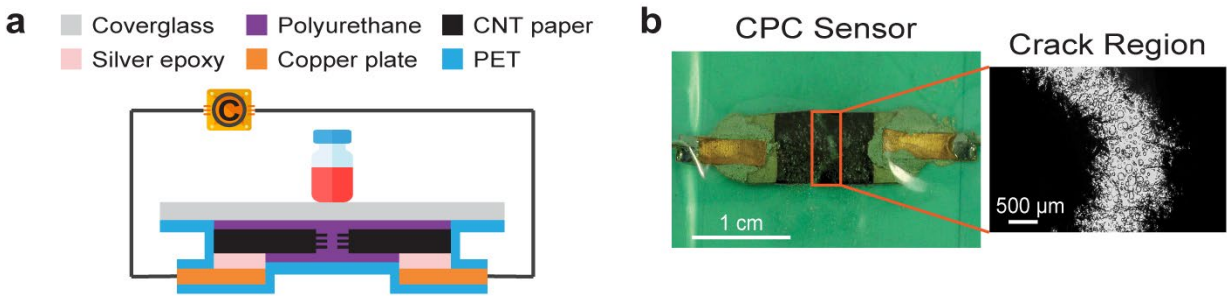

Fig. 3.2. (a) Schematic of the Carbon nanotube-Paper Composite (CPC) capacitance sensor (Not drawn to scale). (b) CPC Sensor: Photograph of a CPC capacitive sensor. Crack region: Zoom-in view of the crack region (4X).

Human whole blood in a glass vial is placed on top of the sensor. The cover glass is supported at the ends through plastic fixtures to avoid stress from sample weight on the carbon nanotube coated cellulose fibers. Near the crack, region untangled cellulose fibers formed numerous conductive cantilevers exhibiting high fringing field for capacitance measurements

3.3.2 Capacitance measuring system

The experimental setup used for capacitance measurement consists of two CPC capacitance sensors, FDC 2214 capacitance evaluation module (Texas Instruments, TX, U.S.A), glass vials (Agilent Technologies, CA, U.S.A), 3D printed plastic fixtures, and a styrofoam box, assembled on the orbital shaker (*KJ-201 BD,* WINCOM, Jiangsu, CHN) as shown in Fig. 3.3.

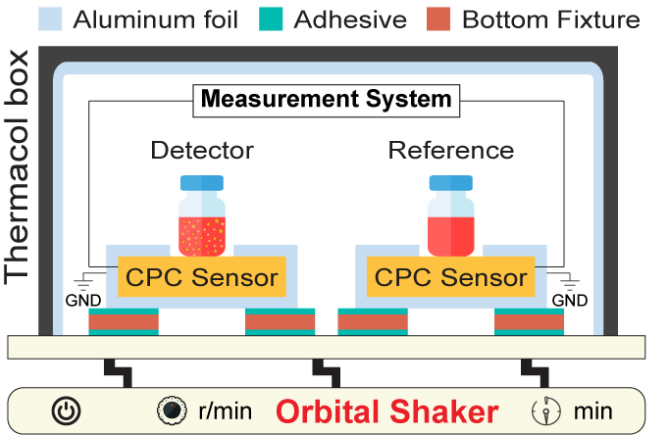

Fig. 3.3. Schematic layout of the experimental setup and method for hemostasis assessment.

A blood sample in glass vials was precisely positioned using plastic fixtures on top of the crack region in the sensor, to ensure maximum fringing field for a high sensitivity capacitance measurement. Fixtures also minimized the variability in sample position between measurements. Bottom fixtures supported the sample weight eliminating any mechanical pressure on the MWCNT-coated cellulose fibers. To reduce the parasitic capacitance, aluminum (Al) foil was used to shield the sensors and the inner surface of the Styrofoam box. FDC 2214 evaluation module used for capacitance measurement. The evaluation module was composed of an inductance-capacitance (*L-C)* circuit to measure capacitance changes as shifts in the resonant frequency of the *L-C* circuit. A 1 nF ceramic capacitor was integrated parallel to the *L-C* circuit to achieve an excitation frequency of 1.3 MHz (Fig. 3.4).

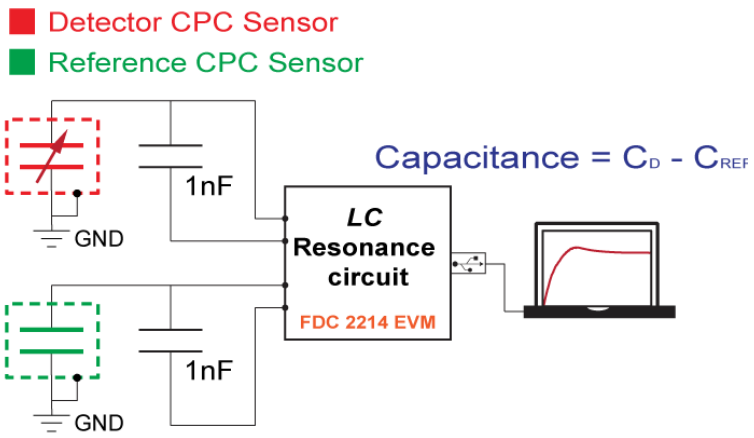

Fig. 3.4. Functional block diagram of the capacitance measuring system.

A laptop with data acquisition and processing software was used as both a power source and data logger.

3.3.3 Measurement protocol for sensor calibration and characterization

Fig. 3.5 illustrates the measurement protocol used for calibration and characterization studies. Briefly, glass vials were placed on top of the sensors and initial capacitance was measured for 5 min. Then, 500 µL of DI water was added to the reference sensor and allowed to equilibrate for 5

min. Subsequently, 500 µL of the testing sample was added to the detector sensor and 80-rpm shaking was applied. Measurement was performed for an additional 5 min. Capacitance change from sample addition (δC) was evaluated as the difference between the averaged capacitance before (7 - 10 min, Fig. 3.5) and after the addition of the testing sample (12 - 15 min, Fig. 3.5).

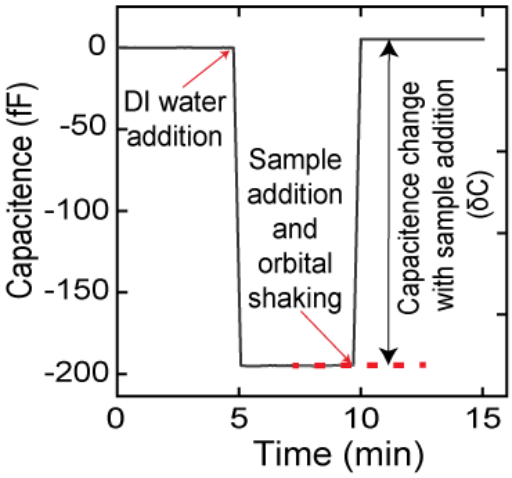

Fig. 3.5. Measurement protocol for sensor calibration and characterization.

3.3.4 Clotting measurement protocol

Clotting measurements were conducted using unmodulated blood and blood sample modulated for a predefined platelet count or platelet function or hematocrit, which are generally referred to as blood samples herein. For a clotting assay (Fig. 3.6), a baseline capacitance was measured for 5 min with the glass vials placed on the sensors. Then, 325 µL of the blood sample was added to the reference sensor. Immediately, 300 µL of the same blood was added to the detector sensor and 80-rpm orbital shaking was applied. The glass vial on the detector sensor was prefilled with 25 µL of 162.5 mM $CaCl_2$ solution (final Ca^{2+} concentration in whole blood: 12.5 mM) for recalcification of the blood sample. Differential capacitance was measured for an additional 30 min after activation. All measurements were conducted at room temperature (23 ^{0}C).

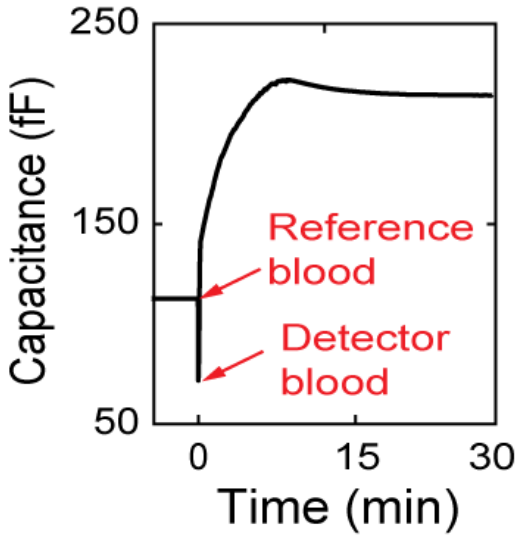

Fig. 3.6. Clotting assay using the CPC capacitance sensor.

3.3.5 Analysis of sensing parameters for hemostasis assessments

Capacitance was measured at a sampling rate of 33 Hz during clotting. A real-time average of 300 data points (approximately 9 sec) was performed to obtain a very low-frequency envelope for capacitance change with the progression of clotting. For data analysis and presentation (graphs), the initial time ($t = 0$) was defined as the time point when the blood sample was activated. From the measured capacitance, three parameters namely T_{Cpeak}, $\Delta C1$ and $\Delta C2$ were chosen for analysis (Fig. 3.7). T_{Cpeak} was the time point for the maximum capacitance value after activation. $\Delta C1$ was evaluated as the magnitude decrease in capacitance from peak to a steady-state value. Steady-state capacitance was the averaged value between 28 - 30 min after activation. $\Delta C2$ was the maximum capacitance value after activation.

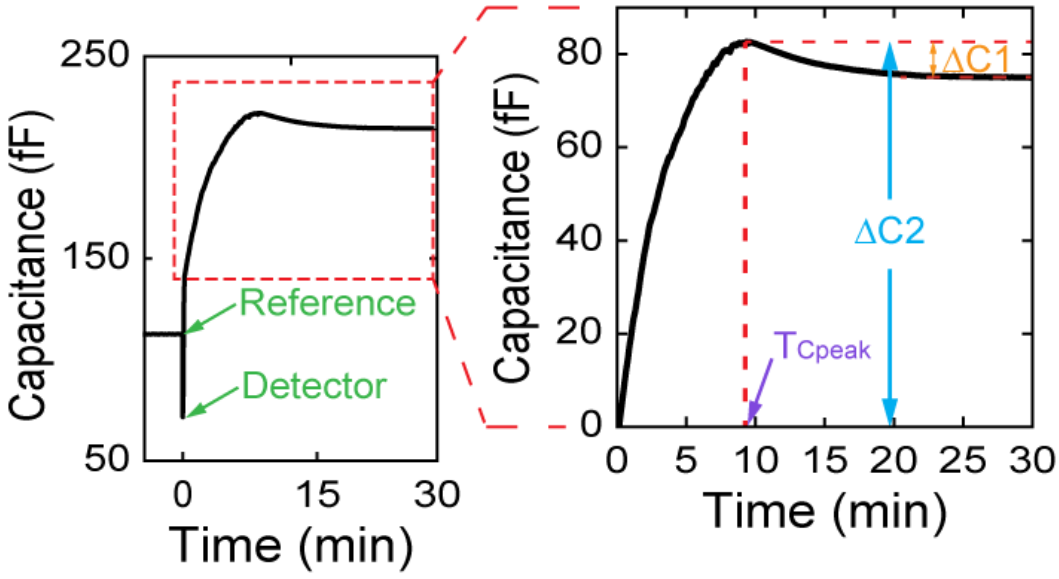

Fig. 3.7. Left: A representative overall capacitance signal for a blood sample activated using $CaCl_2$ (12.5 mM). Right: Zoom-in view of the region of interest with the sensing parameters, T_{Cpeak}, $\Delta C1$, and $\Delta C2$ for analyses.

3.3.6 Blood samples

Fresh whole blood in standard 3.2 % citrate tubes was purchased from Bloodworks Northwest Seattle, WA. Unless specified, all blood samples were from de-identified, healthy volunteers without previously known coagulation or platelet disorders, and had not received any antithrombotic medication in the two weeks before sample collection. Blood tubes were transported and stored in a styrofoam box at room temperature and used within 4 hours from the blood draw. $CaCl_2$ solution in phosphate buffered saline (PBS, pH 7.4; Sigma-Aldrich, MO, U.S.A) was prepared on the day of experiments. In some experiments, the blood samples were treated *in vitro* to modulate platelet count or platelet function or hematocrit to systematically study their effects on the sensing parameters (T_{Cpeak}, $\Delta C1$ *and* $\Delta C2$). Blood samples with a predefined platelet count or hematocrit were prepared from the two-step centrifugation technique. First, citrated whole blood was centrifuged at 200 *g* for 10 min to pellet down the

erythrocytes. The desired volume of the resultant supernatant, platelet-rich plasma (PRP) was carefully removed. Subsequently, a part of the collected PRP was further centrifuged at 4000 *g* for 5 min to obtain platelet-poor-plasma (PPP). The erythrocyte pellet was then resuspended in the remaining PRP by gently inverting the tube to get a reconstituted hematocrit modulated sample. The reconstituted sample was then divided into portions and diluted with a calculated volume of PRP and PPP to yield a blood sample with a predefined hematocrit (15, 20, 40 and 50 %) or platelet count (100, 120, 140, 160 and 180 x 10^3 platelets μl^{-1}).

Platelet counts in all hematocrit modulated samples were maintained constant as 165 ± 27 x10^3 platelets μl^{-1}. Similarly, the hematocrit of all platelet count modulated samples was 40 ± 3 %. Platelet functional inhibition was done by incubating the samples with a predefined concentration of aspirin (0, 0.1, 0.51 mM). Aspirin (Sigma-Aldrich, MO, U.S.A) was dissolved in dimethyl sulfoxide (DMSO; Sigma-Aldrich, MO, U.S.A) and diluted with PBS to the desired concentration before adding to blood samples. In the aspirin study, an appropriate amount of PBS buffer was added to the control samples to maintain approximal cell counts and hemodilution as the aspirin-treated samples. Platelet counts and hematocrit in whole blood, PRP and PPP were measured using a hematology analyzer (*XP-300*, Sysmex America OR, U.S.A) with an accuracy of 1.5 % for hematocrit and ± 6 x 10^3 μl^{-1} for platelet counts. In general, ethylenediaminetetraacetic acid (EDTA) is preferred for blood cellularity measurements to avoid hemodilution (Briggs, 2009). However, EDTA irreversibly chelates the free calcium in the blood and permanently affects the progression of the coagulation cascade and the ability of the blood cells to form aggregates and deform from retraction forces (Green et al., 2008). Therefore, blood

counts were measured on blood samples anticoagulated with sodium citrate and reported with 10% hemodilution.

3.3.7 Thromboelastography (TEG)

TEG measurements were performed by trained personnel at the Department of Laboratory Medicine, University of Washington using TEG 5000 thromboelastography hemostasis analyzer (Haemonetics, U.S.A). *R-time* parameter is the time from the start of the measurement to the initial detection of clot formation (in min) and is indicative of the coagulation function. *MA* is a measure of clot strength as determined by the ability of platelets to bind via $\alpha_{IIb}\beta_3$ integrin as well as the elasticity of the fibrin mesh (Gottumukkala et al., 1999). The newly introduced sensing parameters, T_{Cpeak} and $\Delta C1$, were compared with the equivalent TEG diagnostics parameters *R-time* and *MA*, respectively. TEG measurements were performed within 5 hours of blood draw. Blood samples were activated with 12.5 mM $CaCl_2$ (Citrated Native TEG), similar to measurements using the CPC capacitance sensor.

3.3.8 Statistical analysis of data

To ensure excellent data repeatability and reliability, the sample size for all clotting studies was predetermined to be five healthy donors to account for biological variability with two replicate measurements each. For the TEG comparison study, blood samples from twelve healthy donors with a single replicate measurement were used. Three hemophilia patient samples and simulated thrombocytopenia samples were used to investigate the potential clinical applications for the sensor. Platelet count and hematocrit of blood samples were obtained as an average of three measurements using a hematology analyzer. The vast majority of the data distributions were found to be normal (Shapiro–Wilk Goodness of Fit for normal distribution, $p > 0.077$) and

were analyzed using parametric methods for statistical analysis. For the two measurements that contained distributions significantly skewed from normal (Fig. 3.23f, Fig. 3.16b), non-parametric methods were used for statistical analysis. Pearson's correlation coefficient (r) was used to evaluate linearity between the pairs of data. One-way analysis of variance (ANOVA) with Tukey's post-hoc or Kruskal-Wallis tests was used to compare the results with three or more groups. A two-sided unpaired t-test was used for comparison between healthy donors and hemophilia patients. A two-sided paired t-test or Wilcoxon matched-pairs signed-rank test was used to compare between healthy and thrombocytopenia samples. * denotes a p-value less than 0.05 and was considered statistically significant. ** denotes a p-value less than 0.01 and NS denotes not significant.

3.4 RESULTS

3.4.1 CPC sensor calibration and characterization

A differential measurement using two CPC capacitance sensors was chosen to minimize the environmental disturbances in the signal. This design provided a capacitance signal with low noise in the order of 205 aF (*peak-to-peak*; Fig. 3.8).

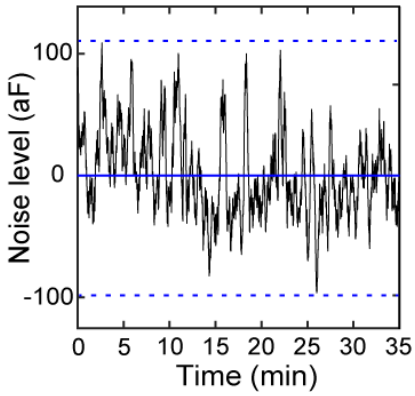

Fig. 3.8. A representative CPC sensor noise level.

DI water as detector and reference sample at 80-rpm orbital shaking; peak-to-peak noise, 205 aF; and RMS noise, 34 aF.

To establish the relationship between the measured differential capacitance to the relative permittivity of a liquid, experiments were conducted with reference permittivity standards namely DI water, isopropyl alcohol (IPA), acetone, ethanol, dimethyl sulfoxide (DMSO), 2.5% & 10% v/v IPA in DI water and 40% v/v ethanol in DI water. DI water was used as the reference sample for all measurements. The experimental protocol followed for measurements and analysis for the readout parameter, δC are described in detail in Section 3.3.3 and shown in Fig. 3.5. Fig. 3.9 shows the average δC for the permittivity standards from five measurements and the error bars represent the standard deviation. One reason for this deviation may be due to the small variation in the pipetting volume between trails. δC showed a strong positive correlation with the relative permittivity ($r = 0.99$, $p < 0.00001$, $n = 7$; Pearson's correlation) with a slope ($\Delta C/\Delta \mathcal{E}$) of 2.22 fF.

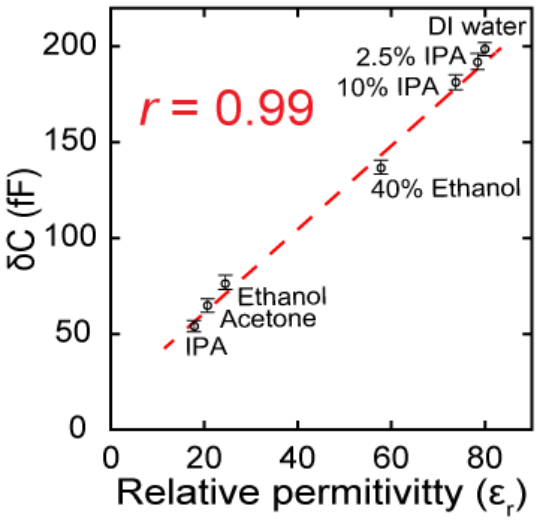

Fig. 3.9. Capacitance change (δC) linearly increases with the increasing relative permittivity (εr) of the sample liquid.

Pearson's r = 0.99; Average slope, 2.22 fF εr^{-1}.

To further characterize the system, we performed additional measurements with aqueous *NaCl* solutions to simulate a relative permittivity change. δC showed a decreasing trend with

increasing molar concentration of *NaCl* in DI water (F (2.02,8.07) = 414.4, $p < 0.00001$, $n = 11$; ANOVA; Fig. 3.10). The capacitance decrement was linear till 1 M but deviated from linearity for higher concentrations and showed saturation around 4 M (inset Fig. 3.10). 0.2 M *NaCl* solution was the smallest concentration for which a statistically significant difference was observed compared to DI water.

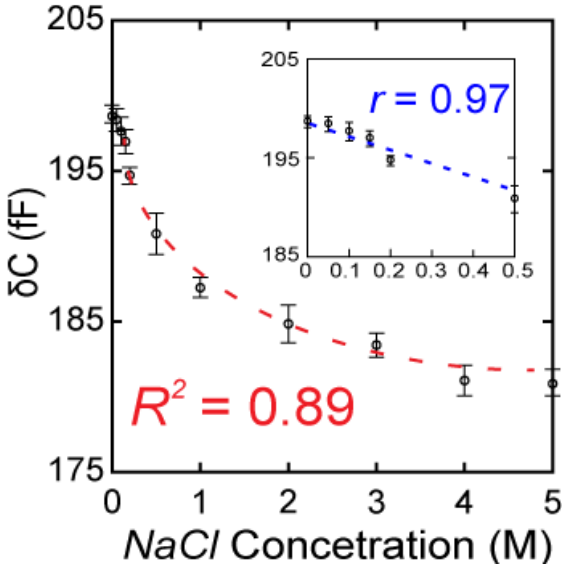

Fig. 3.10. *δC* exponentially decreases with increasing molar concentrations of *NaCl*. *(0, 0.05, 0.1, 0.15, 0.2, 0.5, 1, 2, 3, 4 and 5 M); goodness of fit, $R^2 = 0.89$. Permittivity of NaCl solutions exponentially decreases with increasing molar concentrations of NaCl and δC sensitively followed this decrement. Inset: The decrement was linear for dilute solutions (≤ 0.5 M); Pearson's r = 0.97*

Previous researchers have reported a similar trend in relative permittivity with increasing molar concentration of *NaCl* (Gavish and Promislow, 2016; Haggis et al., 1952; Hasted et al., 1948). One explanation for this phenomenon is the inhibition of the applied external field by the local field generated by the ions (Gavish and Promislow, 2016). The polar water molecules in the solution get reoriented due to the local ionic field creating a hydration shell around each ion, thereby lowering the response to the applied external field causing a reduced polarization. However, the relative permittivity decrement is linear only for dilute solutions (typically less

than 1.5 M) and showed significant nonlinearity at higher salt concentrations and saturation around 45 (Hasted et al., 1948). This was likely due to overlapping hydration shells ensuing reduced inter-ionic distances (geometric restrictions) and the effective screening effect saturates (Persson, 2017). Our results show that readout parameter δC followed this relative permittivity decrement, reaffirming the strong positive relationship of the readout with the relative permittivity of the sample liquid. Collectively, the results from the calibration (Fig. 3.9) and characterization (Fig. 3.10) studies confirmed the CPC sensor readout is sensitive to relative permittivity changes in a liquid.

3.4.2 Characterization of the capacitance-based hemostasis assessment system

To characterize the system for blood hemostasis assessments, preliminary experiments were conducted with citrated and recalcified whole blood samples from healthy volunteers. Erythrocytes in whole blood reversibly aggregate to form rouleaux (resembling a stack of coins) under static or low-shear conditions, but disintegrate at physiological shear flows (Elad and Einav, 2004). Fibrinogen in the plasma is believed to play a significant role in the rouleaux formation acting as bridges binding to the surface of erythrocytes (Bäumler et al., 1999; Maeda et al., 1987; Teige and Starý, 1946). The relative permittivity of the blood changes during rouleaux formation (Asami and Sekine, 2007; Hayashi et al., 2017) and this may reduce the specificity of the signal towards clotting. Therefore, to minimize the differential capacitance variation due to rouleau formation and subsequent cell sedimentation, blood samples were gently agitated on an orbital shaker. A preliminary parametric study was conducted to find the optimal rotational speed (rpm), which minimized rouleaux formation in the reference (inactivated blood) yet allowed for a clot formation without dissolution in the detector sample (activated blood). Citrated whole blood samples from healthy volunteers were subjected to different rotational

speeds (40, 60 and 80 rpm). From visual observation of pictures taken every 10 mins, it was found that 80-rpm sufficiently minimized the cell sedimentation of the erythrocyte rouleaux as shown in Fig. 3.11

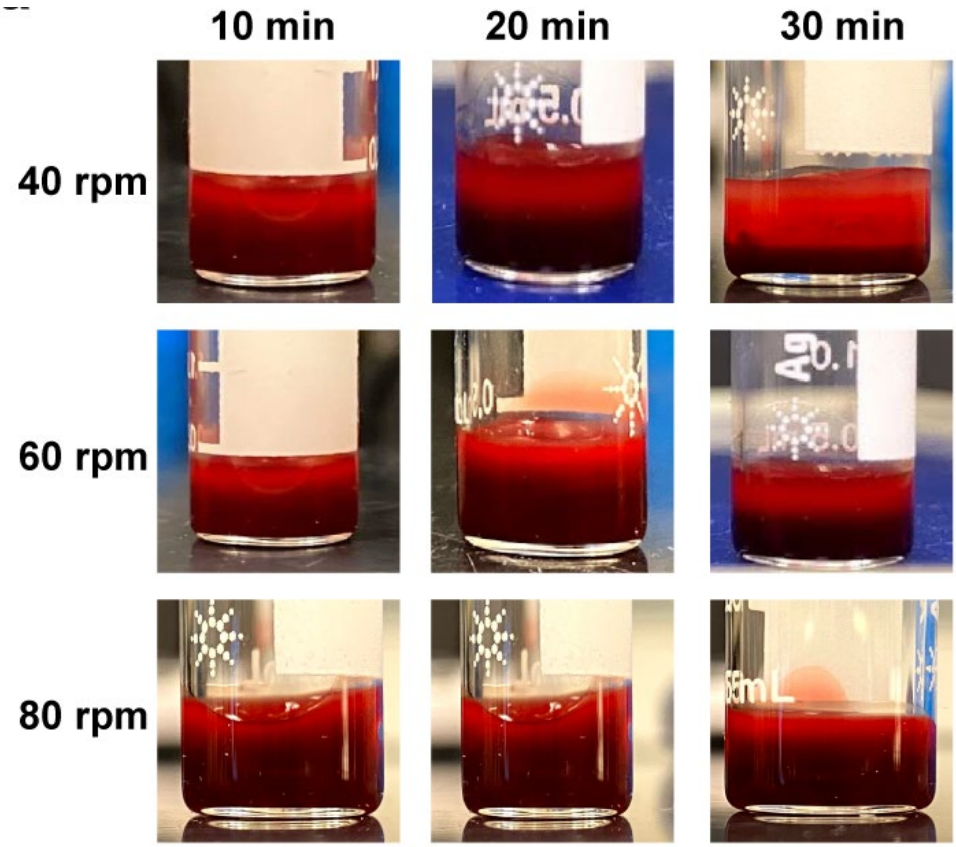

Fig. 3.11. Visual observation of erythrocyte rouleau sedimentation at different orbital rotational speeds (rpm).

Orbital shaking at 80-rpm sufficiently minimized sedimentation and maintained homogeneity in the citrated blood sample.

Next, a repetitive orbital shaking study was conducted to evaluate the stability of the signal during orbital shaking. Capacitance was fairly stable during orbital shaking as shown in Fig. 3.12 (80-rpm cycle). It can be seen that the cessation of orbital rotation caused an exponential increase in the readout, and on resumption of shaking rapidly decreasing to a steady value, similar to that in the preceding shaking cycle. The increase in capacitance during the static cycle was due to the

relative permittivity changes from the rouleaux formation of the erythrocytes (inset Fig. 3.12). Previous researchers have reported a similar increase in blood permittivity with erythrocyte rouleaux formation (Hayashi et al., 2015; Debnath Maji et al., 2018).

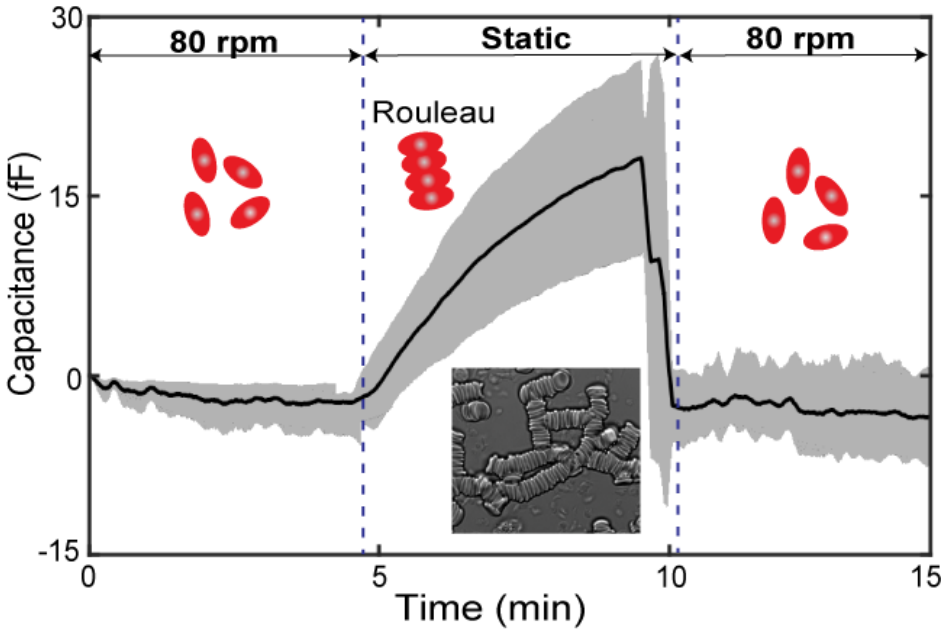

Fig. 3.12. Time course variation of capacitance for healthy citrated whole blood subjected to a repetitive cycle of orbital shaking and static.

Capacitance increases with erythrocyte rouleau formation during the static cycle; n = 3. The shaded region denotes S.D; Blue dotted lines indicate the timepoint for switching cycles.

Additionally, it was also found that 80-rpm orbital shaking did not generate a non-physiologically high shear environment to activate the platelets for clotting in the samples. Capacitance was stable for the inactivated sample during orbital shaking for 40 min, with a *peak-to-peak* change of 414 aF as shown in Fig. 3.13a. Moreover, the shaking also did not interfere with the natural progression of clotting for the activated blood sample (Fig. 3.13b). Hence, an 80-rpm shaking was applied for all clotting assays to get a capacitance readout with high specificity to the clotting dynamics.

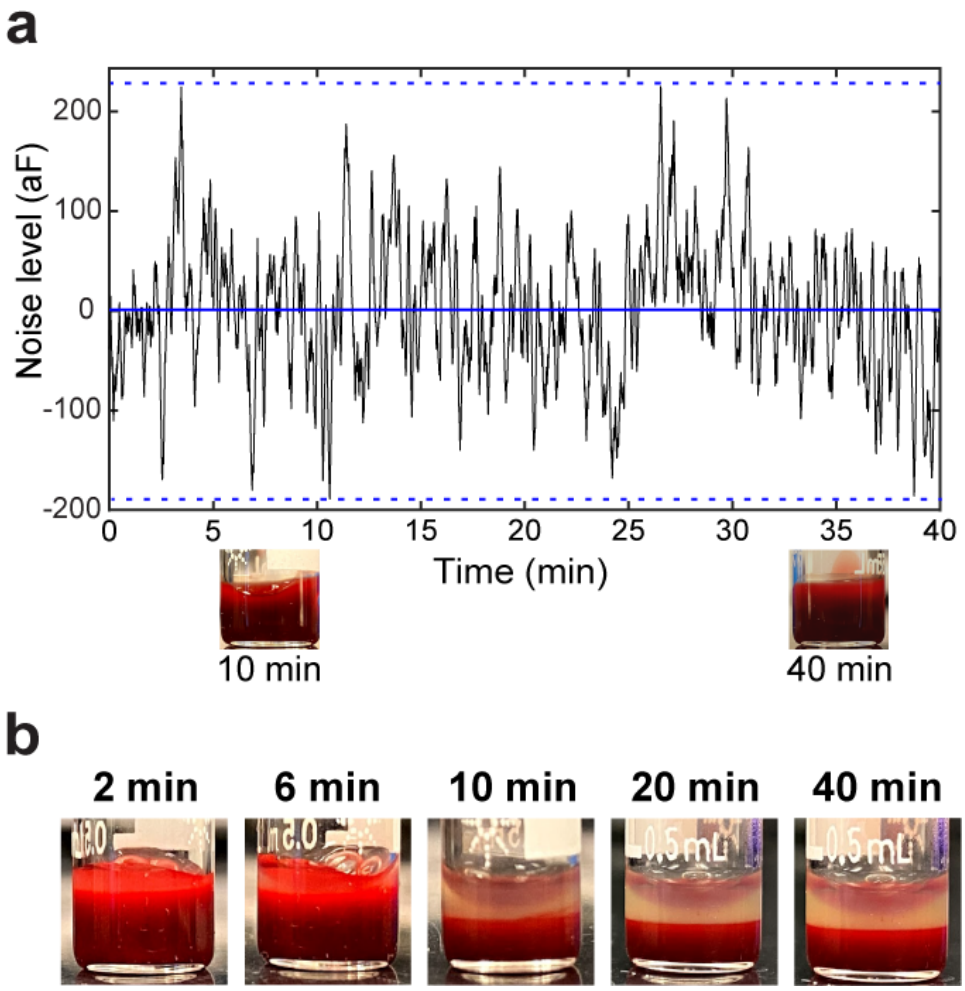

Fig. 3.13. CPC capacitance signal and blood sample stability during 80-rpm orbital shaking.

(a) Stability of the capacitance signal at 80-rpm orbital shaking for non-activated blood sample; peak-to-peak noise, 414 aF; and RMS noise, 68 aF. No visual clot formation was observed in the citrated blood sample photographed at 10 min and 40 min of orbital shaking. (b) Orbital shaking at 80-rpm did not interfere with the natural progression of clotting when the detector blood sample was activated using 12.5 mM of $CaCl_2$.

The permittivity response of whole blood is frequency-dependent (Hayashi et al., 2015; D. Maji et al., 2018). Hence, to find the optimal frequency for measurements capacitance measurements were conducted at various operating frequencies (120k, 550k, 1.3M, 3.1M, and 5.3M Hz), using blood samples with a predefined hematocrit (0, 10, 20, 30 %), following the

protocol described in Section 3.3.3. δC at 1.3 MHz was by approximately 125 % higher than at 120 kHz for 30 % hematocrit (Fig. 3.14). This finding suggests that the frequency-dependent permittivity response of blood was pronounced at 1.3 MHz, similar to previous studies (Abdalla, 2011; Maji et al., 2017). At this frequency, δC also linearly increased with higher hematocrit (r = 0.92, $p < 0.001$, $n = 3$; Pearson's correlation, red-dotted lines).

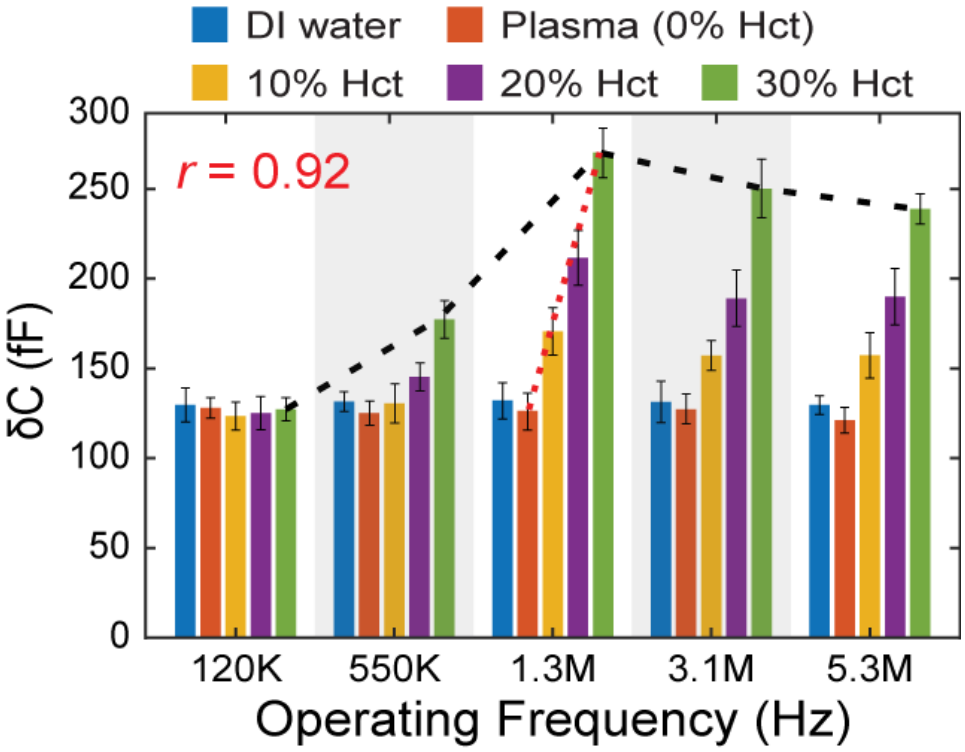

Fig. 3.14. Capacitance change with sample addition (δC) for various operating frequencies.

Peak δC was observed at 1.3 MHz for all hematocrits; n = 3 with single replicates; Bars represent mean values; error bar, S.D. At 1.3 MHz, δC linearly increases with hematocrit; Pearson's r = 0.92.

3.4.3 A multiparameter assessment of hemostasis: simultaneous assessment of coagulation time, platelet count or function, and hematocrit

When testing a blood sample with $CaCl_2$ (final concentration: 12.5 mM), it was observed that the capacitance increased and reached a peak value before decreasing to a steady-state value

(Fig. 3.7). To examine the ability of the sensor to simultaneously assess coagulation function, platelet function and hematocrit, the blood samples from healthy donors were modulated for a predefined clotting activation level (Ca^{2+} concentration), platelet count or function, or hematocrit. Results from these studies are described below.

T_{Cpeak} decreased with increasing $CaCl_2$ concentration (6.3, 12.5 and 25 mM; Fig. 3.15b), which indicated a trend in T_{Cpeak} and coagulation time (F (2,27) = 27.16, $p < 0.00001$; ANOVA). For the remaining studies, 12.5 mM $CaCl_2$ was used to activate clotting in the samples. Measurements using blood samples with a predefined platelet count (100, 120, 140, 160 and 180 x 10^3 platelets μl^{-1}) showed that *ΔC1* linearly increased with increasing platelet count ($r = 0.94$, $p < 0.00001$; Pearson's correlation; Fig. 3.15c). Additionally, *ΔC1* dose-dependently decreased for blood samples incubated with aspirin (0, 0.1, 0.51 mM), which inhibits platelet activation (F (2,27) = 17.68, $p < 0.0001$; ANOVA; Fig. 3d). Together, the above two results (Fig. 3.15c, d) showed that *ΔC1* was sensitive to both platelet count and function. Measurements on blood samples with a predefined hematocrit (15, 20, 40 and 50 %), showed that *ΔC2* linearly increased with increasing hematocrit ($r = 0.96$, $p < 0.00001$; Pearson's correlation; Fig. 3.15e). Collectively, the above results showed that the sensor can offer a multiparameter assessment of hemostasis by providing concurrent information on coagulation function, platelet count or function, and hematocrit.

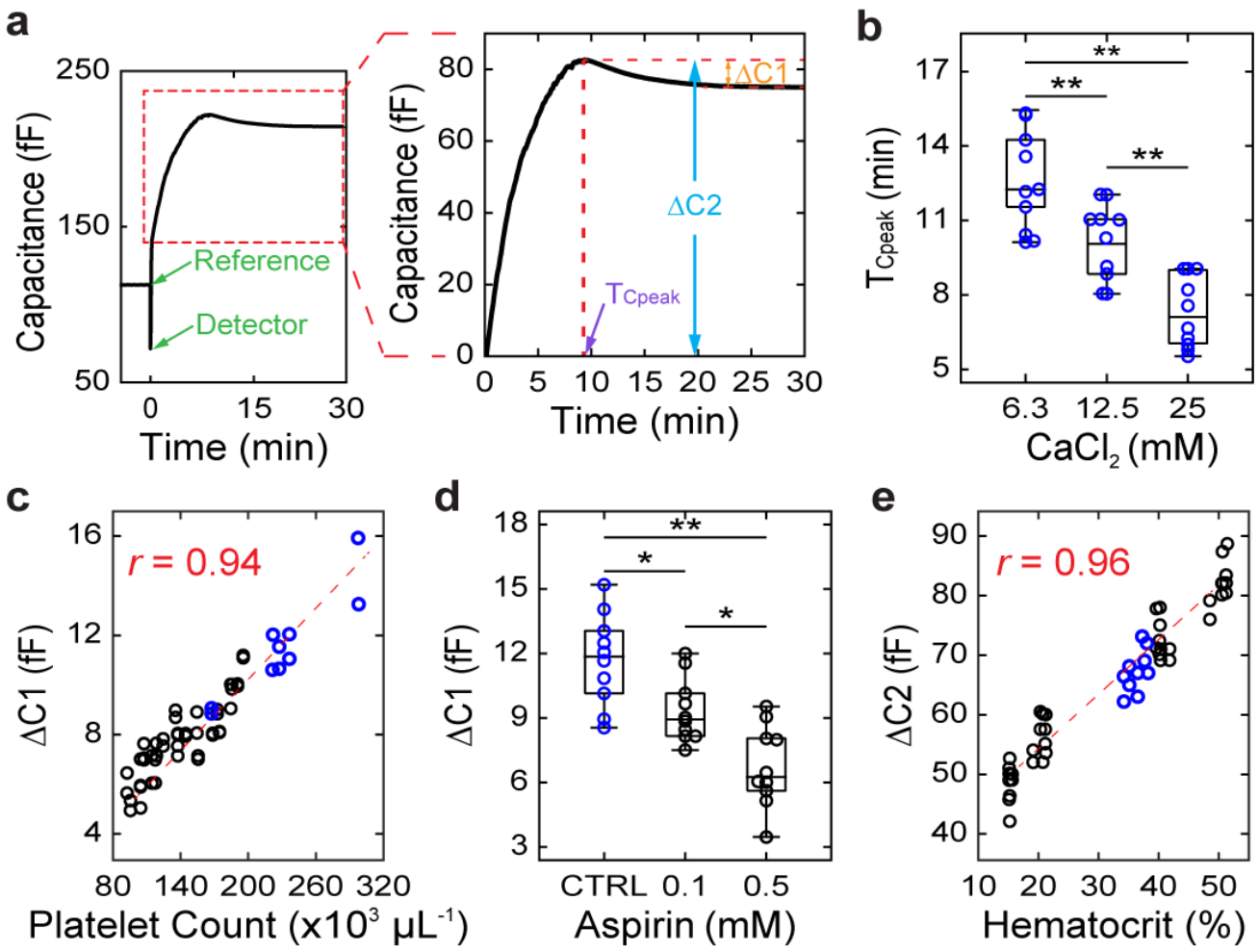

Fig. 3.15. Multiparameter hemostasis assessment: Simultaneous evaluation of coagulation function, platelet count or function and hematocrit.

(a) Left: A representative overall capacitance signal for a blood sample activated using $CaCl_2$ (12.5 mM). Right: Zoom-in view of the region of interest with the sensing parameters, TCpeak, ΔC1, and ΔC2 for analyses. (b) TCpeak decreases with increasing concentration of activating CaCl2 (mM). (c) ΔC1 linearly increases with platelet count in the range 93 – 298 x 103 platelets μl^{-1}; Pearson's r = 0.94. (d) ΔC1 decreases dose-dependently with aspirin treatment. (e) ΔC2 linearly increases with hematocrit in the range 15.1 % - 51.2 %; Pearson's r = 0.96.

Additionally, the sensing parameters, T_{Cpeak}, *ΔC1,* and *ΔC2*, showed distinctive sensitivities towards coagulation function, platelet count or function and hematocrit, respectively. T_{Cpeak} did not change significantly with platelet count ($r = 0.18$, $p = 0.17$; Pearson's correlation; Fig.

3.16a), aspirin concentration ($F(2,27) = 0.082$, $p = 0.92$; ANOVA; Fig. 3.16b), and hematocrit ($r = 0.08$, $p = 0.57$; Pearson's correlation; Fig. 3.16c). *ΔC1* did not show a statistically significant difference with $CaCl_2$ concentration ($F(2,27) = 0.14$, $p = 0.87$; ANOVA; Fig. 3.16d) and hematocrit ($r = 0.037$, $p = 0.80$, Pearson's correlation; Fig. 3.16e). *ΔC1* was higher for unmodulated blood samples compared to blood samples modulated to a predefined hematocrit ($p < 0.0001$; Paired t) due to variations in platelet count between the two groups (Blue circles: 249 ± 37, Black circles: 165 ± 27, x 10^3 platelets μl^{-1}). This finding was consistent with the previous result in Fig. 3.15c, suggesting platelet count to be a major factor affecting *ΔC1*. *ΔC2* had a positive correlation only with hematocrit and no statistically significant changes was detected with variations in $CaCl_2$ concentration ($F(2,27) = 0.064$, $p = 0.94$; ANOVA; Fig. 3.16f), platelet count ($r = -0.19$, $p = 0.15$; Pearson's correlation; Fig. 3.16g) and aspirin concentration ($F(2,27) = 0.23$, $p = 0.8$, ANOVA; Fig. 3.16h).

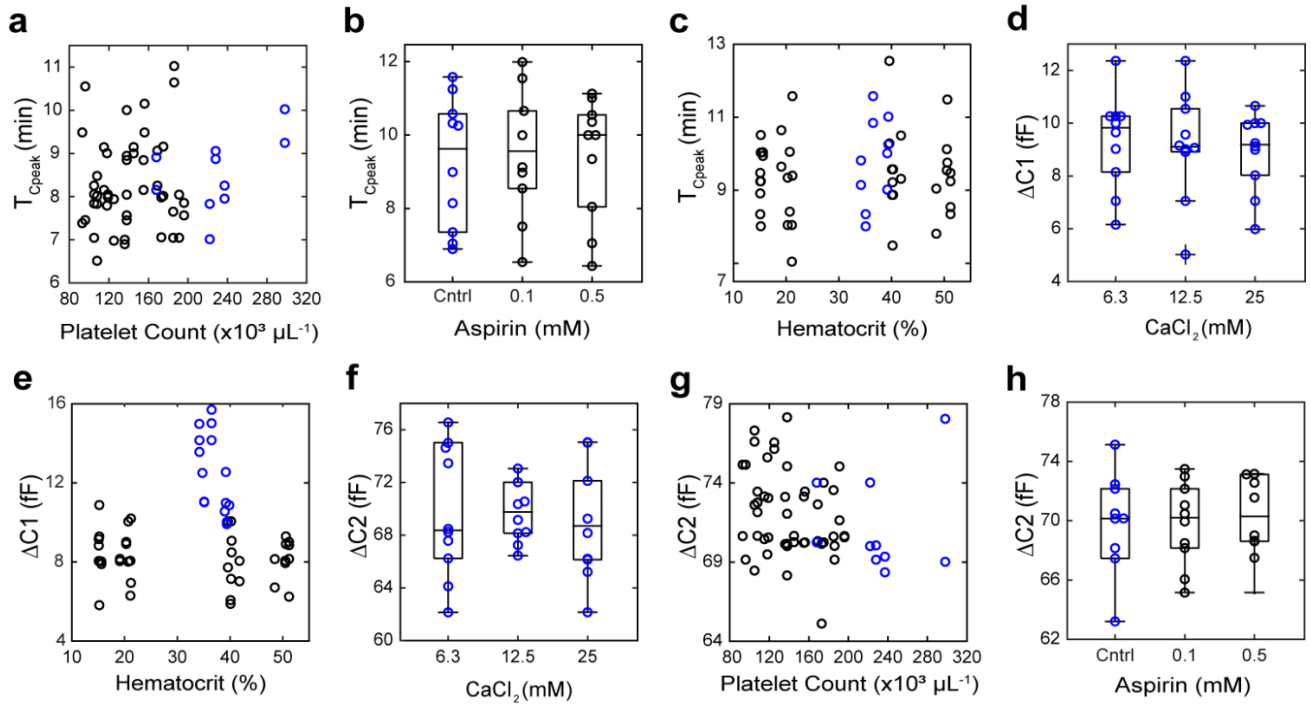

Fig. 3.16. Sensing parameters, *T_{Cpeak}, ΔC1 and ΔC2*, show distinctive sensitivities towards coagulation function, platelet count and function, and hematocrit, respectively.

Independence of T_{Cpeak} with (a) Platelet count in the range 93 – 298 x 103 platelets µL^{-1}, (b) Aspirin treatment, and (c) Hematocrit in the range 15.1 % - 51.2 %. Independence of ΔC1 with (d) Activating CaCl2 concentration and (e) Hematocrit in the range 15.1 % - 51.2 %. Unmodulated raw samples (blue circles) had higher platelet counts (Average: 249 ± 37 x 103 platelets µl-1) compared to modulated samples (black circles; Average: 165 ± 17 x 103 platelets µl-1), hence shows increased ΔC1 values. Independence of ΔC2 with (f) Activating CaCl2 concentration, (g) Platelet count in the range 93 – 298 x 103 platelets µl-1, and (h) Aspirin treatment.

3.4.4 Effects of sample idle time and stability of the hemostasis assessments by CPC capacitance sensor

Fig. 3.17 shows the changes in δC for blood samples tested as different storage durations. Measurements were conducted using a protocol detailed in Section 3.3.3 and shown in Fig. 3.5

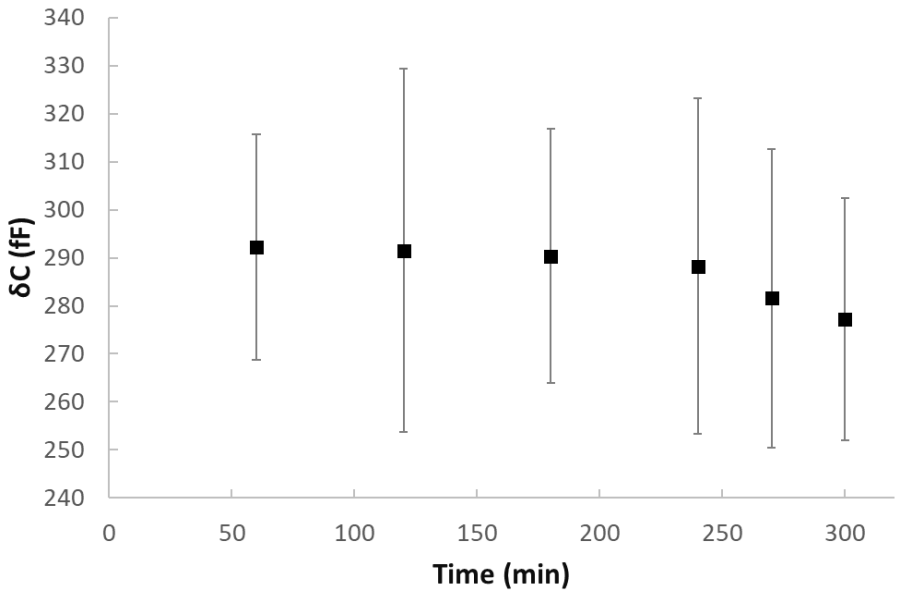

Fig. 3.17. Capacitance change (δC) with idle time for a fixed hematocrit.

To evaluate the stability of the hemostasis assessments, repeated measurements were conducted using room temperature stored blood samples with predefined storage durations (45, 90, 180, 270 and 330 min) after blood draw. T_{Cpeak} was significantly reduced for blood samples stored for 270 and 330 min, relative to measurements at 45 min (F (4,20) = 6.72, $p \leq 0.045$; ANOVA Tukey's post-hoc, Fig. 3.18a). No significant difference was observed for blood samples tested at 90 and 180 min compared with 45 min ($p \geq 0.96$; ANOVA Tukey's post-hoc). No significant difference was observed in $\Delta C1$ (H(4) = 0.89, $p = 0.93$; Kruskal-Wallis test; Fig. 3.18b) and $\Delta C2$ (F(4,20) = 0.28, $p = 0.89$; ANOVA; Fig. 3.18c) for all groups. These results have shown good repeatability in the newly introduced sensing parameters for *in vitro* evaluation of hemostasis using citrated blood.

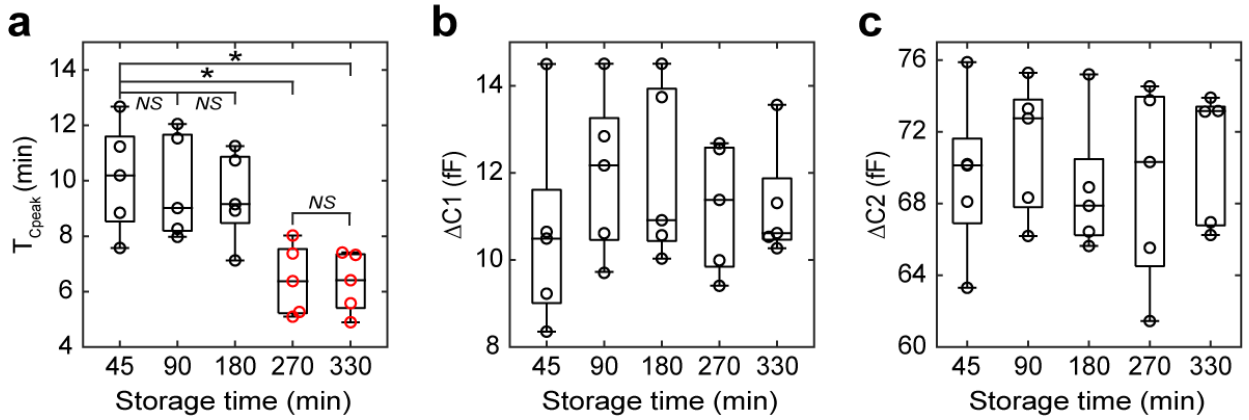

Fig. 3.18. Stability of hemostasis assessments by the CPC capacitance sensor.

(a) *T_{Cpeak} drops for whole blood tested after 270 min from the blood draw, indicating a trend towards hypercoagulability.* ***(b)*** *ΔC1, and* ***(c)*** *ΔC2 remained stable up-till 330 min*

Furthermore, all sensing parameters, *T_{Cpeak}*, *ΔC1,* and *ΔC2*, demonstrated a Gaussian distribution trend for the healthy volunteers tested ($p \geq 0.16$, $n = 26$; Shapiro-Wilk test; Fig. 3.19).

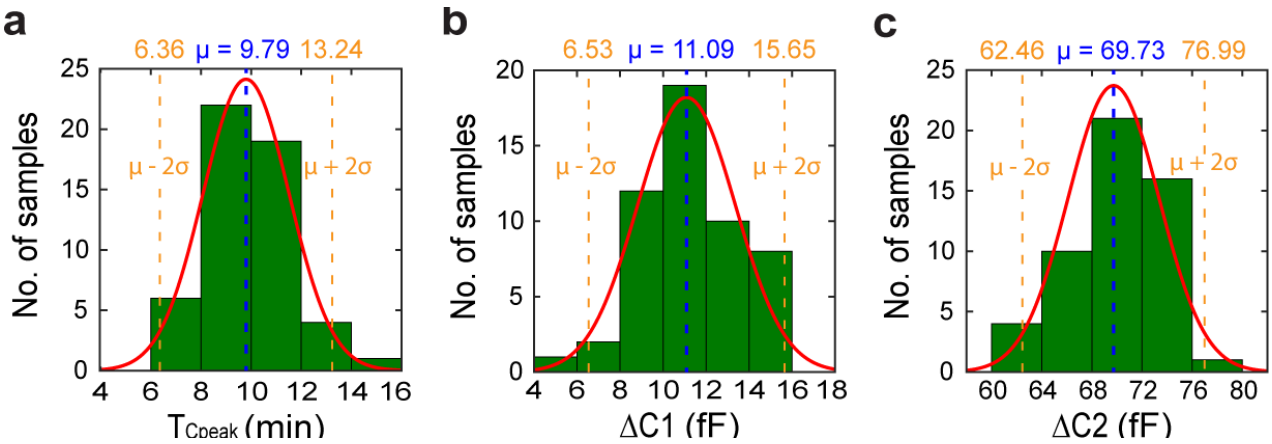

Fig. 3.19. Distribution of sensing parameters for healthy volunteers.

Normal distribution of (a) T_{Cpeak} ($p = 0.16$), (b) ΔC1 ($p = 0.72$) and (c) ΔC2 ($p = 0.66$) for 26 healthy samples with two replicate measurements. p-values were calculated from Shapiro–Wilk Goodness of Fit for normal distribution ($p > 0.05$ is considered normally distributed).

3.4.5 Comparison with Thromboelastography (TEG)

Conventional coagulation tests like aPTT and PT provide valuable information on the activity of coagulation factors but they ignore the contribution of cellular components and endogenous anticoagulant factors in the sample (Mallett et al., 2013). TEG and TEM measure the viscoelastic properties of the clot and provide information about the quality of the clot and kinetics of its formation and are hence routinely used for global hemostasis assessment (Bolliger et al., 2012; Mallett et al., 2013). To evaluate the potential clinical utility of the sensor, the coagulation time and platelet parameters were compared with the clinically relevant diagnostic parameters of citrate native thromboelastography (CN-TEG) assay. TEG measurements were performed by trained laboratory personnel at the coagulation testing facility at the University of Washington – Medicine hospital. The procedure followed is described in detail in Section 3.3.7. A representative TEG trace curve and tests parameters are shown in Fig. 3.20

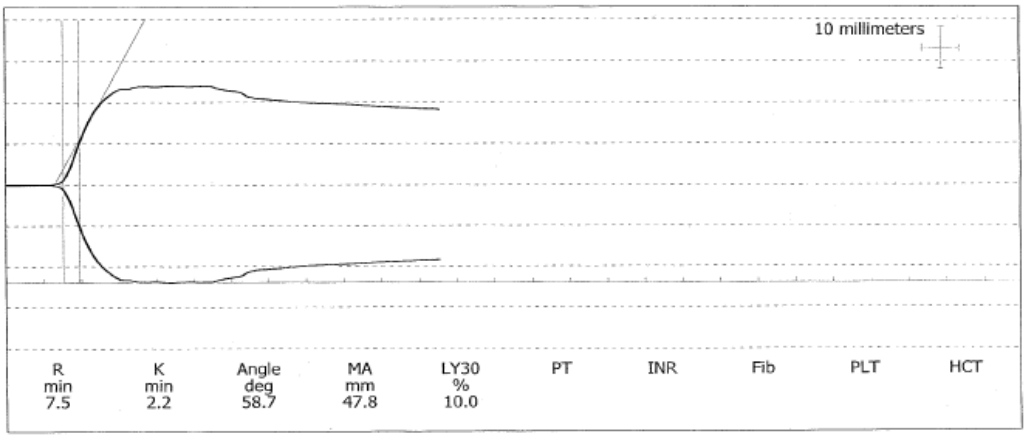

Fig. 3.20. A representative TEG trace for a healthy blood sample.

Among the TEG parameters recorded we were specifically interested in two readout parameters namely the *R-time* and *MA.* The TEG *R-time,* is the time to the initial detection of clot formation (min) from the initiation of the measurement, as determined when the TEG readout reaches an amplitude of 2 mm. The TEG *MA* is the maximum amplitude (mm) of the

TEG readout and is the measure of the clot firmness/strength and stability that is influenced by platelet activity and fibrin (McCrath et al., 2005). Therefore, we choose to compare our CPC sensor readout T_{Cpeak} with the TEG *R-time*, as they are both indicative of the coagulation time, and the system readout $\Delta C2$ with the TEG-*MA*, as they are dependent on platelet activity. Results illustrated a strong positive correlation between T_{Cpeak} and Reaction time (*R-time)* (r = 0.95, $p < 0.00001$, n = 12; Pearson's correlation, Fig. 3.21a). The obtained data validated the effectiveness of the CPC sensor in evaluating coagulation function and is in good agreement with the viscoelastic TEG assay.

There was a relatively less degree of correlation between $\Delta C1$ and Maximum Amplitude (*MA)* (r = 0.58, p = 0.050, n = 12; Pearson's correlation, Fig. 3.21b). The reason for such discrepancy is likely because the *MA* parameter, which measures clot strength, may be affected by both the number of cells in the clot and passive fibrin elasticity (Gottumukkala et al., 1999). To examine the hypothesis, we rearranged the data as illustrated in Fig. 3.21c. Interestingly, a much stronger correlation between $\Delta C1$ and platelet count than to *MA* was observed ($\Delta C1$: r = 0.91, $p < 0.0001$; *MA*: r = 0.62, p = 0.033; Pearson's correlation), suggesting $\Delta C1$ may be solely dependent on the platelet count. This also implies that $\Delta C1$ might be a better alternative in evaluating platelet count-related diseases as it may have a higher sensitivity and specificity to platelet count. Furthermore, the common clinical practice to assess the individual contribution of fibrin(ogen) and platelets to *MA,* is to use a modified TEG assay, where an $\alpha_{IIb}\beta_3$ antagonist is introduced to ensure all viscoelastic parameters measured are the result of fibrin formation alone (Gottumukkala et al., 1999; Whiting and DiNardo, 2014). Our results suggest that the proposed sensor could potentially eliminate the need of using additional specialized inhibitors to assay

platelets in whole blood, which could further minimize the chances of pre-analytical errors that complicate existing assays (Adcock Funk et al., 2012).

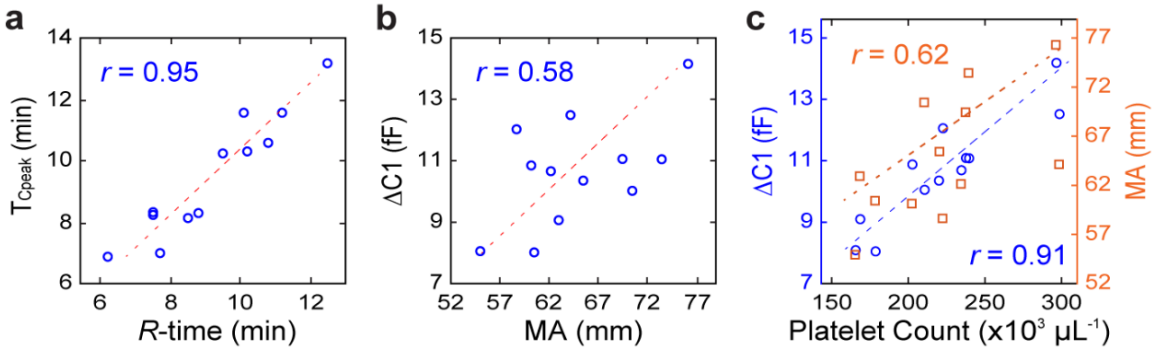

Fig. 3.21. Comparison with Thromboelastography (TEG).

(a) *T_{Cpeak} shows a strong positive correlation with the Reaction time (R-time) parameter demonstrating a good agreement with TEG in evaluating coagulation function; Pearson's r = 0.95* ***(b)*** *Less degree of correlation between ΔC1 and Maximum Amplitude (MA) parameter of TEG; Pearson's r = 0.58.* ***(c)*** *ΔC1 shows a stronger positive correlation with platelet count in comparison to MA; Pearson's r - MA: r = 0.62, ΔC1: r = 0.91. For all graphs: n = 12 healthy donors with the single replicate measurement using the presented CPC capacitance sensor and concurrent Citrate Native TEG.*

3.4.6 Evaluation of clotting function in hemophilia patient samples

To examine the potential usefulness of our sensor in the context of hematologically altered conditions, measurements were conducted using blood samples with clotting disorders. First, the clinical relevance of the measurement in the context of a coagulation disorder was investigated by testing blood samples from three hemophilia patients (2 Hemophilia A, 1 Hemophilia B). The absence of functional factor VIII or factor IX resulted in a significantly higher T_{Cpeak} relative to healthy samples ($t = 8.47$, $df = 5.5$, $p < 0.001$; Unpaired t; Fig. 3.22a). This finding showed that T_{Cpeak} was sensitive to coagulation factor deficiency and can potentially be used to monitor coagulation function in hemophilia patients. Platelet count and hematocrit were in the normal or close to normal ranges for the hemophilia patient samples (Platelet count: 184 ± 37 platelets μl^{-1},

Hematocrit: 35.8 ± 2.77 %; $n = 3$), hence no significant differences was found in both $\Delta C1$ ($t = 1.11$, $df = 5.56$, $p = 0.31$; Unpaired t; Fig. 3.22b) and $\Delta C2$ ($t = 0.66$, $df = 5.85$, $p = 0.54$; Unpaired t; Fig. 3.22c) for hemophilia patients compared to healthy individuals. These results suggested that platelet function or count, and hematocrit were not significantly impacted by a coagulation factor deficiency in these patient samples.

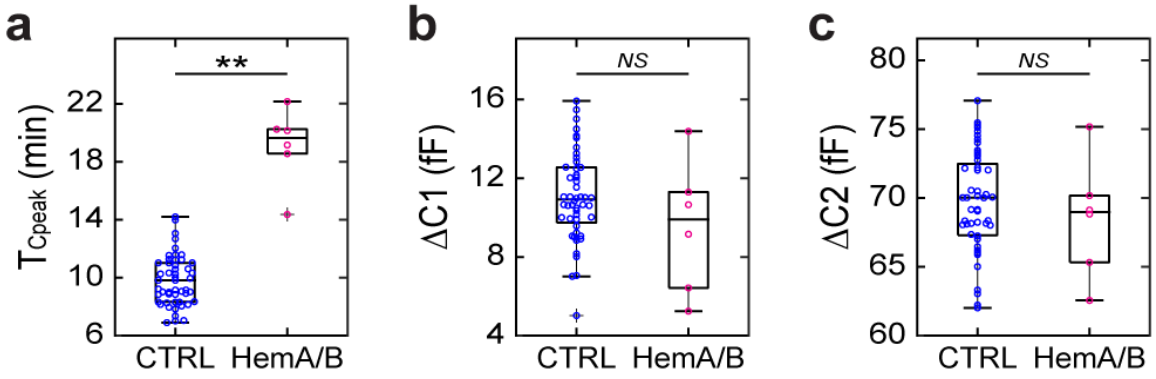

Fig. 3.22. Multiparameter hemostasis assessment for hemophilia condition.

(a) *T_{Cpeak} is prolonged in hemophilia patients indicating the presence of coagulation factor deficiency.* ***(b)*** *$\Delta C1$ and* ***(c)*** *$\Delta C2$ showed no significant difference between healthy and hemophilia patients.*

3.4.7 Effects of thrombocytopenia in hemostasis

As mentioned previously, platelets play a vital role in thrombus formation and stabilization in the event of a vascular injury (Dougald M. Monroe et al., 2002). Platelets are responsible for the formation of a primary plug at the injury site that involves adhesion of platelets to the exposed sub-endothelium, promoting aggregation sites accompanied by the release of aggregating agonists, and eventually the formation of larger platelet aggregates (Frenette et al., 1995). It is therefore evident that the presence of a sufficient number of platelets in the blood is vital to maintain hemostasis. The condition where platelet count falls below 150,000 platelets μL^{-1} of blood is known as thrombocytopenia whereas severe thrombocytopenia occurs when the platelet

count falls below 50,000 platelets per μL^{-1} (Gauer and Braun, 2012). Such quantitative platelet defects may lead to major thrombotic complications, and treatment of patients with these complications requires a rapid hemostasis assessment.

To evaluate the effects of such quantitative platelet disorder in clotting ability, platelet counts in healthy blood samples were modulated to be less than 50 $x10^3$ platelets μl^{-1} to induce a thrombocytopenia condition. Interestingly, we observed a statistically significant increase in T_{Cpeak} for blood samples with an extremely low platelet count compared to healthy samples (t = 3.23, df = 5, p = 0.023; Paired t; Fig. 3.23a). This was in contrast to the previous result, where T_{Cpeak} demonstrated characteristic sensitivity to coagulation function by showing no significant difference with variations in platelet count in the range of 93 to 298 $x10^3$ platelets μl^{-1} (Supplementary Fig. 5a). The reduced T_{Cpeak} observed in blood samples with platelet count less than 50 $x10^3$ platelets μl^{-1} is indicative of the multifaceted role played by platelets in hemostasis. In addition to their key role in primary hemostasis, platelets also play an active role in secondary hemostasis (coagulation cascade) by providing binding sites for coagulation factors in thrombin generation (Michelson, 2019; van der Meijden and Heemskerk, 2019). Therefore, it is possible that a lower activated platelet population could diminish the interaction and localization of the coagulation factors, which further slows down the thrombin generation. As expected, we observed a significant decrease in $\Delta C1$ compared to healthy samples (t = 8.79, df = 5, $p < 0.001$; Paired t; Fig. 3.23b), reaffirming the sensitivity of $\Delta C1$ to platelet counts. Since hematocrit of thrombocytopenia samples was close to healthy samples (Thrombocytopenia: 40.7 ± 2.9 %; Healthy: 38.1 ± 2.1, n = 3), no statistically significant difference was observed in $\Delta C2$ (W = 9, p = 0.44; Wilcoxon matched-pairs signed-rank test; Fig. 3.23c).

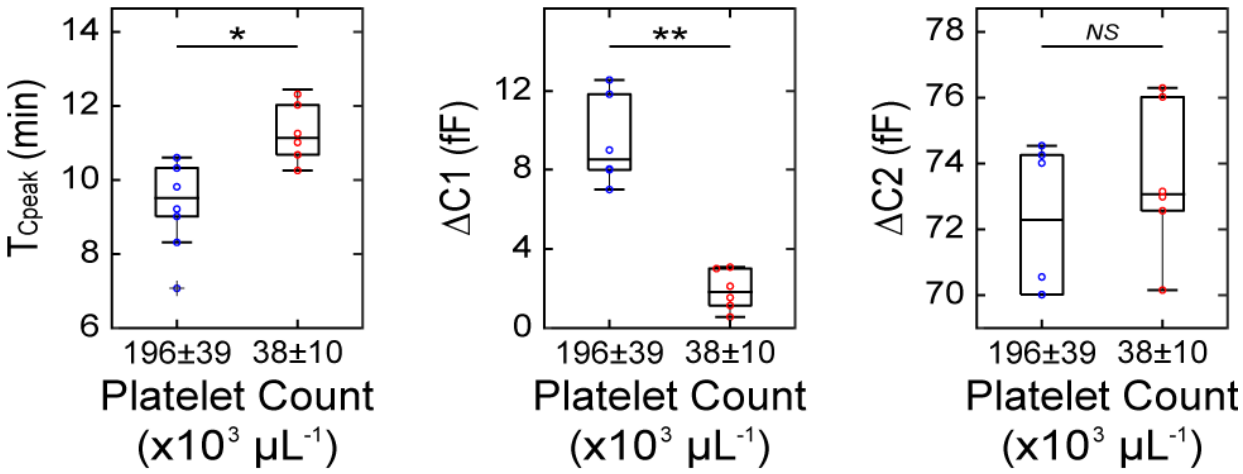

Fig. 3.23. Effects of thrombocytopenia on whole blood hemostasis.

(a) TCpeak is prolonged for blood samples with a thrombocytopenia condition. (b) ΔC1 is significantly reduced from a severe quantitative platelet depletion. (c) ΔC2 showed no significant difference between healthy and severe thrombocytopenia conditions

3.5 DISCUSSION

Motivated by the importance of having a rapid, accurate, and convenient hemostasis assessment device, a new multiparameter hemostasis assessment was developed in this chapter. This is the first capacitance-based non-contact approach. This technology has a unique ability to multiplex the assessment of coagulation function, platelets, and hematocrit in a single clotting assay. Additionally, the CPC sensor system also provides several attractive advantages over existing clinical assays and devices as summarized in Table 3.5. Its ease of use without the necessity of extensive sample preparation or to be performed only by a highly trained laboratory personnel, and additional benefits, such as non-contact measurement, high reusability, and low cost, makes it an ideal tool to readily evaluate clotting status while significantly reducing the financial burden on primary care resources. It may also be used for therapeutic monitoring of anticoagulants, antiplatelet agents, and factor replacement.

Table 3.5. Potential advantages of the CPC capacitance sensor over currently available alternate approaches.

FEATURES	CPC CAPACITANCE SENSOR	VISCOELASTIC ASSAYS	TRADITIONAL LABORATORY ASSAYS	BLOOD GAS OR HAND-HELD ANALYZERS
Provide global assessment of hemostatic and evaluate bleeding risk in a single device	✓			
Provide global assessment of hemostatic status (coagulation time + platelet function)	✓	✓		
Can measure platelet count	✓		✓	
Can measure hematocrit	✓		✓	✓
Rapid Turnround Time (TAT): No need for blood sample processing	✓	✓		✓
Ease of use: No need for trained laboratory staff	✓			✓
Cost-efficient: Reusability	✓			✓

The principle of blood permittivity variation during clotting has been described previously (Hayashi et al., 2010). Earlier attempts using impedance-based sensors have demonstrated the clinical utility by differentiating limited aspects of coagulation and platelet function between normal and pathophysiologic states (Hayashi et al., 2015; Maji et al., 2017). However, the presented capacitance-based approach also offers a simultaneous hematocrit assessment not found in any existing clinical devices including the previous impedance-based sensors. Simultaneous assessment of clotting function and hematocrit can facilitate the development of an automated alert or correction algorithm for blood samples with elevated hematocrit (> 60%), and eliminate the need for *in vitro* citrate adjustment (Marlar et al., 2006).

Another unique feature of the sensor is the ability to provide diagnostic parameters with distinctive sensitivity to coagulation function, platelet count or function, and hematocrit. Specifically, the coagulation and platelet function assessments were not interfered with by variations in hematocrit (Fig. 3.16c & e). This was in contrast to viscoelastic whole blood assays, which can provide inaccurate assessments for abnormal hematocrit settings (Nagler et al., 2013; Ogawa et al., 2012). *ΔC2* provided an exclusive assessment of hematocrit by not changing significantly with variations in clotting activation levels, platelet count and platelet function (Fig. 3.16f - h). The blood permittivity response at 1.3 MHz was from the accumulation of charge carriers at the interface between the erythrocyte membrane and its cytoplasm (Chelidze, 2002). The results from this study suggest that the magnitude of capacitance change (∞ permittivity change) due to redistribution of these accumulated charge carriers from cellular aggregation and encapsulation of the aggregate structures in a fibrin mesh during the clot growth phase, was dependent on the erythrocyte concentration in the whole blood.

Additionally, this study also implies that the CPC sensor affords a simple approach for studying the synergistic relationship between cellular and non-cellular components of hemostasis in normal and different disease states. For example, platelet function in hemophilia patients has been debated and few studies have reported various alterations, such as increased platelet P-selectin expression, lower aggregation upon co-incubation with tissue factor, or reduced platelet contractile forces during clot formation in comparison to healthy individuals (Grünewald et al., 2002; Jensen et al., 2013; van Bladel et al., 2011). However, these conclusions were from assays on platelet suspensions or platelet-rich plasma which only partially reflect platelet function in hemostasis *in vivo* (Harrison, 2009). In this study, results from a limited number of hemophilia

patients suggested that platelet function was not significantly impacted by hemophilia conditions (Fig. 3.22b). Data obtained from a small number of thrombocytopenia samples revealed a prolonged T_{Cpeak} (i.e., coagulation time) (Fig. 3.23a). Similar observations have been made from previous assays (Baughman et al., 1993; Chakraverty et al., 1996; Levi and Opal, 2006). However, these existing assays cannot interpret such prolongation in coagulation time as arising from a severe platelet depletion without an independent platelet count measurement. In our device, in addition to a prolonged T_{Cpeak}, we also observed a significant decrease in $\Delta C1$, as it primarily depends on platelet count, therefore the prolongation in coagulation time may be better deciphered as originating from the reduced platelet count. Additionally, it is also possible to integrate an array of CPC capacitance sensors to conduct parallel assays to analyze blood samples with complex or multiple clotting disorders. These highlight the research-enabling aspect of this technology and the ability to test or create new hypotheses. In a clinical setting, parallel clotting assays could potentially expedite the assessment of bleeding risks in patients, who are not easily diagnosed from a single assay.

Unfortunately, like all other assessment modalities, the presented device does have certain limitations. Firstly, after activation, sedimentation of microthrombi over time due to the growing size of the aggregates (Fig. 3.11b) may convolute the measurement. In the developed system, the sedimentation occurs perpendicular to the electrode plane, hence it's likely to have contributed to capacitance increase during the initial stage of clotting (Asami and Hanai, 1992). The possibility of adding additional sensors in a plane parallel to the sedimentation direction to minimize the signal artifacts from sedimentation will be explored in future work. Two identical CPC capacitance sensors fabricated from a single batch were reused for all measurements in this

study. There might be some minor differences in the intrinsic capacitance value and sensitivity between the sensors due to variations in MWCNTs dispersion and composite fracture. Nevertheless, by conducting a single-point calibration study using the pair of sensors one could establish the sensitivity of the system.

To circumvent the reference signal changes due to rouleau formation and subsequent sedimentation, the system requires constant mechanical vibration/shaking, which limits the realization as a handheld analyzer like CoaguChek (Roche Diagnostics), Xprecia Stride (Siemens Healthineers), or i-STAT (Abbott). While these handheld analyzers may offer a more convenient way to extract physiological properties of blood at the bedside, they have been shown to exhibit variable performance and are limited to specific applications like monitoring patients on warfarin therapy (Harris et al., 2013). Furthermore, they do not provide information on platelet function or count, resulting in a crude snapshot of the hemostatic status. The majority of the clotting assays are still limited to sophisticated laboratories with well-trained operators and personnel for interpreting the results (Harris et al., 2013). The long delay associated with these assays limits their use in acute care settings or patients with active bleeding (Gillissen et al., 2018). In comparison, the CPC sensor system can easily be realized as an automated device with minimal human interventions because of no need for sample processing, limited disposables and minimal steps involved for a clotting measurement. In Chapter 4, the development of an automated compact self-contained bench-top version is presented system.

3.6 CONCLUSION

In this chapter, the first non-contact capacitance-based hemostasis assessment using a carbon nanotube-paper composite (CPC) sensor was presented. Clotting assays at 1.3 MHz provided

three sensing parameters, namely T_{Cpeak}, $\Delta C1$ and $\Delta C2$, to independently assess coagulation function, platelet function or count, and hematocrit, respectively. CPC sensor was first characterized using reference permittivity liquids and then applied to evaluate the hemostatic ability of blood samples with varying clotting activation levels, quantitative and qualitative platelet defects, and different hematocrits. The testing results showed good agreements with a conventional TEG analyzer. The potential clinical usefulness of the technology was demonstrated by testing hemophilia patient samples and blood samples simulated with thrombocytopenia condition. In summary, the CPC sensor system is a promising new device for convenient comprehensive evaluation of hemostasis with attractive advantages such as whole blood-based non-contact evaluation of multiple key clotting biomarkers with high accuracy, high sensitivity, and low cost. Since the sensor system can offer rapid results on the status of multiple clotting elements it can also be used as a medical triage device to identify patients with an emergency need.

Future studies will be focused on exploring the ability of the system to analyze disorders arising from numerous pathological conditions.

Chapter 4. AN AUTOMATED HEMOSTASIS ANALYZER FOR GLOBAL EVALUATION OF HEMOSTASIS

4.1 INTRODUCTION

One of the main challenges in hematology is that existing assays for hemostasis need to be conducted in a central laboratory with highly trained personnel. Access to such specialized testing facilities is often limited in community hospitals and other low-resource settings. In such cases, the sample needs to be transported to a nearby facility, which significantly increases the turnaround time. Even evolving whole blood-based TEG and ROTEM assays that may be performed at the bedside still demand significant operator training. Thiers results are heavily operator-dependent, hard to interpret and are prone to processing/sampling errors (Abdelfattah and Cripps, 2016; Mallett et al., 2013; Whiting and DiNardo, 2014). Several automated technologies have been explored to minimize human errors that complicate existing hemostasis assays.

In Chapter 3, a CPC sensor-based hemostasis assay was introduced and was shown to be sensitive to multiple clotting parameters. The technological superiority of the CPC-based assay compared to existing technologies was summarized in Table 3.5. Its ease of use without the necessity for blood centrifugation, minimal assay steps, high reusability, low-cost and non-contact assessment, makes it an ideal technology for system automation. This chapter presents the development of the first version of a fully automated prototype.

4.1 DESIGN OF THE HEMOSTASIS ANALYZER

The overall workflow for a clotting assay using the CPC sensor system involves the following steps of the following steps:

1. Blood sample collection in standard 3.2 % citrate tube *[5-10 min].*
2. Transporting the sample to the measurement system *[5-30 min, depending on the settings].*
3. Performing the clotting assay *[30 min].*
4. Data analysis for the sensing parameters (T_{Cpeak}, $\Delta C1$, and $\Delta C2$) using an automated algorithm *[< 1 min]*.

In this section, we will present the development of a system to automate steps 3 and 4 in the workflow. The overall 3D design schematic of the analyzer is shown in Fig. 4.1. The prototype system was designed as three subsystems

- Sample and glass vial assembly and discard system
- Orbital shaking system
- Electrical circuitry for automation control and capacitance measurements

This setup separated the operational steps in the assay into individual subsystems to minimize the design complexity and allow for future upgrades.

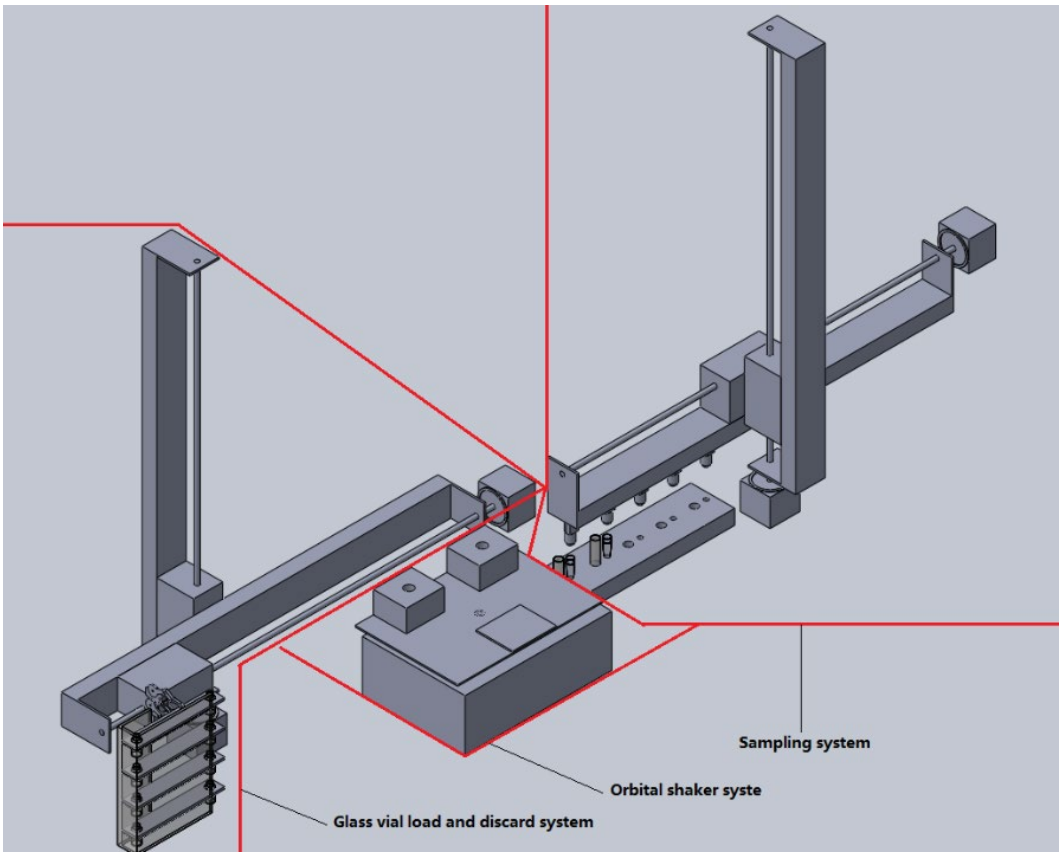

Fig. 4.1. Design of the automated hemostasis analyzer.

4.1.1 Sample and glass vial delivery and discard system

The blood sample for a CPC sensor-based clotting assay is placed in glass vials on top of the sensors. The primary function of this subsystem is to load the glass vials, deliver the blood sample and assay reagent (agonist) to the glass vials and finally discard the vials after measurements. The primary components of this subsystem include

1. 3-axis motorized gantry
2. Electronic pipettes
3. Support fixtures for glass vials and samples.
4. Robotic gripper arm

A commercial gantry system from Opentron was used for a highly precise 3-axis maneuvering. The gantry had an operating dimension of 63*57*66 cm and runs on an AC power source of 240 V. It also had a glass enclosure to provide an isolated testing environment.

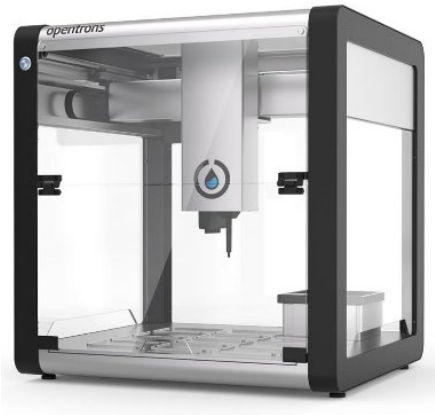

Fig. 4.2. Opentron gantry system.

The robot has slots to attach electronic pipettes for sample aspiration. Two electronic pipettes, one for a blood sample and the other for $CaCl_2$ were attached to the system (Fig. 4.3). The pipettes had an automatic tip loading and ejector mechanism; which enabled hands-free sample aspiration and delivery. The operating volume of the pipettes was 1000 µL for blood samples and 300 µL for $CalCl_2$, with a volume accuracy of ± 2%.

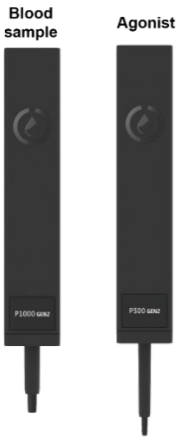

Fig. 4.3. Electronic pipettes.

3D printed fixtures were used to support the glass vials (Fig. 4.4a, b) and sample tubes (Fig. 4.4d). These fixtures precisely controlled the position of the vials on top of the CPC sensor. The support fixture had two openings to load the vials and a cylindrical holder for convenient pick and drop. Pins at the bottom of the fixture precisely positioned the unit on the orbital shaking platform. Before assay, the unit was placed on a 3D printed rack (Fig. 4.4c). The blood sample tubes (3.2 % vacutainer tubes) were placed in a 3D printed rack that can accommodate up to 15 tubes (Fig. 4.4d).

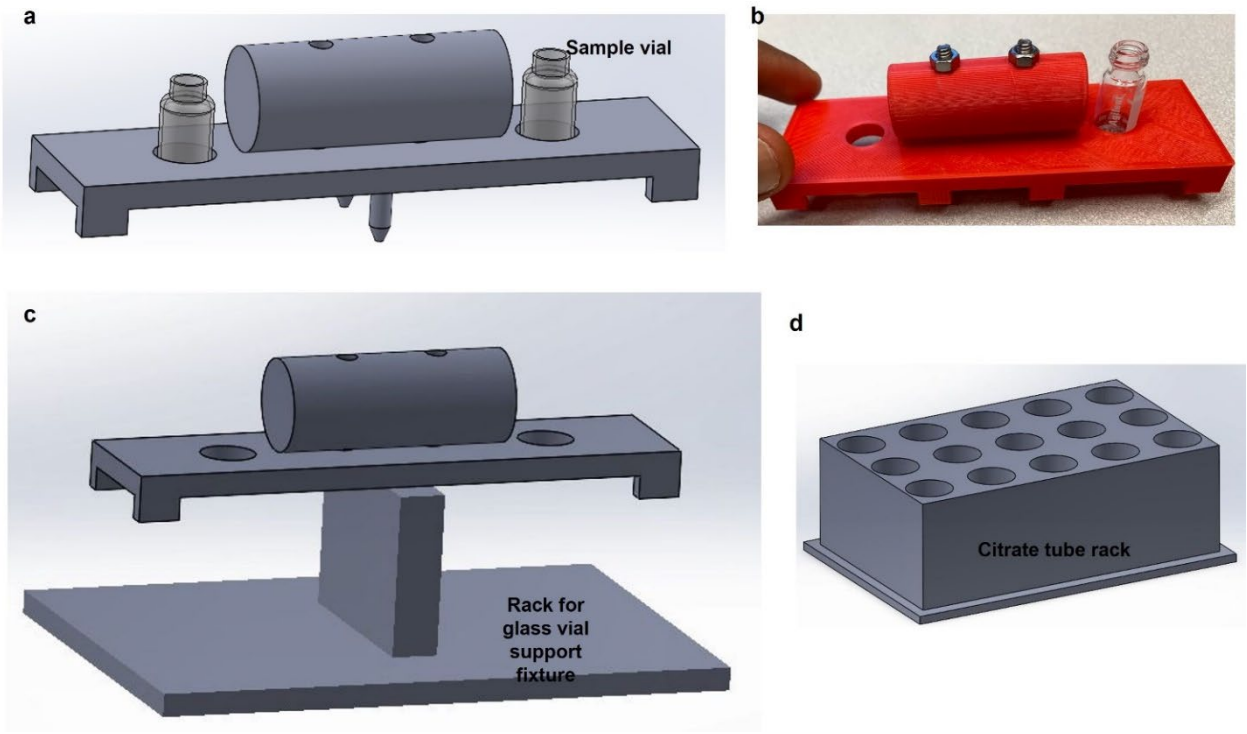

Fig. 4.4. Fixtures for glass vial support and blood sample & reagents.

A robotic claw was used to pick and place the glass vial fixture on the orbital shaking platform. The robotic claw was securely attached to the side of the blood sample pipette using 3D printed connectors. This design enabled both liquid aspiration and glass vials delivery to be controlled using the same gantry system. A tiny servo motor was used to accomplish the claw open-close motion.

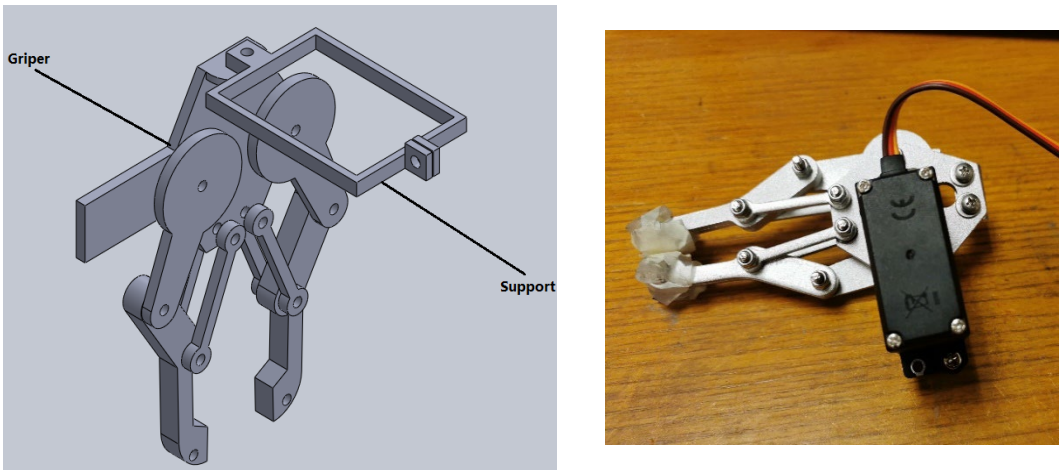

Fig. 4.5. Robotic claw for glass vial support fixture maneuvering.

4.1.2 Orbital shaking system

It was shown in Chapter 3 that to circumvent the reference CPC sensor signal changes during the hemostasis assay, the blood samples need to gently oscillate at 80-rpm. Fig. 4.6 shows the exploded view of the orbital shaker design. The subsystem parts were manufactured using 3D printing techniques.

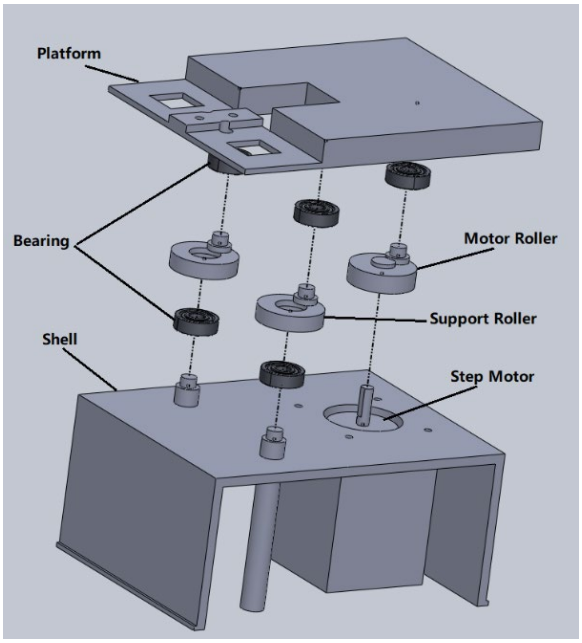

Fig. 4.6. Exploded model view of the orbital shaker components.

The CPC sensors were securely attached to the orbital shaking platform. Ball bearings were used for smooth rotation and the system was driven by a stepper motor with 200 steps/revolution. The orbital diameter was designed to be 22 mm. The stepper motor was operated at 80-rpm but can operate up to 250 rpm. The orbital shaking platform had slots to securely place the glass vial support fixture as shown in Fig. 4.7.

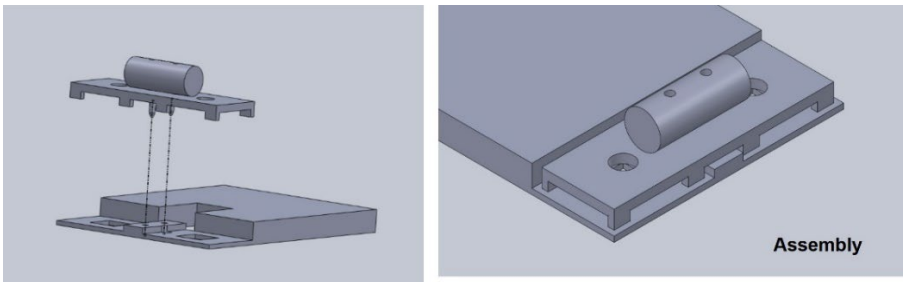

Fig. 4.7. Glass vial support fixture assembly on the orbital shaker.

4.1.3 Capacitance sensing and control system

The sensing unit of the analyzer is the CPC capacitance sensor described in Chapter 3. Two CPC sensors were assembled on the orbital shaking platform. An FDC 2214 evaluation module was used for capacitance measurements. Two 1nF ceramic capacitors were used to obtain a 1.3 MHz operating frequency, which was shown to be sensitive to blood clotting dynamics. A raspberry Pi 4 was used as the main controlling unit including the gantry system and the servo motor through a driver circuit.

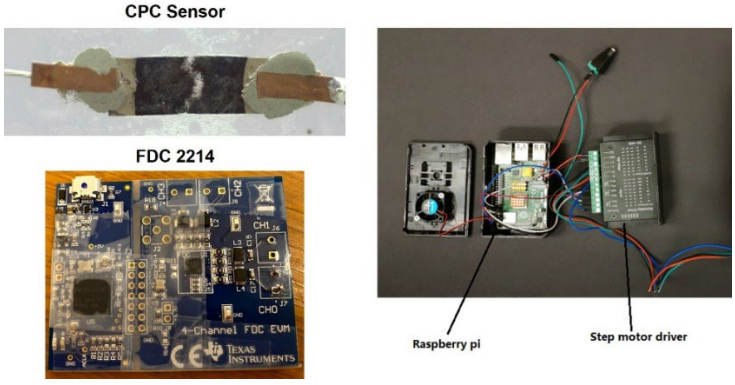

Fig. 4.8. Sensors and electronics for the hemostasis analyzer.

4.2 HEMOSTASIS ANALYZER ASSEMBLY AND OPERATING PROCEDURE

Table 4.6 is the list of all the components of the hemostasis analyzer and their functions.

Table 4.6. Functions and components of the hemostasis analyzer.

Subsystem	Part	Number	Function
Sample and glass vial assembly and discard	Opentron gantry	1	3-axis maneuvering
	Opentron 300μL Pipette and Tips	1	Aspiration and delivery of $CaCl_2$ tips
	Opentron 1000 μL Pipette and Tips	1	Aspiration and delivery of citrated blood samples.
	Support fixture for glass vials	1	Fixture to support and secure the glass vials for blood
	Rack for blood samples		Rack to hold citrate blood tubes
	Robot claw	1	For grabbing and moving glass vial support
	Support for robot claw	1	3D printing structure to secure the claw on the z-axis gantry
	Server Motor	1	MG995 RC, SEAMUING, For driving robot claw
Orbital Shaking System	Shell	1	Enclosure for the orbital shaker
	Bearings	5	Ball bearings for connectors. ID: 8mm, OD: 22mm, Maximum load 310lb for each
	Step motor	1	NEMA 23HS30-3004S, driving the Orbital Shaker rotating
	Platform	1	3D printing structure, for setting blood coagulation sensors
	Support Rollers	2	3D printing structure, connecting bearing platform and shell
	Motor Roller	1	Connecting step motor and platform
Sensing system electronics	CPC capacitance sensor	2	Sensing unit of the analyzer
	FDC 2214 EVM	1	4-channel capacitance measurement module.
	1nF ceramic capacitors	2	To obtain a 1.3 MHz resonant frequency for the L-C oscillator in FDC 2214
	Raspberry Pi 4	1	Controlling step motor drive with wires. Controlling server motor with wires. Controlling OT-2 wirelessly.
	Step motor driver	1	STEPPERONLINE DM542T, for controlling step motor

Fig. 4.9 is the photograph of the automated hemostasis analyzer.

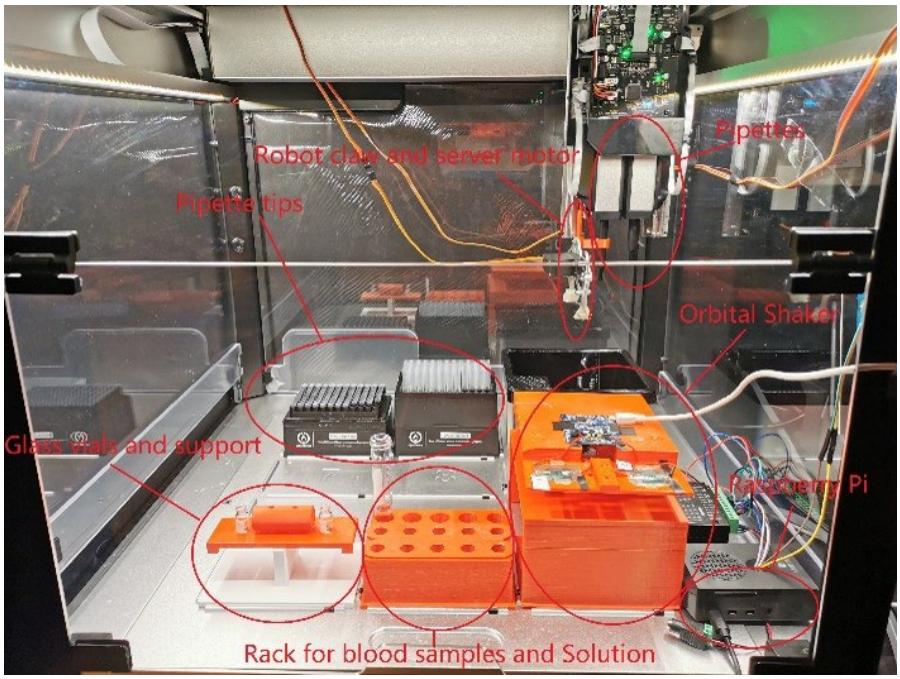

Fig. 4.9. Photograph of the first-generation automated hemostasis analyzer.

The steps involved in a hemostasis assay using the newly developed prototype system

1. Initialize the system (*needs to be performed once at the time of system start-up*)
    a. Coordinate zeroing for the gantry system.
    b. Load the glass vials and the citrated blood sample tube in the respective 3D printed fixtures.
    c. Perform a system warm-up measurement for 5 min.
2. The robotic claw picks up the glass vial fixture and places it on the orbital shaking platform.
3. The gantry system loads the electronic pipettes with the corresponding pipetting tips for both blood sample and $CaCl_2$ solution.

4. 25 µL of $CaCl_2$ is aspirated from a tube and added to the glass vial on the detector CPC sensor.
5. Then, 625 µL of citrated blood sample is aspirated from the blood tube and transferred to the glass vials on the sensors. 325 µL of the blood is delivered to the reference CPC sensor and the remaining 300 µL is added to the detection CPC sensor.
6. Immediately after blood sample delivery, the orbital shaking platform starts rotating at 80-rpm.
7. Detector and reference sensor capacitance were continuously measured through the FDC 2214 evaluation module for 30 min.
8. Finally, the sample holder containing the glass vials is discarded after the measurements.

4.3 Discussion and Conclusion

Recent years have seen an increase in the utilization of robotics for automation in laboratory settings. Automation allows for the successful completion of processes at faster speeds which require a considerable human resource to replicate. It also offers higher levels of process consistency, increases the laboratory throughput, and drastically reduces sampling errors. Traditional hemostasis assays require significant human resources for preparing PRP or PPP samples from whole blood centrifugation. Automating the overall workflow for such assays can be particularly challenging and may not be ideal from a cost perspective. On the other hand, several handheld devices which are easy-to-use with minimal training and no sample processing are currently commercially available (Hughes, 2002). However, they exhibit variable performance and are primarily limited to a specific application such as monitoring patients on warfarin anticoagulant therapy, while other devices have low thromboplastin and partial thromboplastin reagent sensitivity (e.g., i- STAT), resulting in only a crude snapshot of the

coagulation process (Harris et al., 2013). Furthermore, they do not provide information on platelet function or count, resulting in a crude snapshot of the hemostatic status. In comparison, the CPC-based hemostasis does not require any sample processing steps and can provide concurrent information on coagulation function, platelets, and hematocrit.

Using rapid prototyping and commercially available components, the entire CPC-based hemostasis assay was automated with minimal human intervention. However, it is to note that was the first attempt in developing a fully automated prototype and the primary focus was on full automation. There are still numerous improvements that are possible with the system. For example, the overall size of the system could be further miniaturized. This can potentially pay the way for other avenues for applicability such as a small doctor clinic. Secondly, the electrical circuitry for capacitance measurement and control system can be incorporated and further miniaturized into a single custom-made circuit board. Also, the gantry and the orbital shaker platform system could be redesigned with a specific focus on reducing the device footprint. We are also planning the second version of the prototype to be operated on a DC power source which could transition the system from a bench-top analyzer to a portable device. This version could potentially be used at the point-of-injury in a remote battel field or emergency setting or a cruise ship or other low-resource environment. The possibility to integrate an array of CPC capacitance sensors to conduct parallel assays will also be explored in future versions. Parallel clotting assays can expedite the assessment of bleeding risks in patients, who are not easily diagnosed from a single assay.

Chapter 5. CONCLUSIONS AND FUTURE WORK

5.1 CONCLUSION

Health is the eternal theme for human beings. One of the important considerations for well-being is maintaining the fluidity of the blood in our vascular system, to allow for oxygen and nutrient transport to all cells and tissues. Abnormalities or disorders in blood hemostatic potential can lead to pathological conditions including cardiovascular diseases, which have been the leading cause of death worldwide, accounting for nearly 32% of global deaths in 2021 (WHO Fact sheet). To fight against these pathological conditions, innumerable efforts have been made from fundamental biological and pathological research to clinical trials by not only biologists and medical scientists but also engineers all over the world. However, we are still far from an ideal state. Motivated by the importance of having a strong hemostasis assay, two innovative approaches were developed and tested for various hemostatic environments including pathological conditions.

The first approach, described in Chapter 2, was focused on evaluating platelet function using a nano thin-film-based capacitance sensor. Platelets are the primary cellular mediators in hemostasis and abnormalities in their functionality can lead to life-threatening conditions. Below is a summary of this research and the key scientific contributions.

1. Fabrication and biofunctionalization of the nano thin-film capacitance sensor and biofunctionalization

- Conventional microfabrication techniques (top-down approach) were used to fabricate the nano thin-film capacitance sensor. The dual-chip design minimized the

system disposables by avoiding direct sample contact with the bottom chip making it reusable.

- The sensing electrode in the T-chip was biofunctionalized with fibronectin, which allowed for sequential assessment of platelet function for adhesion and after activation.

2. An experimental protocol to evaluate platelet function at multiple functional stages

- The platelet assay offered a multiparameter assessment of platelet function in terms of the hemostatic ability for adhesion, aggregation, granular secretion, and cytoskeletal contraction which was not possible by existing assays.
- Platelet functionality has been successfully decoupled from fibrin formation and plasma clotting factors, resulting in a measurement that is sensitive to several aspects of platelet function.

3. Testing with human plasma samples

- The sensor signal was sensitive to platelet counts, platelet activation levels and multiple activation pathways.
- In comparison to a live microscopy technique, this approach was rapid in differentiating between normal and drug-treated platelets devoid of phototoxic functional inhibition.
- The sensor system could not only differentiate between normal and drug-treated samples but also showed significant differences between the aspirin and ticagrelor drug dosage levels.

3. Key scientific discoveries and contributions from this research

- It was found that a high dose of aspirin (1.3 mM) and ticagrelor (2800 ng ml^{-1}) caused a short-term inhibitory effect in platelet response, but their cumulative long-term antiplatelet effect was similar to the medium doses of the drugs (Aspirin – 0.51 mM; Ticagrelor - 785 ng ml^{-1})
- Aspirin and ticagrelor had a different effective time course of drug action, even though they wielded similar levels of antiplatelet effects.
- High dose (1.3 mM) aspirin inhibits the ability of platelets to attach to FN, which implied that aspirin could have a direct effect on the function of GP IIb/IIIa and GP Ic/IIa receptors.

In conclusion, the presented sensor system along with the standardized experimental and automated data analysis protocol is a promising new diagnostic device for a comprehensive evaluation of platelet function, encompassing multiple aspects of platelet function, in addition to serving as a potential tool for mechanistic studies in the field of experimental hematology and platelet physiology.

The second approach, described in Chapter 3, was a whole-blood-based hemostasis assay, which in addition to evaluating platelet function also assessed the contributions from erythrocytes and coagulation factors in hemostasis. The research summary and scientific findings are listed below.

1. Fabrication, calibration, and characterization of the carbon nanotube paper-composite sensor

- A bottom-up fabrication technique was used to fabricate the low-cost reusable paper-based sensor.

- CPC sensor provided a high fringing field which enabled a non-contact assessment of whole blood hemostasis.
- A differential measurement setup automatically calibrated the system for variations in environmental conditions and biosamples.

2. CPC-based whole blood hemostasis assay

- Clotting measurements at 1.3 MHz provided three sensing parameters, namely T_{Cpeak}, ΔC1 and ΔC2, with high sensitivities toward multiple clotting elements.
- T_{Cpeak} was sensitive to coagulation function.
- ΔC1 was sensitive to both platelet count and platelet function.
- ΔC2 had a strong positive correlation with the hematocrit.
- Additionally, all the sensing parameters, T_{Cpeak}, ΔC1 and ΔC2 showed distinctive sensitivities towards coagulation function, platelet count or function and hematocrit, respectively.

3. Comparison with a conventional thromboelastography (TEG)

- A strong positive correlation with the TEG-Reaction time confirmed the effectiveness of the sensor in assessing coagulation function.
- ΔC1 showed higher sensitivity to platelet count relative to TEG-Maximum Amplitude parameter.

3. Clotting measurements on blood samples with a hemostatic disorder

- T_{Cpeak} was prolonged for hemophilia patient samples.
- ΔC1 was significantly reduced for blood samples with a quantitative platelet disorder (thrombocytopenia).

4. Key findings and contributions from this research

- It was found that coagulation function is impaired in blood samples with a thrombocytopenia (< 50,000 platelets μl^{-1}) condition. This finding indicated that platelets play a multifaceted role in hemostasis.
- Results from a limited number of hemophilia patient samples suggested that platelet function was not significantly impacted by hemophilia conditions.
- It was found that variations in hematocrit in the range (15-50 %) did not affect platelet function and coagulation function.

In this research, a capacitance-based non-contact multiparameter hemostasis assessment was realized for the first time. Multiple key clotting biomarkers were evaluated simultaneously with high sensitivity & accuracy. The sensor system can potentially be realized as an automated hemostasis analyzer.

In Chapter 4, the development of a fully automated prototype of the hemostasis analyzer was presented. The system components were designed using conventional solid modeling software and fabricated using rapid prototyping techniques. The CPC-based hemostasis assay was completely automated in the presented system. Further system optimizations with a focus on miniaturization and portability will be explored in future work.

5.2 FUTURE WORK

The future work will be primarily focused on the following aspects.

1. Scientific explorations with the CPC capacitance sensor
2. Optimization of the performance of the novel multiparameter hemostasis assays
3. Development of a market fit, the second generation of the hemostasis analyzer for clinical studies

4. Extensive clinical evaluation (clinical trials) to establish the functional equivalence of the assay to existing FDA-approved assays/devices.

More details about each work have been listed below

5.2.1 Scientific explorations with the CPC capacitance sensor

The CPC sensor-based hemostasis assessments were shown to be sensitive to coagulation function, platelet function, platelet count and hematocrit. Another key hematological parameter is fibrinogen. During a thrombus formation, plasma fibrinogen is converted to fibrin which is critical for rapid encapsulation of blood cells and the propagation of platelet contractile forces (Michelson, 2019; Sørensen et al., 2011; Versteeg et al., 2013). The impact of fibrinogen variations in the CPC sensor responses will be explored in a future study. A plausible approach for this study would be to obtain fibrinogen-depleted plasma samples and artificially spike them with a predefined concentration of the protein.

On the other hand, various other blood physiological parameters such as blood types, concentration of ions (such as Na^{+}, Ca^{2+} and K^{+}), proteins (such as albumin) and vitamins (such as Vitamin K) may also have an impact on blood hemostatic ability (Chakraverty et al., 1996; Gissel et al., 2016; Mann, 1999; Rasmussen et al., 2016). Variations in these parameters could also influence the inferences from the CPC-based hemostasis assays. In future work, we plan to systematically study the effects of these parameters and further explore the ability of the sensor to diagnose pathological conditions arising from abnormalities in these parameters.

5.2.2 Optimization of the performance of the novel multiparameter hemostasis assay

The studies in this aim will be designed to optimize the performance of the novel simultaneous multiparameter hemostasis assay. Specifically, studies will be conducted to optimize the assay performance for linearity, detection limits, precisions, the saturation cut-offs for all the assay parameters, and the impact of interferences. The plan is to use blood samples from human subjects modulated for desired platelet count, platelet function, clotting factors, and hematocrit. After this, the second main goal for this aim is to further reduce the hemostasis assay time by half from 30 min to 10-15 min. A pilot study on a small number of human samples will be conducted to confirm that the reduction in assay time does not have any impact on the performance.

5.2.3 Development of a market fit, the second generation of the hemostasis analyzer for clinical studies

There are numerous improvements possible in the first version of the system. To begin with, the overall size of the system could be further miniaturized. Secondly, the electrical circuitry for capacitance measurement and control system of the analyzer could be incorporated into a single custom-made circuit board. The system components could be redesigned with an optimization focus on the device footprint. We are also planning the second generation of the system to be operated on a DC power source, transitioning from a bench-top to a portable analyzer. This version could potentially be used at the point-of-injury in a remote battel field or emergency setting or a cruise ship or any low-resource environment. The possibility to integrate an array of CPC capacitance sensors to conduct parallel assays, to increase the device throughput will also be considered in the next version.

5.2.4 Extensive clinical evaluation (clinical trials) to establish the functional equivalence of the assay to existing FDA-approved assays/devices.

Any new biological assay or a device needs to be subjected to an extensive series of clinical tests to evaluate their applicability for a wide-ranging human population. The plan is to perform multiple center-clinical studies to establish the functional equivalence of the technology to existing FDA-approved assays/devices. Specifically, we will compare the results from our assay with commercially available assays such as thromboelastography (TEG) analyzer and automated CBC analyzer. User indication and clinical settings will be established. The results of these clinical studies will be used for seeking FDA approval. Table 5.7 is the compilation of the focus areas we are currently planning to evaluate the device applicability, and the roadmap to realize the plan.

Table 5.7. Focus areas and study plan.

Focus Areas	Action items	Plan
Emergency Rooms Urgent care and Outpatient Clinic Triage	Optimize the existing device function such as linear range, precision, repeatability, and reproducibility of the output parameters	Establish the range and linearity for the sensor parameters: • T_{Cpeak} (coagulation time) • *ΔC1 (Platelet count)* and • *ΔC2 (Hematocrit)*
	Optimize the system design	Further miniaturization of the analyzer. **Target size - 30 x 30 x 30 cm**
	Funding agencies	STTR grant application
Management of patients with acute bleeding and assist with blood product replacement therapy	Understand fibrinogen impact	Test blood samples artificially spiked with a predefined fibrinogen concentration
	Substantial functional equivalence determination	Establish a relationship with UW-RTS or Bloodworks NW to perform concurrent thromboelastography (TEG) measurements
Remote setting such as battlefield, cruise ship, and other low-resource settings	Optimize the system design for portability	Develop a DC battery version of the system - Modify the electrical circuitry for the control system. - Bluetooth operated data transfer to a smartphone/tablet - Data analysis in either a smartphone or inboard processor
	Funding agencies	BARDA, DoD

APPENDIX

A Data analysis routine for capacitance signal markers from platelet function assay:

```
# In[ ]:
import numpy as np
import pandas as pd
pd.set_option("display.max_rows",1000)    # or pd.options.display.max_rows=1000
pd.set_option("display.max_columns",200)   # or
pd.options.display.max_columns=20
pd.set_option('precision',3)
pd.set_option('large_repr', 'truncate')
import os
import warnings
warnings.filterwarnings('ignore')
import errno
notebook_version = 1.5
print('Notebook version: ',notebook_version)
from IPython.core.interactiveshell import InteractiveShell
InteractiveShell.ast_node_interactivity = "all"


# In[ ]: Make a new folder function
def make_folder(path):
    '''Create new path if it does not already exist'''
    try:
        os.makedirs(path)
    except OSError as e:
        if (e.errno != errno.EEXIST):
            raise
# In[ ]: Range
def drange(start, stop, step):
    r = start
    while r < stop:
        return r
        r += step
# In[ ]:
# Setup the folder and data file
basefolder=r'C:\Users\PRAVE\Google Drive\python codes\Measurement'
currentrun='Thrombin'
testrun='PC2_5E5'
fname='Trail1.csv'
path=basefolder+'\\'+currentrun+'\\'+testrun
os.chdir(path)
```

```
    df=pd.read_csv(fname,index_col=0) # read data and put it into a dataframe
(dataframe=matrix in python)

    # Output folder setup
    output_folder=os.path.join(basefolder,'Processed files')
    make_folder(output_folder)
    os.chdir(output_folder)
    df.to_csv('Trail 2.tsv',sep='\t',index=False)
    # In[ ]:
    df.head() # first 5 lines of the dataframe
    # In[ ]:
    # specify the time points(in secs) for addition of PRP and agonist
    # baseline=300
    # adhesion_time = 1800
    # washout=600
    # contractile=5400
    # convert mins on timer to sec eg 5 min 40 secs = 340 sec
    # In[ ]:
    t_prp = 302 # time point of addition of PRP in secs (make sure all PRP is added into
the well)
    t_ag = 2720 # addition of agonist in secs (first spike while adding Agonist)
    tm=[0]
    z=0;
    for x in list(range(1,len(df))):
        y=z+0.129 # datalogging frequency (depends on the LCR meter, 4980AL)
        tm.append(y)
        z=y
    df['Time']= tm
    # In[ ]:
    df.head() # first 5 lines of the dataframe-checking for time column
    # In[ ]:
    # seperate the data into three different dataframes
    # baseline : before the addition of PRP
    # Adhesion: 30 mins after addition of PRP
    # Cont: 5 mins before the addition of Ag
    # In[ ]:
    base_df=df[(df['Time']<(t_prp-5))]
    adhesion_df=df[(df['Time']>t_prp) & (df['Time']<(t_prp+1780))] # discard last 20
sec of adhesion
    activation_df=df[(df['Time']>(t_ag-300))] # include 300 secs (5min) before addition
of agonist in the data frame
    # In[ ]:
    # Adding a scaled capacitance column for adhesion dataframe
    adhesion_df['Delta C']=adhesion_df['Capacitance']-
adhesion_df['Capacitance'].iloc[0]
    adhesion_df['Delta t']=adhesion_df['Time']-adhesion_df['Time'].iloc[0]
```

```
    adhesion_df.plot(x='Delta t',y='Delta C',color='blue')
    # In[ ]:
    # Calculating adhesion data variables - Max and rate of change of capacitance
    slp_region=adhesion_df[(adhesion_df['Time']>300) & (adhesion_df['Time']< 900)]
#slope region 300 - 900 sec after PRP addition
    rt_adhesion,b=np.polyfit(slp_region['Time'],slp_region['Capacitance'],1)
    delta_adhesion=adhesion_df['Capacitance'].iloc[0:80].mean() -
adhesion_df['Capacitance'].iloc[-80:].mean()
    print("Change in Capacitance:",format(delta_adhesion,'.4g'))
    print("Rate of change in Capacitance: ",format(abs(rt_adhesion),'.4g'))
    # In[ ]:
    # Adding a scaled capacitance column for activation dataframe
    activation_df['Delta C']=activation_df['Capacitance']-
activation_df['Capacitance'].iloc[0]
    activation_df['Delta t']=activation_df['Time']-activation_df['Time'].iloc[0]
    activation_df.plot(x='Delta t',y='Delta C',color='red')
    # In[ ]:
    # Calculating activation data variables - Max and rate of change of capacitance
    activation_slp_region=activation_df[(activation_df['Delta t']>500) &
(activation_df['Delta t']<550)]

    # 200-250 sec after addition of agonist (300 sec data added before, so 500-550)
    p1=np.polyfit(activation_slp_region['Time'],activation_slp_region['Capacitance'],2)
    p2=([2*p1[0],p1[1]])
    sl=np.polyval(p2,(activation_slp_region['Delta t']))
    rt_capacitance=abs(np.mean(sl))
    delta_activation=activation_df['Capacitance'].iloc[0:80].mean() -
activation_df['Capacitance'].iloc[-80:].mean()
    #trendpoly=np.poly1d(p1)

    print("Change in Capacitance: ",format(delta_activation,'.4g'))
    print("Rate of change in Capacitance: ",format(rt_capacitance,'.4g'))
    # In[ ]:
    # Overall data
    df.plot(x='Time',y='Capacitance')
```

B Data analysis code for whole blood hemostasis assay

```
# In[ ]:
import numpy as np
import pandas as pd
pd.set_option("display.max_rows",1000)    # or pd.options.display.max_rows=1000
pd.set_option("display.max_columns",200)   # or pd.options.display.max_columns=20
pd.set_option('precision',5)
pd.set_option('large_repr', 'truncate')
```

```
import os
import warnings
warnings.filterwarnings('ignore')
import errno
notebook_version = 1.5
print('Notebook version: ',notebook_version)
from IPython.core.interactiveshell import InteractiveShell
InteractiveShell.ast_node_interactivity = "all"
# In[ ]:
def make_folder(path):
    '''Create new path if it does not already exist'''
    try:
        os.makedirs(path)
    except OSError as e:
        if (e.errno != errno.EEXIST):
            raise
# In[ ]:
def drange(start, stop, step):
    r = start
    while r < stop:
        return r
        r += step
# In[ ]:
basefolder=r'C:\Users\Praveen\Documents\Data'
fname='Trail2.xlsx'
pt=basefolder
currentrun ='Aspirin'
testrun='Highdose'
path=basefolder+'\\'+currentrun+'\\'+testrun
os.chdir(path)
df=pd.read_excel(fname,index_col=0)

output_folder=os.path.join(path,'Processed files')
make_folder(output_folder)
os.chdir(output_folder)
#df.to_csv('Trail2.tsv',sep='\t',index=False)
# In[ ]:
df.head()
# In[ ]:
tm=[0]
z=0;
for x in list(range(1,len(df))):
    y=z+0.0005
    tm.append(y)
    z=y
df['Time(min)']= tm
```

```
# In[ ]:
df['Diff_C']=df['DATA0_pF']-df['DATA1_pF']
df=df.drop(columns=['evmSampleDeltaMs','logDeltaMs','DATA2_pF','DATA3_pF','DAT
A0','DATA1','DATA2','DATA3','DATA0_MHz','DATA1_MHz','DATA2_MHz','DATA3_M
Hz'])
# In[ ]:
df.head()
# In[ ]:
#df.plot(x='Time(sec)',y=['Data0_pF','Data1_pF'])
# # specify the time point for the addition of both the liquids in row number
# In[ ]:
# as row number
df_copy=df.iloc[10000:]
df_copy.head()
# In[ ]:
df_copy['Scaled Diff_C']=df_copy['Diff_C']-df_copy['Diff_C'].iloc[0]
df_copy['Scaled Time(min)']=df_copy['Time(min)']-df_copy['Time(min)'].iloc[0]
# In[ ]:
df_copy.head()
# In[ ]:
DeltaC1=df_copy['Scaled Diff_C'].max()
TCpeak_index=df_copy['Scaled Diff_C'].idxmax()
TCpeak=df_copy['Scaled Time(min)'].iloc[TCpeak_index]
DeltaC2=DeltaC1 - df_copy['Scaled Diff_C'].iloc[56000:].mean()
# In[ ]:
DeltaC1
# In[ ]:
TCpeak
# In[ ]:
DeltaC2
# In[ ]:
df_copy.to_csv('Tissuepaper_Trail 1_processed.tsv',sep='\t',index=False)
```

C Control codes for automated hemostasis analyzer

C.1 OT-2 Gantry Initialization

```
from opentrons import protocol_api, types
from opentrons.types import Point, Mount
from opentrons.hardware_control.types import Axis
from time import sleep
metadata = {'apiLevel': '2.9'}
def run_position(protocol):

protocol._implementation.get_hardware().hardware.current_position(mount=Mount.RIG
HT)
```

```
    protocol._implementation.get_hardware().hardware.move_rel(mount=Mount.RIGHT,
delta=Point(x=0, y=0, z=-10))
protocol._implementation.get_hardware().hardware.current_position(mount=Mount.LE
FT)
    protocol._implementation.get_hardware().hardware.move_rel(mount=Mount.LEFT,
delta=Point(x=0, y=0, z=-10))
def run(protocol: protocol_api.ProtocolContext):
    try:
        plate = protocol.load_labware('opentrons_15_tuberack_falcon_15ml_conical', 2)
#define tube rack
        tiprack_300 = protocol.load_labware('opentrons_96_tiprack_300ul', 10)
#define pipettes
        tiprack_1000 = protocol.load_labware('opentrons_96_tiprack_1000ul', 11)

        pipette_right = protocol.load_instrument('p1000_single', 'right',
tip_racks=[tiprack_1000])     #define pipette tips rack
        pipette_left = protocol.load_instrument('p300_single', 'left',
tip_racks=[tiprack_300])
        #pipette.aspirate(100, plate.wells('A1'))
        #pipette_right.aspirate(100, plate['A1'])
        # define speed
        pipette_left.default_speed = 100
        pipette_right.default_speed = 100

        # define griper
        Griper_offset_x = -24.0
        Griper_offset_y = 19.0
        Griper_offset_z = -45.0
       # grab vials
        print('start moving to grab')
        pipette_left.move_to(protocol.deck.position_for('1').move(types.Point(z=170)))  #
move to slot 1 maximum height 170
        # Move to the position to grab
        grab_move_x = 63.8
        grab_move_y = 42.3
        grab_move_z = -112.0
        protocol._implementation.get_hardware().hardware.move_rel(mount=Mount.LEFT,
delta=Point(x=0, y=grab_move_y – Griper_offset_y, z=0), speed=100.0)
        protocol._implementation.get_hardware().hardware.move_rel(mount=Mount.LEFT,
delta=Point(x=grab_move_x – Griper_offset_x, y=0, z=0), speed=100.0)
        protocol._implementation.get_hardware().hardware.move_rel(mount=Mount.LEFT,
delta=Point(x=0, y=0, z=grab_move_z – Griper_offset_z), speed=60.0)
        print('grab finish')
        sleep(5)
        protocol._implementation.get_hardware().hardware.move_rel(mount=Mount.LEFT,
delta=Point(x=0, y=0, z=-(grab_move_z – Griper_offset_z)), speed=60.0)
```

```
    # load vials
    print('start moving to load')
    # Move to 50mm above the front left of slot 1
    pipette_left.default_speed = 20
    pipette_left.move_to(protocol.deck.position_for('2').move(types.Point(z=170)))
    protocol._implementation.get_hardware().hardware.move_rel(mount=Mount.LEFT,
delta=Point(x=0, y=0, z=30.0), speed=10.0)
    # Move to the position to load
    load_move_x = 63.8 + 134.5 #63.8+132
    load_move_y = 22.7
    load_move_z = -68  # 55 for test 64 for load
    protocol._implementation.get_hardware().hardware.move_rel(mount=Mount.LEFT,
delta=Point(x=load_move_x – Griper_offset_x, y=0, z=0), speed=40.0)
    protocol._implementation.get_hardware().hardware.move_rel(mount=Mount.LEFT,
delta=Point(x=0, y=load_move_y – Griper_offset_y, z=0), speed=10.0)
    sleep (2)
    protocol._implementation.get_hardware().hardware.move_rel(mount=Mount.LEFT,
delta=Point(x=0, y=0, z=load_move_z – Griper_offset_z), speed=10.0)
    sleep(7)
    print('load finish')
    protocol._implementation.get_hardware().hardware.move_rel(mount=Mount.LEFT,
delta=Point(x=0, y=0, z=-(load_move_z – Griper_offset_z)), speed=10.0)
    pipette_left.default_speed = 100
    pipette_left.move_to(protocol.deck.position_for('5').move(types.Point(z=170)))
    #upload tips
    pipette_left.pick_up_tip(tiprack_300['A1'])
    pipette_right.pick_up_tip(tiprack_1000['A1'])
    # aspirating
    aspirate_left_move_x = 13.3
    aspirate_left_move_y = 67.8
    pipette_left.default_speed = 100
    pipette_left.move_to(protocol.deck.position_for('2').move(types.Point(z=140)))
    protocol._implementation.get_hardware().hardware.move_rel(mount=Mount.LEFT,
delta=Point(x=0, y=aspirate_left_move_y, z=0), speed=100.0)
    protocol._implementation.get_hardware().hardware.move_rel(mount=Mount.LEFT,
delta=Point(x=aspirate_left_move_x, y=0, z=0), speed=100.0)
protocol._implementation.get_hardware().hardware.prepare_for_aspirate(mount=Moun
t.LEFT, rate = 1.0)
    protocol._implementation.get_hardware().hardware.move_rel(mount=Mount.LEFT,
delta=Point(x=0, y=0, z=-120), speed=100.0)
    protocol._implementation.get_hardware().hardware.aspirate(mount=Mount.LEFT,
volume = 25.0, rate = 1.0)
    sleep(2)
    pipette_right.aspirate(625, plate['A2'])  #aspiratre 625ul blood
```

```
protocol._implementation.get_hardware().hardware.move_rel(mount=Mount.RIGHT,
delta=Point(x=0, y=0, z=50), speed=50.0)
    sleep(4)

    # pipetting CaCl2
    pipette_left_move_x = 27.8
    pipette_left_move_y = 22.8
    pipette_left.move_to(protocol.deck.position_for('3').move(types.Point(z=140)))
    protocol._implementation.get_hardware().hardware.move_rel(mount=Mount.LEFT,
delta=Point(x=0, y=pipette_left_move_y, z=0), speed=100.0)
    protocol._implementation.get_hardware().hardware.move_rel(mount=Mount.LEFT,
delta=Point(x=pipette_left_move_x, y=0, z=0), speed=100.0)
    protocol._implementation.get_hardware().hardware.move_rel(mount=Mount.LEFT,
delta=Point(x=0, y=0, z=-20), speed=10.0)

protocol._implementation.get_hardware().hardware.blow_out(mount=Mount.LEFT)
    protocol._implementation.get_hardware().hardware.move_rel(mount=Mount.LEFT,
delta=Point(x=0, y=0, z=20), speed=200.0)
    protocol._implementation.get_hardware().hardware.move_rel(mount=Mount.LEFT,
delta=Point(x=0, y=0, z=-5), speed=200.0)
    protocol._implementation.get_hardware().hardware.move_rel(mount=Mount.LEFT,
delta=Point(x=0, y=0, z=5), speed=200.0)
    protocol._implementation.get_hardware().hardware.move_rel(mount=Mount.LEFT,
delta=Point(x=0, y=0, z=-5), speed=200.0)
    protocol._implementation.get_hardware().hardware.move_rel(mount=Mount.LEFT,
delta=Point(x=0, y=0, z=5), speed=200.0)

# pipetting blood
    pipette_right_move_x = 100.2
    pipette_right_move_y = 22.8
    pipette_right.move_to(protocol.deck.position_for('3').move(types.Point(z=140)))

protocol._implementation.get_hardware().hardware.move_rel(mount=Mount.RIGHT,
delta=Point(x=0, y=0, z=3), speed=10.0)

protocol._implementation.get_hardware().hardware.move_rel(mount=Mount.RIGHT,
delta=Point(x=0, y=pipette_right_move_y, z=0), speed=100.0)

protocol._implementation.get_hardware().hardware.move_rel(mount=Mount.RIGHT,
delta=Point(x=pipette_right_move_x, y=0, z=0), speed=100.0)

protocol._implementation.get_hardware().hardware.move_rel(mount=Mount.RIGHT,
delta=Point(x=0, y=0, z=-20), speed=10.0)
```

```
protocol._implementation.get_hardware().hardware.dispense(mount=Mount.RIGHT,
volume = 325.0, rate = 1.0)

protocol._implementation.get_hardware().hardware.move_rel(mount=Mount.RIGHT,
delta=Point(x=0, y=0, z=20), speed=200.0)

protocol._implementation.get_hardware().hardware.move_rel(mount=Mount.RIGHT,
delta=Point(x=0, y=0, z=-5), speed=200.0)

protocol._implementation.get_hardware().hardware.move_rel(mount=Mount.RIGHT,
delta=Point(x=0, y=0, z=5), speed=200.0)

protocol._implementation.get_hardware().hardware.move_rel(mount=Mount.RIGHT,
delta=Point(x=0, y=0, z=-5), speed=200.0)

protocol._implementation.get_hardware().hardware.move_rel(mount=Mount.RIGHT,
delta=Point(x=0, y=0, z=5), speed=200.0)   # shaking

protocol._implementation.get_hardware().hardware.move_rel(mount=Mount.RIGHT,
delta=Point(x=-71.5, y=0, z=0), speed=100.0)

protocol._implementation.get_hardware().hardware.move_rel(mount=Mount.RIGHT,
delta=Point(x=0, y=0, z=-20), speed=10.0)

protocol._implementation.get_hardware().hardware.dispense(mount=Mount.RIGHT,
volume = 300.0, rate = 1.0)

protocol._implementation.get_hardware().hardware.move_rel(mount=Mount.RIGHT,
delta=Point(x=0, y=0, z=20), speed=200.0)

protocol._implementation.get_hardware().hardware.move_rel(mount=Mount.RIGHT,
delta=Point(x=0, y=0, z=-5), speed=200.0)

protocol._implementation.get_hardware().hardware.move_rel(mount=Mount.RIGHT,
delta=Point(x=0, y=0, z=5), speed=200.0)

protocol._implementation.get_hardware().hardware.move_rel(mount=Mount.RIGHT,
delta=Point(x=0, y=0, z=-5), speed=200.0)

protocol._implementation.get_hardware().hardware.move_rel(mount=Mount.RIGHT,
delta=Point(x=0, y=0, z=5), speed=200.0)
      pipette_left.drop_tip()    #left discard tip
      pipette_right.drop_tip()    #right discard tip
      protocol.home()            # home
   except:
```

```
    pipette_left.default_speed = 100
    pipette_left.move_to(protocol.deck.position_for('5').move(types.Point(z=170)))
    protocol.home()
```

C.2 Hemostasis assay

```
import RPi.GPIO as GPIO
from time import sleep
from time import time
import os
from subprocess import call

GRIP_PIN = 12
DIR_PIN = 2   # Direction GPIO Pin
STEP_PIN = 27  # Step GPIO Pin
CW = 1     # Clockwise Rotation
CCW = 0    # Counterclockwise Rotation
SPR = 200   # Steps per Revolution (360 / 7.5)
step_size = 8
GPIO.setmode(GPIO.BCM)
GPIO.setup(GRIP_PIN, GPIO.OUT)
pwm=GPIO.PWM(GRIP_PIN, 50)
pwm.start(0)
GPIO.setup(DIR_PIN, GPIO.OUT)
GPIO.setup(STEP_PIN, GPIO.OUT)
GPIO.output(DIR_PIN, CCW)
step_count = SPR*step_size
delay = .25/step_count
print(delay)
Angle_grab = 72  #angle of grab
Angle_put = 0   #angle of discard

# define server motor
def SetAngle(angle):
    duty = angle / 18 + 2.5
    #GPIO.output(03, True)
    pwm.ChangeDutyCycle(duty)
    sleep(1)
    #GPIO.output(03, False)

# define step motor
def Rotate(time_length, dir):
    time_start = time()
    time_now = time()
    time_span = time_now - time_start
    GPIO.output(DIR_PIN, dir)
```

```
    while (time_span < time_length):
        for x in range(step_count):
            # move backward
            GPIO.output(STEP_PIN, GPIO.HIGH)
            sleep(delay)
            GPIO.output(STEP_PIN, GPIO.LOW)
            sleep(delay)
        time_pre = time_now
        time_now = time()
        time_span = time_now - time_start
        speed_RPM = 1/(time_now - time_pre)*60
        print("Rotational Speed: %s RPM" %(speed_RPM))

sleep(5)

# start OT-2 load glass vials
call(["gnome-terminal","-e","ssh -i ot2_ssh_key root@192.168.0.107 \"sh -l -c
'opentrons_execute /data/user_storage/coagulation_test_1.py '\""])

sleep(42)
# grab and put glass vials
SetAngle(Angle_grab)  # grab
sleep(20)
SetAngle(Angle_put)  # put
pwm.ChangeDutyCycle(0)  #zero
sleep(73)
Rotate(1800,CCW)

# start OT-2 discard glass vials
call(["gnome-terminal","-e","ssh -i ot2_ssh_key root@192.168.0.107 \"sh -l -c
'opentrons_execute /data/user_storage/coagulation_discard_1.py '\""])

sleep(45)
SetAngle(Angle_grab) # grab

sleep(23)
SetAngle(Angle_put) # descard
pwm.ChangeDutyCycle(0)

pwm.stop()
GPIO.cleanup()
```

VITA

Praveen K. Sekar was a Ph.D. candidate, working under the guidance of Prof. Dayong Gao at the University of Washington – Mechanical Engineering at the time of authoring this thesis. During his research training in Dr. Gao's lab, Praveen worked on developing micro-sensors for bio-medical application including hemostasis assessment and cryopreservation. His work resulted in publishing 9 journals, 2 conference proceedings, 1 book chapter and 1 pending patent application (Google Scholar). Apart from research and technology development in an academic setting, he has also worked in the R&D departments of four multinational companies.

BIBLIOGRAPHY

Abdalla, S., 2011. . AIP Adv. 1, 012104.

Abdelfattah, K., Cripps, M.W., 2016. . Int. J. Surg. 33, 196–201.

Adcock Funk, D.M., Lippi, G., Favaloro, E.J., 2012. . Semin. Thromb. Hemost. 38, 576–585.

Ageno, W., Gallus, A.S., Wittkowsky, A., Crowther, M., Hylek, E.M., Palareti, G., 2012. . Chest 141, e44S-e88S.

Ahrens, I., Lip, G.Y.H., Peter, K., 2010. . Thromb. Haemost. 104, 49–60.

Aktas, B., Pozgajova, M., Bergmeier, W., Sunnarborg, S., Offermanns, S., Lee, D., Wagner, D.D., Nieswandt, B., 2005. . J. Biol. Chem. 280, 39716–39722.

Angiolillo, D.J., 2009. . Am. J. Cardiol. 103, 27A-34A.

Annich, G.M., 2015. . J. Thromb. Haemost.

Asami, K., Hanai, T., 1992. . Colloid Polym. Sci. 270, 78–84.

Asami, K., Sekine, K., 2007. . J. Phys. D. Appl. Phys. 40, 2197–2204.

Baron, T.H., Kamath, P.S., McBane, R.D., 2013. . N. Engl. J. Med. 368, 2113–2124.

Baughman, R.R., Lower, E.E., Flessa, H.C., Tollerud, D.J., 1993. . Chest 104, 1243–1247.

Bäumler, H., Neu, B., Donath, E., Kiesewetter, H., 1999. . Biorheology 36, 439–442.

Becker, R.C., Voora, D., Shah, S.H., 2013. , in: Genomic and Personalized Medicine. Lippincott Williams & Wilkins, pp. 602–611.

Bhatt, D L, Topol, E.J., 2003. . Nat. Rev. Drug Discov. 2, 15–28.

Bhatt, Deepak L., Topol, E.J., 2003. . Nat. Rev. Drug Discov. 2, 15–28.

Blumberg, N., Heal, J.M., Phillips, G.L., 2010. . F1000 Med. Rep. 2.

Bolliger, D., Seeberger, M.D., Tanaka, K.A., 2012. . Transfus. Med. Rev. 26, 1–13.

Briggs, C., 2009. . Int. J. Lab. Hematol. 31, 277–97.

Carll, T., Wool, G.D., 2020. . Transfusion 60, S1–S9.

Chakraverty, R., Davidson, S., Peggs, K., Stross, P., Garrard, C., Littlewood, T.J., 1996. . Br. J. Haematol. 93, 460–463.

Chee, Y.-L., Greaves, M., 2003. . Hematol. J. 4, 373–378.

Chelidze, T., 2002. . J. Non. Cryst. Solids 305, 285–294.

Chen, A., Stecker, E., Warden, B.A., 2020. . J. Am. Heart Assoc. 9, 17559.

Chen, D., Song, S., Ma, J., Zhang, Z., Wang, P., Liu, W., Guo, Q., 2017. . Biosens. Bioelectron. 91, 465–471.

Chen, X., Wang, M., Zhao, G., 2020. . ACS Sensors 5, 282–291.

Chiba, S., Uchibori, K., Fujiwara, T., Ogata, T., Yamauchi, S., Shirai, T., Masuo, M., Okamoto, T., Tateishi, T., Furusawa, H., Fujie, T., Sakashita, H., Tsuchiya, K., Tamaoka, M., Miyazaki, Y., Inase, N., Sumi, Y., 2015. . J. Sci. Res. Reports 4, 180–188.

CHO, J., MOSHER, D.F., 2006. . J. Thromb. Haemost. 4, 1461–1469.

Chowdhury, A.D., Takemura, K., Li, T.-C., Suzuki, T., Park, E.Y., 2019. . Nat. Commun. 10, 3737.

Collet, J.-P., Montalescot, G., 2009. . J. Cardiovasc. Pharmacol. Ther. 14, 157–169.

Cotton, B., Holcomb, J.B., Pommerening, M., Jastrow, K., Kozar, R.A., 2015. , in: Brunicardi, F.C., Andersen, D.K., Billiar, T.R., Dunn, D.L., Hunter, J.G., Matthews, J.B., Pollock, R.E. (Eds.), Schwartz's Principles of Surgery, 10e. McGraw-Hill Education, New York, NY.

Cui, F., Zhou, Z., Zhou, H.S., 2020. . J. Electrochem. Soc. 167, 037525.

Dahlbäck, B., 2000. . Lancet 355, 1627–1632.
Davie, E.W., Kulman, J.D., 2006. . Semin Thromb Hemost 32 Suppl 1, 3–15.
Dichiara, A.B., Song, A., Goodman, S.M., He, D., Bai, J., 2017. . J. Mater. Chem. A 5, 20161–20169.
Drelich, D.A., Bray, P.F., 2015. The Traditional Role of Platelets in Hemostasis, The Non-Thrombotic Role of Platelets in Health and Disease.
Durila, M., Kalinčík, T., Jurčenko, S., Pelichovská, M., Hadačová, I., Cvachovec, K., 2010. . Blood Coagul. Fibrinolysis 21, 770–774.
Elad, D., Einav, S., 2004. . Chapter 3 Phys. FLOW Prop. BLOOD.
Ertürk, G., Mattiasson, B., 2017. . Sensors 17, 390.
Frenette, P.S., Johnson, R.C., Hynes, R.O., Wagner, D.D., 1995. . Proc Natl Acad Sci U S A 92, 7450–7454.
Fuentes, E., Palomo, I., 2014. . J. Funct. Foods.
Gale, A.J., 2011. . Toxicol. Pathol.
Ganter, M.T., Hofer, C.K., 2008. . Anesth. Analg. 106, 1366–1375.
Gauer, R.L., Braun, M.M., 2012. . Am. Fam. Physician 85, 612–22.
Gavish, N., Promislow, K., 2016. . Phys. Rev. E 94, 1–14.
George, J.N., 2000. . Lancet 355, 1531–1539.
Gillissen, A., Van Den Akker, T., Caram-Deelder, C., Henriquez, D.D.C.A., Bloemenkamp, K.W.M., De Maat, M.P.M., Van Roosmalen, J.J.M., Zwart, J.J., Eikenboom, J., Van Der Bom, J.G., 2018. . Blood Adv. 2, 2433–2442.
Gissel, M., Brummel-Ziedins, K.E., Butenas, S., Pusateri, A.E., Mann, K.G., Orfeo, T., 2016. . J. Thromb. Haemost. 14, 2001–2010.
Golebiewska, E.M., Poole, A.W., 2015. . Blood Rev 29, 153–162.
Gonzalez, E., Moore, E.E., Moore, H.B., Chapman, M.P., Chin, T.L., Ghasabyan, A., Wohlauer, M. V., Barnett, C.C., Bensard, D.D., Biffl, W.L., Burlew, C.C., Johnson, J.L., Pieracci, F.M., Jurkovich, G.J., Banerjee, A., Silliman, C.C., Sauaia, A., 2016. . Ann. Surg. 263, 1051–9.
Gottumukkala, V.N.R., Sharma, S.K., Philip, J., Camenzind, V., Bombeli, T., Seifert, B., Jamnicki, M., Popovic, D., Pasch, T., Spahn, D.R., 1999. . Anesth. Analg. 89, 1453–1455.
Green, D., McMahon, B., Foiles, N., Tian, L., 2008. . Am. J. Clin. Pathol. 130, 811–5.
Grünewald, M., Siegemund, A., Grünewald, A., Konegen, A., Koksch, M., Griesshammer, M., 2002. . Platelets 13, 451–458.
Haggis, G.H., Hasted, J.B., Buchanan, T.J., 1952. . J. Chem. Phys. 20, 1452–1465.
Harris, L.F., Castro-López, V., Killard, A.J., 2013. . TrAC - Trends Anal. Chem. 50, 85–95.
Harrison, P., 2009. . Hamostaseologie 29, 25–31.
Harrison, P., 2005. . Blood Rev. 19, 111–123.
Hasted, J.B., Ritson, D.M., Collie, C.H., 1948. . J. Chem. Phys. 16, 1–21.
Hayashi, Y., Brun, M.A., Machida, K., Lee, S., Murata, A., Omori, S., Uchiyama, H., Inoue, Y., Kudo, T., Toyofuku, T., Nagasawa, M., Uchimura, I., Nakamura, T., Muneta, T., 2017. . Biorheology 54, 25–35.
Hayashi, Y., Brun, M.A., Machida, K., Nagasawa, M., 2015. . Anal. Chem. 87, 10072–10079.
Hayashi, Y., Katsumoto, Y., Omori, S., Yasuda, A., Asami, K., Kaibara, M., Uchimura, I., 2010. . Anal. Chem. 82, 9769–9774.
Hayashi, Y., Oshige, I., Katsumoto, Y., Omori, S., Yasuda, A., Asami, K., 2008. . Phys. Med. Biol. 53, 2553–2564.

Heileman, K., Daoud, J., Tabrizian, M., 2013. . Biosens. Bioelectron.
Henriques, S.S., Sandmann, R., Strate, A., Köster, S., 2012. . J. Cell Sci. 125, 3914–3920.
Hughes, M., 2002. . Point Care 1.
Huth-Kühne, A., Baudo, F., Collins, P., Ingerslev, J., Kessler, C.M., Lévesque, H., Castellano, M.E.M., Shima, M., St-Louis, J., 2009. . Haematologica 94, 566–575.
Ill, C.R., Engvall, E., Ruoslahti, E., 1984. . J. Cell Biol. 99, 2140–2145.
Jackson, S.P., 2011. . Nat. Med. 17, 1423–1436.
Jain, A., Graveline, A., Waterhouse, A., Vernet, A., Flaumenhaft, R., Ingber, D.E., 2016. . Nat. Commun. 7, 10176.
Jensen, M.S., Larsen, O.H., Christiansen, K., Fenger-Eriksen, C., Ingerslev, J., Sørensen, B., 2013. . Haemophilia 19, 403–408.
Jin, J., Quinton, T.M., Zhang, J., Rittenhouse, S.E., Kunapuli, S.P., 2002. . Blood 99, 193–198.
Judith, R.M., Fisher, J.K., Spero, R.C., Fiser, B.L., Turner, A., Oberhardt, B., Taylor, R.M., Falvo, M.R., Superfine, R., 2015. . Lab Chip 15, 1385–1393.
Kaufman, R.M., Djulbegovic, B., Gernsheimer, T., Kleinman, S., Tinmouth, A.T., Capocelli, K.E., Cipolle, M.D., Cohn, C.S., Fung, M.K., Grossman, B.J., Mintz, P.D., O'Malley, B.A., Sesok-Pizzini, D.A., Shander, A., Stack, G.E., Webert, K.E., Weinstein, R., Welch, B.G., Whitman, G.J., Wong, E.C., Tobian, A.A.R., 2015. . Ann. Intern. Med. 162, 205–213.
Kirley, K., Qato, D.M., Kornfield, R., Stafford, R.S., Caleb Alexander, G., 2012. . Circ. Cardiovasc. Qual. Outcomes 5, 615–621.
Koscielny, J., Ziemer, S., Radtke, H., Schmutzler, M., Pruss, A., Sinha, P., Salama, A., Kiesewetter, H., Latza, R., 2004. . Clin. Appl. Thromb. 10, 195–204.
Kumar, A., Mhaskar, R., Grossman, B.J., Kaufman, R.M., Tobian, A.A.R., Kleinman, S., Gernsheimer, T., Tinmouth, A.T., Djulbegovic, B., AABB Platelet Transfusion Guidelines Panel, 2015. . Transfusion 55, 1116–27; quiz 1115.
Kvolik, S., Jukic, M., Matijevic, M., Marjanovic, K., Glavas-Obrovac, L., 2010. . Surg. Oncol. 19, e33–e46.
Lages, B., Weiss, H.J., 1980. . Thromb Haemost 43, 147–153.
Lam, W.A., Chaudhuri, O., Crow, A., Webster, K.D., Li, T.D., Kita, A., Huang, J., Fletcher, D.A., 2011. . Nat Mater 10, 61–66.
Lei, K.F., Chen, K.H.K.-H.K.H., Tsui, P.-H.P.H.P.-H., Tsang, N.-M.N.M., 2013. . PLoS One 8, e76243.
Lemke, G., Silverman, G.J., 2020. . Nat. Rev. Immunol.
Levi, M., Opal, S.M., 2006. . Crit. Care 10, 222.
Levy, J.H., Dutton, R.P., Hemphill, J.C., Shander, A., Cooper, D., Paidas, M.J., Kessler, C.M., Holcomb, J.B., Lawson, J.H., 2010. . Anesth. Analg. 110, 354–364.
Li, Z., Li, X., McCracken, B., Shao, Y., Ward, K., Fu, J., 2016. . Small 12, 3926–3934.
Li, Z., Zhang, G., Le Breton, G.C., Gao, X., Malik, A.B., Du, X., 2003. . J. Biol. Chem. 278, 30725–30731.
Liang, X.M., Han, S.J., Reems, J.A., Gao, D., Sniadecki, N.J., 2010. . Lab Chip 10, 991–998.
Lin, C.-H., Liu, C.-Y., Shih, C.-H., Lu, C.-H., 2014. A sample-to-result system for blood coagulation tests on a microfluidic disk analyzer, Biomicrofluidics.
Lippi, G., Favaloro, E.J., 2018. . Semin. Thromb. Hemost. 44, 239–248.
Luka, G., Samiei, E., Dehghani, S., Johnson, T., Najjaran, H., Hoorfar, M., 2019. . Sensors 19, 258.
Lukinavičius, G., Reymond, L., D'Este, E., Masharina, A., Göttfert, F., Ta, H., Güther, A.,

Fournier, M., Rizzo, S., Waldmann, H., Blaukopf, C., Sommer, C., Gerlich, D.W., Arndt, H.D., Hell, S.W., Johnsson, K., 2014. . Nat. Methods 11, 731–733.
Lusher, J.M., 1996. . Am. J. Obstet. Gynecol. 175, 778–783.
Mackenzie, I.S., Coughtrie, M.W.H., MacDonald, T.M., Wei, L., 2010. . J. Intern. Med.
Maeda, N., Seike, M., Kume, S., Takaku, T., Shiga, T., 1987. . BBA - Biomembr. 904, 81–91.
Mahadhy, A., Stahl-Wernersson, E., Mattiasson, B., Hedstrom, M., 2014. . Biotechnol Rep 3, 42–48.
Maji, D., De La Fuente, M., Kucukal, E., Sekhon, U.D.S., Schmaier, A.H., Sen Gupta, A., Gurkan, U.A., Nieman, M.T., Stavrou, E.X., Mohseni, P., Suster, M.A., 2018. . J. Thromb. Haemost. 16, 2050–2056.
Maji, D., Suster, M.A., Kucukal, E., Sekhon, U.D.S., Gupta, A. Sen, Gurkan, U.A., Stavrou, E.X., Mohseni, P., 2017. . IEEE Trans. Biomed. Circuits Syst. 11, 1459–1469.
Maji, Debnath, Suster, M.A., Mohseni, P., 2018. . 2018 IEEE Biomed. Circuits Syst. Conf. BioCAS 2018 - Proc. 1–4.
Mallett, S. V., Armstrong, M., 2015. . Anaesthesia 70, 73–77.
Mallett, S. V., Chowdary, P., Burroughs, A.K., 2013. . Liver Int.
Mann, K., 1999. . Thromb. Haemost. 82, 165–174.
Marlar, R.A., Potts, R.M., Marlar, A.A., 2006. . Am. J. Clin. Pathol. 126, 400–405.
Matchar, D.B., Samsa, G.P., Cohen, S.J., Oddone, E.Z., 2000. . J. Thromb. Thrombolysis 9, S7-11.
Mattiasson, B., Hedström, M., 2016. . TrAC Trends Anal. Chem. 79, 233–238.
McCrath, D.J., Cerboni, E., Frumento, R.J., Hirsh, A.L., Bennett-Guerrero, E., 2005. . Anesth. Analg. 100, 1576–1583.
McFadyen, J.D., Schaff, M., Peter, K., 2018. . Nat. Rev. Cardiol. 15, 181–191.
McKenzie, M.E., Malinin, A.I., Bell, C.R., Dzhanashvili, A., Horowitz, E.D., Oshrine, B.R., Atar, D., Serebruany, V.L., 2003. . Blood Coagul. Fibrinolysis 14, 249–253.
Mega, J.L., Simon, T., 2015. . Lancet 386, 281–291.
Michelson, A.D., 2019. Platelets, Platelets. Elsevier.
Michelson, A.D., 2004. . Circulation 110, 489–493.
Miller, C.H., 2009. , in: Transfusion Medicine and Hemostasis. Elsevier, pp. 617–621.
Miyazaki, Y., Suwannasom, P., Sotomi, Y., Abdelghani, M., Tummala, K., Katagiri, Y., Asano, T., Tenekecioglu, E., Zeng, Y., Cavalcante, R., Collet, C., Onuma, Y., Serruys, P.W., 2017. . Nat Rev Cardiol 14, 294–303.
Monroe, D M, Hoffman, M., Roberts, H.R., 2002. . Arter. Thromb Vasc Biol 22, 1381–1389.
Monroe, Dougald M., Hoffman, M., Roberts, H.R., 2002. . Arterioscler. Thromb. Vasc. Biol. 22, 1381–9.
Müller, L., Sinn, S., Drechsel, H., Ziegler, C., Wendel, H.P., Northoff, H., Gehring, F.K., 2010. . Anal. Chem. 82, 658–663.
Nabovati, G., Ghafar-Zadeh, E., Letourneau, A., Sawan, M., 2019. . IEEE Trans. Biomed. Eng. 66, 1094–1104.
Nagler, M., Kathriner, S., Bachmann, L.M., Wuillemin, W.A., 2013. . Thromb. Res. 131, 249–253.
Nair, S.C., Dargund, Y., Chitlur, M., Srivastava, A., 2010. . Haemophilia 16, 85–92.
Nathwani, A.C., Tuddenham, E.G.D., 1992. Epidemiology of coagulation disorders, Bailliere's Clinical Haematology. Baillière Tindall.
Ogawa, S., Szlam, F., Bolliger, D., Nishimura, T., Chen, E.P., Tanaka, K.A., 2012. . Anesth.

Analg. 115, 16–21.
Orme, R., Judge, H.M., Storey, R.F., 2017. . Semin Thromb Hemost 43, 311–319.
Padovani, F., Duffy, J., Hegner, M., 2017. . Nanoscale.
Pakala, R., Waksman, R., 2011. . Cardiovasc. Revascularization Med. 12, 312–322.
Paknikar, A.K., Eltzner, B., Köster, S., 2019. . Prog. Biophys. Mol. Biol. 144, 166–176.
Pallister, C., Watson, M., n.d. Haematology.
Paniccia, R., Priora, R., Liotta, A.A., Abbate, R., 2015. . Vasc. Health Risk Manag. 11, 133–148.
Patrono, C., 1994. . N. Engl. J. Med. 330, 1287–94.
Pengo, V., Pegoraro, C., Cucchini, U., Iliceto, S., 2006. . J. Thromb. Thrombolysis 21, 73–77.
Persson, R.A.X., 2017. . Phys. Chem. Chem. Phys. 19, 1982–1987.
Pethig, R., 1984. . IEEE Trans. Electr. Insul. EI-19, 453–474.
Pierschbacher, M.D., Ruoslahti, E., 1984. . Nature 309, 30–33.
Prusty, A.K., Bhand, S., 2020. . J. Electroanal. Chem. 863, 114055.
Puckett, L.G., Lewis, J.K., Urbas, A., Cui, X., Gao, D., Bachas, L.G., 2005. . Biosens. Bioelectron. 20, 1737–1743.
Ramiz, S., Hartmann, J., Young, G., Escobar, M.A., Chitlur, M., 2019. . Am. J. Hematol.
Ranucci, M., Baryshnikova, E., 2020. . J. Clin. Med. 9, 189.
Raskob, G., Angchaisuksiri, P., Blanco, A.N., Buller, H., Gallus, A., Hunt, B.J., Hylek, E.M., Kakkar, A., Konstantinides, S. V., McCumber, M., Ozaki, Y., Wendelboe, A., Weitz, J.I., 2014. . Thromb. Haemost.
Rasmussen, K.C., Højskov, M., Johansson, P.I., Kridina, I., Kistorp, T., Salling, L., Nielsen, H.B., Ruhnau, B., Pedersen, T., Secher, N.H., 2016. . Medicine (Baltimore). 95, e2720.
Rugeri, L., Levrat, A., David, J.S., Delecroix, E., Floccard, B., Gros, A., Allaouchiche, B., Negrier, C., 2007. . J. Thromb. Haemost.
Seiffge, D.J., De Marchis, G.M., Koga, M., Paciaroni, M., Wilson, D., Cappellari, M., Macha, MD, K., Tsivgoulis, G., Ambler, G., Arihiro, S., Bonati, L.H., Bonetti, B., Kallmünzer, B., Muir, K.W., Bovi, P., Gensicke, H., Inoue, M., Schwab, S., Yaghi, S., Brown, M.M., Lyrer, P., Takagi, M., Acciarrese, M., Jager, H.R., Polymeris, A.A., Toyoda, K., Venti, M., Traenka, C., Yamagami, H., Alberti, A., Yoshimura, S., Caso, V., Engelter, S.T., Werring, D.J., 2020. . Ann. Neurol. 87, 677–687.
Sniecinski, R.M., Levy, J.H., 2015. . Best Pract. Res. Clin. Anaesthesiol. 29, 189–202.
Sørensen, B., Tang, M., Larsen, O.H., Laursen, P.N., Fenger-Eriksen, C., Rea, C.J., 2011. . Thromb. Res. 128, S13–S16.
Spiezia, L., Radu, C., Marchioro, P., Bertini, D., Rossetto, V., Castelli, M., Pagnan, A., Sørensen, B., Simioni, P., 2008. . Thromb. Haemost. 100, 1106–1110.
Teige, K., Starý, Z., 1946. . Nature 158, 794.
Tynngård, N., Lindahl, T.L., Ramström, S., 2015. . Thromb. J. 13, 8.
Ur, A., 1970. . Nature 226, 269–270.
van Bladel, E.R., Roest, M., de Groot, P.G., Schutgens, R.E.G., 2011. . Haematologica 96, 888–895.
van der Meijden, P.E.J.J., Heemskerk, J.W.M.M., 2019. . Nat. Rev. Cardiol. 16, 166–179.
Vane, J.R., Botting, R.M., 2003. , in: Thrombosis Research. pp. 255–258.
Versteeg, H.H., Heemskerk, J.W.M., Levi, M., Reitsma, P.H., 2013. . Physiol. Rev. 93, 327–358.
Wang, Y., Wang, M., Ni, Y., Liang, Z., 2020. . Hematology 25, 63–70.
Wendelboe, A.M., Raskob, G.E., 2016. . Circ. Res. 118, 1340–1347.
White, H.D., 2011. . Am. Heart J. 161, 450–461.

Whiting, D., DiNardo, J.A., 2014. . Am. J. Hematol. 89, 228–232.
Wier, L.M., Steiner, C.A., Owens, P.L., 2015. Surgeries in hospital-owned outpatient facilities, 2012.
Wiviott, S.D., Steg, P.G., 2015. . Lancet 386, 292–302.
Xu, X., Zhu, J., Yu, J., Chen, Z., 2019. . IEEE J. Sel. Top. Quantum Electron. 25, 1–6.
Yeung, J., Holinstat, M., 2012. . J Blood Med 3, 33–42.
Zhang, J., Goodman, S.M., Wise, H.G., Dichiara, A.B., Chung, J.-H., 2021. . J. Mater. Chem. C 9, 4544–4553.
Zuo, Z., Wang, K., Gao, L., Ho, V., Mao, H., Qian, D., 2019. . Sensors 19, 325.